Reverse Water Gas Shift Reaction over Supported Cu-Ni Nanoparticle Catalysts

Maxime Lortie

Thesis submitted to the Faculty of Graduate and Postdoctoral Studies in partial fulfillment of the requirements for the M.A.Sc degree

In

Department of Chemical and Biological Engineering
University of Ottawa

© Maxime Lortie, Ottawa, Canada, 2014

Abstract

CuNi nanoparticles were synthesized using a new polyol synthesis method. Three different Cu_xNi_{1-x} catalysts were synthesized where x = 20, 50 and 80. The nanoparticles were deposited on carbon, C, gamma-alumina, γ-Al_2O_3, yttria-stabilized zirconia, YSZ, and samarium-doped ceria, SDC. Each set of catalysts was tested using the Reverse Water Gas Shift, RWGS, reaction under atmospheric pressure and at temperatures ranging from 400°C-700°C. The experiments were repeated 3 times to ensure stability and reproducibility. Platinum nanoparticles were also deposited on the same supports and tested for the RWGS reaction at the same conditions. The CuNi nanoparticles were characterized using a variety of different techniques. X-ray diffraction, XRD, measurements demonstrate the presence of two CuNi solid solutions: one Cu rich solid solution, and the other a Ni rich solid solution. X-ray photo electron spectroscopy, XPS, measurements show Cu enrichment on all catalytic surfaces. Scanning electron microscopy, SEM, measurements show CuNi nanoparticles ranging in size from 4 nm to 100 nm. Some agglomeration was observed. SDC showed the best yield with all catalysts. Furthermore, high oxygen vacancy content was shown to increase yield of CO for the RWGS reaction. $Cu_{50}Ni_{50}$/SDC shows the combination of highest yield of CO and the best stability among CuNi catalysts. It also has similar yields (39.8%) as Pt/SDC at 700°C, which achieved the equilibrium yield at that temperature (43.9%). The catalyst was stable for 48 hours when exposed to high temperatures (600-700°C). There was no CH_4 observed during any of the experiments when the partial pressure of the reactant gases was fed stoichiometrically. Partial pressure variation experiments demonstrated the presence of CH_4 when the partial pressure of hydrogen was increased to twice the value of the partial pressure of CO_2.

Résumé

Des nanoparticules de CuNi ont été synthétisées à l'aide d'un nouveau procédé de synthèse polyol. Trois différents catalyseurs de Cu_xNi_{1-x} ont été synthétisés où x = 20, 50 et 80. Les nanoparticules sont déposées sur : C, γ-Al_2O_3, YSZ et SDC. Chaque série de catalyseurs a été testée en utilisant la réaction « Reverse Water Gas Shift », RWGS, sous pression atmosphérique et à des températures allant de 400°C-700°C. Les expériences ont été répétées trois fois pour assurer la stabilité et la reproductibilité. Des nanoparticules de platine ont été également déposées sur les mêmes supports et testés pour la réaction RWGS dans les mêmes conditions. Les nanoparticules ont été caractérisées en utilisant une variété de techniques différentes. La diffraction par rayons-X, XRD, démontre deux alliages de CuNi: un alliage étant riche en Cu et l'autre étant riche en Ni. La spectroscopie photoélectronique des rayons-X, XPS, démontre un enrichissement en Cu sur toutes les surfaces catalytiques. La Microscopie électronique à balayage, SEM, a démontré que les nanoparticules de CuNi ont une taille allant de 4 nm à 100 nm. L'agglomération de certaine particule a été observée. SDC a montré le meilleur rendement parmi les supports avec tous les catalyseurs. La haute teneur en déficience d'oxygène est suggérée d'avoir augmenté le rendement de CO pour la réaction RWGS. $Cu_{50}Ni_{50}$ / SDC montre la combinaison de rendement de CO le plus élevé et la meilleure stabilité des catalyseurs parmi CuNi. Ce catalyseur obtient des rendements similaires (39,8%) à Pt / SDC à 700 °C, qui a atteint une conversion à l'équilibre à cette température (43,9%). Le catalyseur est stable pendant 48 heures consécutives lorsqu'il est exposé à des températures élevées (600-700 °C). Il n'y avait pas de CH_4 observé au cours des expériences lorsque la pression partielle des gaz réactifs est alimentée de façon stoechiométrique. Des expériences variant la pression partielle des réactifs démontre la formation du CH_4 lorsque la pression partielle de H_2 est deux fois celle du CO_2.

Acknowledgements

I would like to begin by thanking my supervisor; Marten Ternan. His countless hours dedicated to my research gave me the opportunity to accomplish all I have worked towards over the course of my Master's degree. I am extremely grateful for his contributions to both my professional career and my personal endeavours.

The Natural Science and Engineering Council (NSERC) and Phoenix Canada Oil Company Limited, represented by Steve Aplin, are also acknowledged for their financial contributions.

I would like to acknowledge the scientific contributions of several University of Ottawa Researchers: Tara Burchell for her XRD assistance, Yun Liu for the SEM images, Elena Baranova for the laboratory equipment and Alexander Mommers for the XPS experiments.

I would also like to thank the Chemical Engineering Technical Officers, Louis Tremblay, Gérard Nina and Franco Ziroldo for their laboratory assistance throughout my degree.

Lastly, I would like to take this opportunity to thank my family and friends for their endless support. I am truly blessed to have such an incredibly loving and caring group of individuals willing to join me on my quest through life. I will never forget the contributions you have brought me during the good and difficult times.

Table of Contents

List of Figures

List of Tables

Nomenclature

Abbreviations

Abbreviation	Definition
ACS	American Chemical Society
ads	Adsorbed
ALE	Atomic layer epitaxy
BET	Brunauer-Emmett-Teller
cat	Catalyst
COMPO	Compositional
EDS	Energy dispersive X-ray spectroscope
EG	Ethylene glycol
eg	For example
EPOC	Electrochemical promotion of catalysts
FESEM	Field emission scanning electron microscope
GHSV	Gas hourly space velocity
ICSD	Inorganic Crystal Structure Database
IPPC	Intergovernmental Panel on Climate Change
LEI	Lower-secondary electron image
LTS	Low temperature shift
Me	Metal
NA	Not available
NDIR	Non-dispersive infrared
NSERC	The Natural Science and Engineering Research Council
PEM	Proton exchange membrane
PGM	Platinum group metals
PVP	Polyvinylpyrrolidone
RWGS	Reverse water gas shift
SDC	Samarium-doped ceria
SEM	Scanning electron microscopy
Spec.	Spectrometer
SOFC	Solid oxide fuel cell
Sup	Support
SV	Space velocity
TEM	Transmission electron microscopy
TPB	Triple phase boundary
TOF	Turn over frequencies
WGS	Water gas shift
XPS	X-ray photoelectron spectroscopy
XRD	X-ray diffraction
YSZ	Yttria-stabilized Zirconia

Symbols

Symbol	Definition
a.u.	Arbitrary unit
atm	Atmosphere
°C	Degrees Celsius
cm^2	Centimeter square
° / deg	Degree
Ea	Activation energy
F	Molar flow rate
g	Gram
(g)	Gas
Gt	Giga tonne
h	Hours
k	Kelvin
kcal	Kilo calorie
kg	Kilogram
kPa	Kilopascal
kV	Kilovolt
K_X	Equilibrium constant of reaction x
L	Liters
ma	Milliamps
mg	Milligram
min	Minute
mL	Milliliters
mmol	Millimole
mol	Mole
mW	Milliwatt
m^2	Square meters
N	Order of reaction
nm	Nanometers
$O_0^X(S)$	Oxygen ion from support
Ppm	Parts per million
P_x	Partial Pressure of X
$V_0^X(S)$	Support vacancy
W	Weight of catalyst
wt	Weight
X	Fractional conversion
[ ]	Concentration
$\square_{Me}$	Conduction band of the metal
2Θ	Diffraction angle
%	Percent

Chapter 1: Introduction

1.1 Motivation:

Carbon dioxide is the third most abundant gas in our atmosphere. Its concentration has greatly increased since the industrial revolution. In the last 60 years, CO_2 concentrations have increased from 315 ppm to 400 ppm. According to the Intergovernmental Panel on Climate Change (IPCC), 1000 ppm is attainable by year 2100. This near exponential increase can cause drastic, irreversible changes to our planet's climate.

Climate changes can be seen everywhere. Most recently, a large iceberg 6 times the size of Manhattan broke off Antarctica plummeting into the ocean. Increase in CO_2 concentrations has also been linked to decreasing pH levels in the ocean. Corals such as the Great Barrier Reef are feared to become extinct with the ongoing climate changes. Many believe that these examples along with numerous others are directly linked to human activity.

Reducing CO_2 emissions has been at the heart of countless research over the past 20 years. There is however a clear separation between researchers wanting to capture and store CO_2 or use alternative energy sources, and others who want to reuse CO_2 as a carbon source for the production of chemicals/fuels. Some consider that using CO_2 as carbon source brings negligible contributions to the climate change [1].

Sizable quantities of CO_2 are planned to be stored using carbon capture and sequestration. It is estimated that by 2031, approximately 3 Gt/year of CO_2 will be stored [2]. However, CO_2 storage is not sustainable. Caverns that are used to store CO_2 will one day be filled. The technology can therefore be seen as a temporary fix over a concrete solution. The stored CO_2

will consequently be available at zero cost. This means that large amounts of available CO_2 could lead to new opportunities in CO_2 utilization in the future.

CO_2 is a thermodynamically stable molecule. Therefore, breaking the C=O bond requires high energy. In order to do so industrially, high temperatures, hydrogen and catalysts are required [3]–[5]. These demands are what limit the use of CO_2 as an efficient carbon source in the industrial field.

In contrast to fuel from crude oil, using fuel from CO_2 is presently much more expensive because of the high energy demands necessary to convert CO_2 to fuel. This may not always be the case. Current traditional extraction methods are slowly being replaced by offshore platforms and oil sands which in turn cause an increase in the energy demand to produce crude oil. These methods also produce high CO_2 outputs consequently increasing CO_2 concentrations. It is feasible to imagine a future where fuel from recycled CO_2 becomes less costly than fuel from crude oil, because the high energy demands required for the recovery of crude oil limit the use of crude oil thereby enabling renewable energy to become more competitive.

Several ways to sever the C=O bond exist. Electrocatalytic reduction of CO_2 has been achieved at room temperature and pressure using carbon supported Pt nanoparticles [6]. However, high electrical requirements limit the current use of the electrocatalytic reduction of CO_2. Other methods like, photochemical reduction [7], [8], electrochemical reduction [9], [10] and the use of enzymes [11], [12] to reduce CO_2 are small scale developing technologies which limit their industrialisation potential.

Hydrogenating CO_2 is an alternative capable of large scale industrialisation. Research has been done converting CO_2 directly to long-chain liquid hydrocarbons [13]–[15]. This research

combines two reaction steps into one process through a series of reactors and separation units. The first reaction is the reverse water gas shift (RWGS) reaction (eq. 1.1) and the second is the Fischer-Tropsch synthesis (eq. 1.2). Products capable of being synthesized through this reaction include different types of fuels like gasoline, dimethyl ether - which is known as a possible alternative to diesel - or light olefins containing up to 6 carbons (C_6H_{12}) [6].

$$CO_2 + H_2 \leftrightarrow CO + H_2O \tag{1.1}$$

$$(2n+1)\ H_2 + n\ CO \rightarrow C_nH_{(2n+2)} + n\ H_2O \tag{1.2}$$

An alternative to the aforementioned process includes hydrogenating CO_2 according to the following synthesis reaction. Here, CO_2 can be converted to methanol or higher molecular weight alcohols.

$$xCO_2 + (2x\text{-}z+y/2)H_2 \leftrightarrow CxHyOz + (2x\text{-}z)H_2O \tag{1.3}$$

Without considering the end product, high operating temperatures required for the endothermic RWGS reaction will undoubtedly require the use of a catalyst. Development of an efficient catalyst capable of withstanding high temperatures and being selective to CO during the RWGS reaction is a necessity if the process is to be used industrially. The process requires standard equipment already available at most processing plants creating a good opportunity to industrialize the hydrogenation of carbon dioxide through the RWGS reaction.

The selectivity of the catalyst is a requirement due to the nature of simultaneous side reactions occurring during the hydrogenation process. Among possible species being formed, methane is the most prominent. CH_4 is an undesired by-product for several reasons. First, the

methanation process requires 4 H_2 molecules as seen in eq. 1.4. In addition, natural gas prices will always be relatively low in comparison to the cost of H_2 manufactured from CH_4.

$$4\ H_2 + CO_2 \leftrightarrow CH_4 + 2\ H_2O \tag{1.4}$$

Currently hydrogen production is mainly accomplished via the steam reforming of methane [1], [16] that is the reverse of the reaction in eq. 1.4. the entire basis of using the RWGS reaction becomes ineffective when using steam reforming, because the production of CO_2 during this reaction is the opposite of the desired RWGS reaction. In addition, the process uses hydrocarbons and heat.

Instead, H_2 should be derived from alternate reaction pathways. The use of biomass, biogas, cyanobacteria and green algae are all being researched with minimal productivity or efficiency [1]. Using nuclear power or renewable energy like solar or wind power on the other hand could be a profitable venture. This would be accomplished via the electrolysis of water.

Hydrogen was first believed to be a strong candidate to replace fuels in cars using proton exchange membrane (PEM) fuel cells. The lack of flexibility to transport the gas coupled with low energy density and an infrastructure already built for liquid hydrocarbons limit its uses as an everyday gas. Converting H_2 to hydrocarbons could effectively solve all of the aforementioned problems since these fuels have higher energy densities, are convenient to transport and are thoroughly established in today's infrastructure.

Electrolysing water using both solar and wind energy is a topic already being thoroughly researched [17]–[19]. Limitations are caused by high overpotential required for the process as well as low overall efficiencies of solar and wind power [1]. Further research in this domain is

needed for the RWGS & Fischer-Tropsch process to become a useful and economical alternative to other energy sources.

It is possible with the use of nuclear energy and renewable energy to create a closed cycle loop for the fuel industry. As seen in Fig. 1.1, the cycle utilizes both products from the RWGS reaction. Water which is generated during the process can be sent to the electrolysing unit to make H_2. CO_2 generated from varying sources can be reduced to fuels and reused.

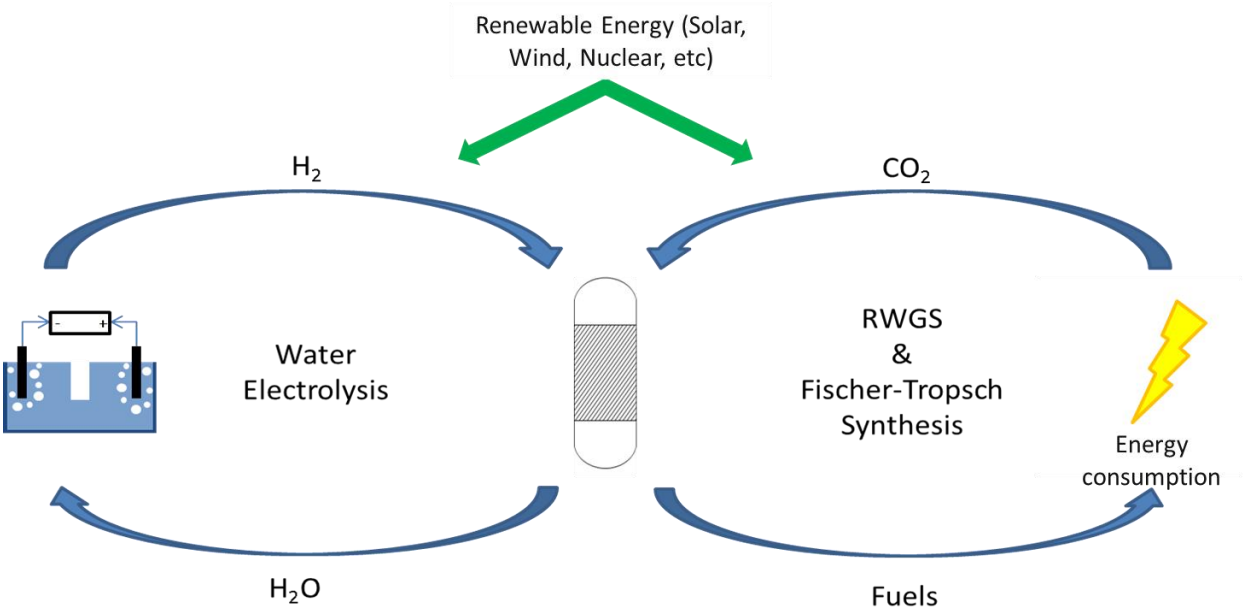

Figure 1.1: Closed cycle using H_2 electrolysis, RWGS and the Fischer Tropsch synthesis.

Instead of being considered a "devil" molecule, CO_2 could, with the proper initiative, become a strategic molecule in the processing industry. Further research dedicated to converting CO_2 to useful fuels parallel to the current research devoted to capturing the gas can reduce CO_2 emissions, and in the long term, reduce atmospheric CO_2 concentrations.

1.2 Objectives:

The development of a stable and selective catalyst is required for the success of the proposed strategy. This was considered to be attainable using platinum (Pt), copper (Cu) and/or

nickel (Ni) nanoparticles deposited on supports having varying oxygen vacancy content. With that in mind, the following four objectives were pursued:

Objective 1: Develop a synthesis method producing CuNi nanoparticles

Objective 2: Characterize the CuNi catalysts

Objective 3: Establish a "best case scenario" using an established noble metal (Pt) based nanocatalyst

Objective 4: Investigate the performance of CuNi nanoparticles deposited on supports having varying oxygen vacancy contents for the RWGS reaction

The thesis is separated into 5 more chapters plus appendices. Chapter 2 provides a detailed literature review pertinent to the research conducted during the Master's project. Chapters 3 and 4 are papers which are intended for submission for publication. Chapter 3 discusses the synthesis of the CuNi nanoparticles (Objective 1), their characterization (Objective 2) as well as how they compare to Pt (Objective 3) when deposited on supports containing no oxygen vacancies. Chapter 4 further compares $Cu_{50}Ni_{50}$ to Pt (Objective 3) when both are supported on supports having varying oxygen vacancy content (Objective 4). Chapter 5 integrates the material in the two articles (Chapters 3 and 4). Lastly, Chapter 6 summarizes the major findings brought forth in this M.A.Sc thesis as well as further suggestions for prospective researchers.

1. 3 References:

[1] G. Centi and S. Perathoner, "Chapter 1: Perspectives and State of the Art in Producing Solar Fuels and Chemicals from CO2," in *Green Carbon Dioxide: Advances in CO2 Utilization*, 2014, pp. 1–24.

[2] E. A. Quadrelli, G. Centi, J.-L. Duplan, and S. Perathoner, "Carbon dioxide recycling: emerging large-scale technologies with industrial potential.," *ChemSusChem*, vol. 4, pp. 1194–215, Sep. 2011.

[3] L. Wang, S. Zhang, and Y. Liu, "Reverse water gas shift reaction over Co-precipitated Ni-CeO2 catalysts," *J. Rare Earths*, vol. 26, pp. 66–70, 2008.

[4] C.-H. Huang, "A Review: CO2 Utilization," *Aerosol Air Qual. Res.*, pp. 480–499, 2014.

[5] W. Wang, S. Wang, X. Ma, and J. Gong, "Recent advances in catalytic hydrogenation of carbon dioxide.," *Chem. Soc. Rev.*, vol. 40, no. 7, pp. 3703–27, Jul. 2011.

[6] B. Hu and S. L. Suib, "Chapter 3: Synthesis of Useful Compounds from CO2," in *Green Carbon Dioxide: Advances in CO2 Utilization*, 2014, pp. 51–97.

[7] J. Hawecker, J. Lehn, and R. Ziessel, "Photochemical and Electrochemical Reductions of Carbon Dioxide to Carbon Monoxide Mediated by (2,2'-Bipyridine)tricarbonylchlorohenium (I) and Related Complexes as Homogeneous Catalysts," *Helv. Chim. Acta*, vol. 69, no. 1986, pp. 1990–2012, 1990.

[8] M. Anpo, H. Yamashita, K. Ikeue, Y. Fujii, S. G. Zhang, Y. Ichihashi, D. R. Park, Y. Suzuki, K. Koyano, and T. Tatsumi, "Photocatalytic reduction of CO2 with H2O on Ti-MCM-41 and Ti-MCM-48 mesoporous zeolite catalysts," *Catal. Today*, vol. 44, no. 1–4, pp. 327–332, Sep. 1998.

[9] K. Hara, A. Kudo, and T. Sakata, "Electrochemical reduction of carbon dioxide under high pressure on various electrodes in an aqueous electrolyte," *J. Electroanal. Chem.*, vol. 391, no. 1–2, pp. 141–147, Jul. 1995.

[10] M. Jitaru, "Electrochemical Carbon Dioxide Reduction - Fundamental and Applied Topics," *J. Univ. Chem. Technol. Metall.*, vol. 42, no. 4, pp. 333–344, 2007.

[11] I. H. Steen, M. S. Madsen, N.-K. Birkeland, and T. Lien, "Purification and characterization of a monomeric isocitrate dehydrogenase from the sulfate-reducing bacterium Desulfobacter vibrioformis and demonstration of the presence of a monomeric enzyme in other bacteria," *FEMS Microbiol. Lett.*, vol. 160, pp. 75–79, 1998.

[12] V. Wiwanitkit, "Plasmodium and host carbonic anhydrase : molecular function and biological process," *Gene Ther. Mol. Biol.*, vol. 10, pp. 251–254, 2006.

[13] A. Boisen, T. V. W. Janssens, N. Schumacher, I. Chorkendorff, and S. Dahl, “Support effects and catalytic trends for water gas shift activity of transition metals,” *J. Mol. Catal. A Chem.*, vol. 315, no. 2, pp. 163–170, Jan. 2010.

[14] M. J. L. Gines, N. Amadeo, M. Laborde, and C. R. Apestegufa, “Activity and structure-sensitivity of the water-gas shift reaction over Cu-Zn-Al mixed oxide catalysts,” *Appl. Catal. A Gen.*, vol. 131, pp. 283–296, 1995.

[15] D. J. Pettigrew and N. W. Cant, “The effects of rare earth oxides on the reverse water-gas shift reaction on palladium / alumina,” *Catal. Letters*, vol. 28, pp. 313–319, 1994.

[16] S. Uemiya, N. Sato, H. Ando, and T. Matsuda, “Steam reforming of methane in a hydrogen-permeable membrane reactor,” *Appl. Catal.*, vol. 67, pp. 223–230, 1991.

[17] R. L. LeRoy, “Industrial water electrolysis: Present and future,” *Int. J. Hydrogen Energy*, vol. 8, no. 6, pp. 401–417, 1983.

[18] M. Carmo, D. L. Fritz, J. Mergel, and D. Stolten, “A comprehensive review on PEM water electrolysis,” *Int. J. Hydrogen Energy*, vol. 38, no. 12, pp. 4901–4934, Apr. 2013.

[19] W. Doenitz, R. Schmidberger, E. Steinheil, and R. Streicher, “Hydrogen Production by High Temperature Electrolysis of Water Vapour,” *Int. J. Hydrogen Energy*, vol. 5, pp. 55–63, 1980.

Chapter 2. Literature Review

2.1 Nanoparticles

Nanoparticles are now at the heart of a variety of different researches. In the past 20 years, these particles which are invisible to the naked eye have transformed how people look at a variety of subjects. These subjects include electronics [1], optical [1], magnetic devices such as sensors [2], photocatalysts [3], heterogeneous catalysis [4] etc.

Nanoparticles in heterogeneous catalysis have been increasingly used over the past two decades [5]. In fact, there has been a near exponential growth of nanoparticle publications in a 13 year span from 1997 - 2010 [6]. This is in part because certain metals used in heterogeneous catalysis are inactive/less active unless they are shrunk to nano-scale consequently changing their properties. In addition, the small nature of these particles increases the number of surface sites available for reaction.

Gold nanoparticles are a good example of changing properties once particle size is reduced to nano-scale. For gold catalysts, there is a direct correlation between the particle size and catalytic efficiency [7]. These gold nanoparticles can be synthesized with a narrow size distribution and be an efficient catalysts while using a fraction of the metal [7]–[9].

Particle size distribution as well as particle shape has a lot to do with the synthesis method used to produce nanoparticles. Laser pulses have been used to synthesize nanoparticles of narrow size distribution capable of layering nanoparticles on certain surfaces resulting in a specific thickness [9], [10]. Other methods use a combination of solvents and microwaves to

produce nanoparticles [11], [12]. However, both methods require high costs and produce relatively small samples.

2.2 Polyol Synthesis Method

The polyol synthesis method is a (poly)ethylene glycol (EG) based method which utilizes EG as both a solvent and a reducing agent. The method usually involves diluting metal salts in EG and then either refluxing or distilling the solution at temperatures ranging from 140°C-196°C [13]–[15].

Modifications can be made to the polyol synthesis method which can enhance the particle size distribution and vary the shape of the resulting particles. These modifications can be reaction conditions, solvent or salt based or can be through the addition of other species such as stabilizing agents or pH adjustors.

Carroll et al. [16] synthesized copper (Cu) and nickel (Ni) nanoparticles using a polyol method and varied several aspects. First, they used two reaction conditions: distillation and reflux. Next, the scientists changed the solvent using ethylene glycol, diethylene glycol or polyethylene glycol. Lastly, they used three different types of metal salts (chlorides, hydroxides and acetates).

In all experiments, they dissolved their metal salts in an ethylene glycol solvent and added NaOH as pH adjuster. A 0.1M metal salt concentration was used in 50 mL of the polyol solvent. The mixture was then heated either through distillation or through reflux for 2 hours. The particles were washed and centrifuged at 25°C.

Varying both solvents and reaction conditions brought shape and size variations. The group noticed circular particles when ethylene glycol was used under reflux and pentagon shapes

when the same solvent was used under distillation. Similar changes were observed when solvents were changed. Slightly smaller triangular particles were observed when using polyethylene glycol under reflux while larger rectangular shaped particles were obtained with diethylene glycol under reflux.

Varying salt precursors showed an effect on the reduction mechanism and resulting metals. When chlorides were used in ethylene glycol under reflux, they observed the presence of a Ni hydroxyl salt. When other salts were used, only base metals were obtained.

Other researchers [13] have also shown that varying metal salt precursors can affect how said salts are dissolved in the polyol solvent. Bonet et al. found that Ni and Cu carbonates did not dissolve completely in an ethylene glycol solution even after 39 hours of mixing at 140°C. They noticed that nitrates salts were more soluble in the same solution.

The group first dissolved Cu and Ni nitrate in ethylene glycol at room temperature without the addition of NaOH. They then refluxed the solution at 196°C. The reflux lasted for 4 hours. They observed the formation of a Ni rich Cu-Ni solid solution shell and a Cu rich Cu-Ni solid solution core. This observation contradicts some research which state that Cu is the main component found on the surface of a CuNi alloy [17]–[19].

Stabilizing agents are also used in the polyol process in order to form nanoparticles of a narrow size distribution. Polyvinylpyrrolidone (PVP) has been widely used as stabilizing agent [20], [21]. It is added prior to the synthesis. The polymer attaches to the formed metal preventing agglomeration between nanoparticles. The PVP can then be burnt off prior to usage.

Meshesha et al. [22] compared the use of PVP with 1-hexadecylamine as stabilizing agent in the synthesis of Cu nanoparticles. In their work, they found that 1-hexadecylamine was

more effective at isolating nanoparticles. The compound successfully capped the synthesized metal and yielded smaller nanoparticles with a smaller size distribution.

Other researchers [20], [23]–[25] have found that PVP can be used to successfully synthesize nanoparticles. Gold, silver, platinum, ruthenium among others are examples of noble metal nanoparticles synthesized with a narrow size distribution using PVP.

NaOH can also be used as additive in the polyol process. Bock et al. [26] varied the NaOH concentration from 0.2 to 0.4 M for the synthesis of PtRu nanoparticles using the polyol process. They observed a relationship between the concentration / solution's initial pH and particle size. The higher pH/NaOH concentration yielded smaller nanoparticles. Other researchers [27] noticed similar trends. Isaifan et al. [27] varied NaOH concentration of their Pt nanoparticles and observed its effect on CO oxidation. They found that smaller particles yielded better turn over frequencies (TOF).

The polyol process is also used to form bimetallic metals. In fact, some metals do not begin to reduce to their metallic form without the presence of a nucleating agent. Ni is a good example of such metal. Chou et al. [28] synthesized $Ni_{99}Pd_1$ nanoparticles using Pd as a nucleating agent. The obtained metal was a bimetallic compound where Ni and Pd were pure metals.

Other researchers have used the polyol process to synthesize core shell particles. Nagaveni et al. [15] synthesized Pd coated Ni nanoparticles using the polyol process. They injected Pd at 196°C in order to coat Ni particles with Pd. In addition, alloys can be synthesized. Nanoparticles of FePt were synthesized by Liu et al [29].

In summary, the Polyol synthesis method provides a simple synthesis method capable of generating nanoparticles of a narrow size distribution and of selected shape. Its flexibility permits numerous extensions of the method to be developed that are capable of synthesizing a variety of different metals.

2.3 Catalysts for the Reverse Water Gas Shift Reaction

Traditionally, catalysts were tested in an arbitrary manner but recently, screening methods are employed to select catalysts with the most potential. These methods can involve simulation software or experimental results. Because of this, catalyst research is becoming more systematic.

Predicting catalytic activity can be a difficult task and therefore requires a certain level of organisation. Zigarnik et al [30] demonstrated their methodology in which a computer program first determines a list of intermediate species for reactions. Then they are able to calculate the activation energies of each step. Table 2.1 demonstrates the activation energies of both directions of the water gas shift reaction (Eq. 2.1). The crystal (111) face of 7 different metals was examined. They determined that the metals should yield the following order of catalytic activity based on kinetic simulations: Cu > Ni > Fe > Pt > Pd > Ag > Au.

$$H_2O + CO \leftrightarrow CO_2 + H_2 \qquad (2.1)$$

Table 2.1: The activation energies (kcal/mol) of steps in the forward and reverse directions in the WGS reaction [30]

Step	Metal													
	Cu(111)		Ag(111)		Au(111)		Ni(111)		Pd(111)		Pt(111)		Fe(110)	
	For	Rev	For	Rev	For	Rev	For	Rev	For	Rev	For	Rev	For	Rev
$H_2O_g = H_2O_{ads}$	0	13.5	0	8.6	0	7.6	0	16.4	0	10	0	9.6	0	19
$CO_g = CO_{ads}$	0	12	0	6.5	0	7	0	27	0	34	0	32	0	36
$CO_{2,\,g} = CO_{2,\,ads}$	0	5.3	0	3.2	0	2.8	0	6.5	0	3.8	0	3.6	0	7.7
$H_{2,\,ads} = H_{ads} + H_{ads}$	12.7	15.3	15.4	10.6	19.4	3.6	8.2	23.3	8.8	22.2	9.5	21	6.2	26.8
$H_{2,\,g} = H_{2,\,ads}$	0	5.4	0	4.7	0	3.7	0	6.8	0	6.6	0	6.4	0	7.4
$H_2O_{ads} = H_{ads} + OH_{ads}$	25.8	1.1	40.4	0	48.8	0	21.2	9.8	26.8	0	28.9	0	18.4	15.3
$CO_{2,\,ads} = CO_{ads} + O_{ads}$	28	10.7	49.7	6	54.2	6.4	13.4	21.9	34.1	24.5	36.9	23.2	1.6	28
$HCOO_{ads} = CO_{ads} + OH_{ads}$	20.4	0	22.3	0	21.2	0	13.2	5.5	7.1	11.3	7.5	10	12.2	11.5
$OH_{ads} = O_{ads} + H_{ads}$	15.5	20.8	18.3	13.2	20.6	7.9	12.8	27.9	14.6	21.6	15.1	20.4	11.5	31.7
$CO_{2,\,ads} + H_{ads} = CO_{ads} + OH_{ads}$	22.5	0	38.5	0	35.1	0	12.6	6.1	17.5	0.9	19	0	8.7	14.9
$HCOO_{ads} = CO_{2,\,ads} + H_{,ads}$	1.4	3.5	0	16.2	0	13.8	3.5	2.4	0	20.8	0	21.5	6.8	0
$CO_{2,ads} + OH_{ads} = HCOO_{ads} + O_{ads}$	17.2	20.4	23.8	2.4	26.6	0	13.8	29.9	21.7	7.9	22.4	6.3	11	38
$H_2O_{ads} + O_{ads} = OH_{ads} + OH_{ads}$	27.3	0	35.7	0	33.1	0	26.7	0	40.2	0	40.5	0	23.7	0
$O_{ads} + H_{2,\,ads} = OH_{ads} + H_{ads}$	14.8	12.1	10.3	10.7	10.9	7.9	15.4	15.6	9	15.4	8.7	14.9	16.6	17.1
$CO_{2,\,ads} + H_2O_{ads} = HCOO_{ads} + OH_{ads}$	27.2	0.4	56.6	0	62.7	0	21.6	11.1	47.6	0	50.4	0	16.7	20.4
$CO_{2,\,ads} + H_{2,\,ads} = HCOO_{ads} + H_{ads}$	14.2	14.6	21.6	0.7	29.6	0	8.5	24.8	16.7	9.3	17.6	7.7	4.4	31.9

Another way of predicting the efficiency of a catalyst for a specific reaction is to observe how it does in other similar reactions. For instance, supported noble metals like Pt, Rh, Ru etc are known as a good hydrogenation catalysts because of their capability to dissociate hydrogen [31]. They could therefore show good activity for the reverse water gas shift (RWGS) reaction. In fact, several have tested Pt group metals (PGM) for the RWGS reaction and have shown considerable conversion [32]–[34]. Supported Pt will be discussed in detail in section 2.3.1.

It is well known that catalysts that are good for a forward reaction should also be good for the reverse reaction. The water gas shift (WGS) reaction has been thoroughly researched for decades. Several catalysts have been established as being efficient depending on the operating temperature. For instance, low temperature (<350°C) WGS reactions often involve Cu-ZnO-

Al_2O_3 catalysts while high temperature (>350°C) WGS reactions take place over Fe_2O_3-Cr_2O_3 catalysts [35].

This section is dedicated to highlighting the most pertinent advances in catalysis relevant to the field of research. These include catalysts containing Pt, Cu and Ni. A section will also be dedicated to the impact of the support. Other PGM metals such as Ru [36], Rh [37], Pd [38] and noble metals such as Ag [39] and Au [40] have all been used for the RWGS reaction but will not be discussed in detail unless it is directly related to the field of study.

2.3.1 Pt for the RWGS reactions

Pt has been used as a catalyst in numerous applications. These include in the catalytic converter of your car, catalytic reforming of naphtha to higher octane gasoline, PEM fuel cell technology, amongst others. However, platinum's high cost limits its use as an effective industrial catalyst.

Research into synthesizing Pt nanoparticles reduces the economic impact that is attached with Pt. Researchers have been able to successfully synthesize Pt nanoparticles of specific size and deposit them on varying supports [26], [41]. Pt nanoparticles have been researched for other reactions [23], [24], [27] and have proven to be efficient at relatively small loadings (1 wt% metal, 99 wt% support).

Supported metallic Pt in the micron scale has been tested for the WGS reaction showing promising results. Among these, Pt-ZrO_2 [42], Pt-Fe_2O_3 [43], Pt-CeO_2 [44] and Pt–TiO_2 [45] have all shown considerable yields within the 250-400°C temperature range [35]. These supported catalysts are compared in Table 2.2 which demonstrates the activation energy and the

catalytic activity. Pt/TiO_2 demonstrates the best catalytic activity at 300°C and Pt/Fe_2O_3 shows the worst. In the work of Ratnasamy and Wagner, catalytic activity is defined as:

$$\text{Activity (mmol/kg}_{cat}) = F_{co} \text{ x } (X_{co}/W_{cat}) \quad (2.2)$$

where the molar flow rate of CO is F_{co} in mol/s, the fractional conversion is X_{co} and the weight of catalyst is W_{cat} in kg.

Table 2.2: Apparent activation energies and catalytic activities (at 300°C) of Pt over supported reducible oxides [35]

Catalyst	Ea (kJ/mol)	Activity (mmol/kg cats)
2% Pt/CeO2	65	15
1.5% Pt/ZrO2	58	20
1.9% Pt/TiO2	23	39
1.5% Pt/FeO3	44	6

In the past 10 years, Pt nanoparticles have been tested for the RWGS reaction. These are typically deposited on reducible supports like TiO_2 and CeO_2 with positive results. The size of the supported Pt particles range from 1 nm to 400 nm depending on the researchers conducting the experiments.

Kim et al [33] tested Pt/TiO_2 at different H_2:CO_2 feed ratios in a temperature range of 300 to 600°C. They used a space velocity (SV) of 12 000 h^{-1}, 500 mg of catalyst and a 1 wt% loading. Pt nanoparticles had an average size of 22 nm. They achieved near equilibrium conversion for their temperature range with no CH_4 production. They also observed an increase in conversion with an increase in H_2:CO_2 feed ratio. However, CH_4 was observed when the ratio was increased to 2. They also observed limited to no deactivation for a period of 72 hours.

The same researchers [46] compared the support's reducibility using Pt nanoparticles. They compared the use of titania (TiO_2) as a reducible support with gamma-alumina (γ-Al_2O_3)

using 500 mg of catalyst, a gaseous feed content of 21% CO_2, 30% H_2, balance of N_2 and a total flow rate of 100 mL min^{-1}. They observed a considerable increase in CO_2 conversion when using Pt/TiO_2. They suggest that the support's reducibility is the main cause of their observation.

A high pressure setup using Pt/CeO_2 was built by Tidona et al [47] where they operated at a pressure range of 200 - 950 bar and 450°C. They found that the increase in pressure yielded higher conversions, as predicted thermodynamically. They observed an increase in conversion with pressure. The researchers explained that higher fluid densities yielding higher CO_2 molar flow rates at the inlet of the reactor causes the increase in conversion. Results were below equilibrium for all their system.

By-products are often formed when trying to conduct RWGS reaction experiments; some of which may even be beneficial. For example, Dorner et al.[48] attempted to modify the reaction conditions in order to form valuable hydrocarbons directly. They used $Co\text{-}Pt/Al_2O_3$ and had H_2:CO_2 feed ratios of 1:1, 2:1 and 3:1. They were able to shift the equilibrium slightly away from the methanation reaction - which is formed by the hydrogenation of CO – by lowering the operating pressure and reducing the H_2:CO_2 ratio. However, they concluded that throughout their experiments, the catalyst behaved like a hydrogenation catalyst and were unable to primarily form longer chain hydrocarbons (C2-C4).

Goguet et al. [49]–[51] worked with Pt/CeO_2 studying catalytic deactivation as well as spectrokinetic investigation for the RWGS reaction. In their work, they observed that CO is the main cause of low temperature deactivation. In addition, high H_2:CO_2 ratios combined with extensive catalytic testing can cause an accumulation of coke on the catalytic surface. Their spectrokinetic research concluded that formates are almost entirely spectator species in the

formation of CO. They also found that Pt bound carbonyls are not a major reaction route. Instead, they concluded that support surface carbonyls are the main reaction intermediate. Figure 2.1 demonstrates their interpretation of the intermediates formed over a Pt/CeO_2 catalyst. These kinetic tests were performed at low temperatures (225°C) and high H_2:CO_2 ratios (4).

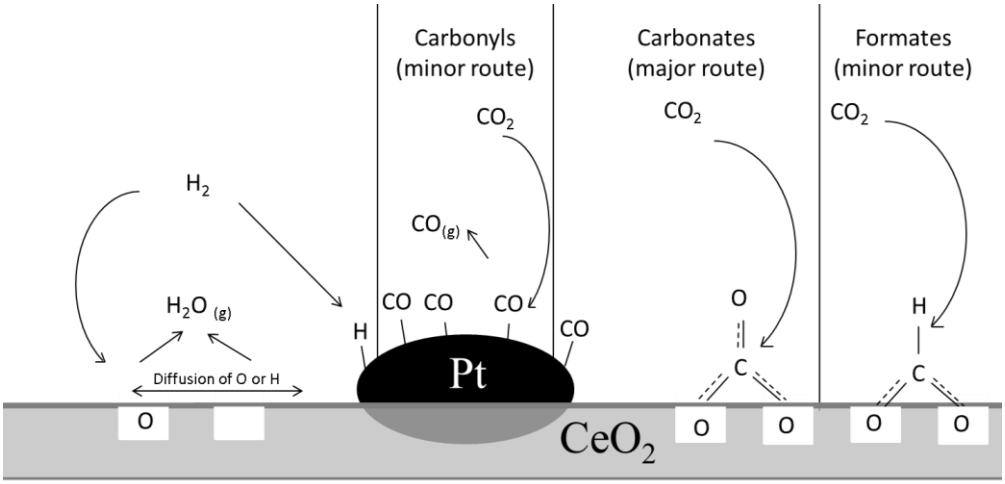

Figure 2.1: Model for the reaction mechanism of the RWGS reaction over Pt/CeO_2. [49]

Pekridis et al. [34] were among the first and only researchers to test Pt/YSZ/Pt for its use in a SOFC with the RWGS reaction. In their work, they operated at different H_2:CO_2 ratios in a temperature range of 650 – 850 °C. They applied both positive and negative potentials in order to examine the impact of migrating O^{2-} species throughout the support. They observed that with positive over potentials, O^{2-} was being pumped to the surface increasing the formation of H_2O and decreasing the formation of CO. When a negative current is applied, O^{2-} is sent away from the surface generating more oxygen vacancies consequently increasing the formation rate of CO. They developed the following mechanism for the support interaction:

$$CO_2 + V_o^x(S) \leftrightarrow CO + O_o^x(S) \quad (2.3)$$

$$H_2O + V_o^x(S) \leftrightarrow H_2 + O_o^x(S) \quad (2.4)$$

In their work, they determined that the formate decomposition describes best the kinetics for the RWGS reaction. They also concluded that the reaction rate seems to be controlled by C-containing intermediates. This is mainly caused by the intermediates' interaction with adsorbed hydrogen to form carbonyl species.

2.3.2 Cu RWGS reaction

Copper (Cu) provides a relatively inexpensive alternative to PGM catalysts. Cu has been most prominently used in both steam reforming and in the WGS reaction. In fact, Cu has proven to be an effective catalyst for low temperature systems like the ones mentioned previously. Issues with Cu arise when operating temperatures increase consequently reducing its catalytic activity [35].

Industrially, Cu is an established metal for low temperature WGS reactions [42]. It is even known as the "... most popularly studied catalytic system for the WGS reaction." [31] In addition, ongoing research published in 2014 continues to be dedicated to enhancing the metal's capabilities for the reaction. Jeong et al. [52] synthesized a Cu/CeO_2 catalyst showing 100% selectivity towards CO_2 and excellent conversion. Others [53], [54] have looked into the interaction of the support (ZrO_2) using Cu metal. Cu deposited on CeO_2 and ZrO_2 have similar activation energy and activity then Pt when deposited on the same supports as seen in Table 2.3. The most popular catalyst for the for low temperature shift (LTS) WGS reaction is CuO-ZnO-Al_2O_3 [35].

Table 2.3: Comparison of Pt and Cu over the same supports under similar testing conditions

Catalyst	Ea (kJ/mol)	Activity (mmol/kg cats)
2% Pt/CeO_2 [35]	65	15
1.5% Pt/ZrO_2 [35]	58	20
2.1% Cu/CeO_2 [35]	43	16
6.1% Cu/ZrO_2 [54]	66.5	19.3

Historically, research has shown that if a catalyst is good in one direction of an equilibrium reaction, it has the potential to be good in the opposite direction [55]. This principle has brought many to explore the use of Cu in the RWGS reaction. A spike of interest for the RWGS reaction over the past 20 years further increased research for the hydrogenation of CO_2 over a Cu-based catalyst.

Early research concerning the catalyzed hydrogenation of CO_2 over Cu metal catalysts was done using ZnO and Al_2O_3 as a support primarily because of its impact on the WGS reaction. Work began on kinetic experiments attempting to understand the mechanism over a Cu based catalyst. The $CuO/ZnO/Al_2O_3$ catalyst often used in LTS WGS reaction was studied by Ginés et al. [56] in an attempt to compare their calculated results with experimental results in order to predict reaction rates. There was a good agreement between both sets of data when they assumed that both the CO_2 dissociation and the water formation determined the overall reaction rate.

Fujita et al. [57] and Campbell et al. [58], [59] studied the RWGS reaction mechanism over Cu/ZnO_2. They both suggested that the mechanism proceeds by a surface oxidation of Cu to CuO. H_2 could then reduce CuO to metallic Cu forming H_2O. Campbell et al. also postulated the formation of formate species as a major intermediate.

Chen et al. [60]–[62] studied the kinetics of metallic Cu over Al_2O_3 and SiO_2. They also suggested the impact of formate species. They discuss that formates are intermediate species caused by the association of adsorbed hydrogen atoms with CO_2. In addition, they showed the presence of Cu_2O formed when oxygen adatoms react with Cu^0.

A significant advantage to using Cu as a catalyst for the RWGS reaction is its tendency to favour the formation of CO (Eq. 2.1) over side reactions such as CO methanation (Eq. 2.5) [63].

$$CO + 3H_2 \leftrightarrow CH_4 + H_2O \quad (2.5)$$

However, Cu alone has shown to sinter at high temperature because of its relatively low melting point of 1084.6°C [64]–[66].

One method proposed by Chen et al. [67] to increase thermal stability was to do atomic layer epitaxy (ALE) to prepare Cu/SiO_2 nanoparticles. They showed increased thermal stability of the Cu nanoparticles claiming that the catalyst had different characterization in contrast to standard Cu. What happens in this case is that the Cu particles were prevented from contacting each other. Additionally, they mention that the deposition method provides high catalytic activity for the transformation of CO_2 to CO. This is because sintering was prevented causing no loss in copper surface area.

Promoting Cu with varying metals has also shown to increase thermal stability and in some cases even conversion. Doping Cu has been done extensively for the WGS reaction. Amongst others, ZnO, Fe_2O_3 and Cr_2O_3 have all been used to dope Cu providing an increase in activity [35], [68]. The same principle is applied for the RWGS reaction as seen in the following section.

2.3.3 Doped Cu for the RWGS Reaction

Doping Cu with more stable metals is a reasonable solution to improving the thermal stability by changing the physical properties of the Cu-containing catalyst. The doping agent could itself be a more stable metal capable of withstanding higher operating temperatures. Hughes [69] suggested the following order for metallic thermal stability:

Ag < Cu < Au < Pd < Fe < Ni < Co < Pt < Rh < Ru < Ir < Os < Re

Iron was amongst the first Cu dopants successfully used in the RWGS reaction. The reasoning behind utilizing Fe containing catalysts is taken from their increased thermal stability as shown previously and its good activity towards the WGS reaction [70]–[72]. In addition, Fe has a much higher melting point (1535°C) than Cu (1083°C) making it a good candidate for high temperature reactions [66].

Chen et al. [65], [73] studied the effect of stabilizing Cu/SiO_2 with an Fe promoter. In their work, 10wt% Fe-Cu/SiO_2 was used. In all, 9.2% of the mixture was Cu while 0.8% was Fe. The iron addition proved effective. Their catalyst was stable for up to 120 hours at 600°C under 40 mL/min of reactants being fed through the catalyst. In contrast, Cu/SiO_2 deactivated almost entirely after the same duration of time when exposed to the same flow rates. The high stability is explained by the formation of small Fe particles formed around Cu particles that inhibit sintering. Otherwise, the Cu/SiO_2 catalyst sinters reducing the active surface area. They also noticed an increase in conversion of 6% with the Fe additive.

Stone et al. [74] researched the impact of doping Cu with ZnO for low temperature RWGS reaction (240°C). Their experimental procedure consisted of varying the Cu:ZnO ratio from Cu rich to ZnO rich in order to examine its impact on conversion. They observed an increase in conversion at high Cu content and highest conversion when the Cu:ZnO ratio was >3. No stability measurements were performed.

Another group [62] studied the effect of potassium on a Cu/SiO_2 catalyst. Their experiments consisted of depositing 9 wt% Cu on the support and adding between 0.52wt% - 5.2 wt% potassium. They noticed a decrease in surface area with increasing amounts of dopant.

However, 0.52 wt% and 1.9 wt% K showed higher conversion than Cu alone in spite of the reduced surface area. An increase of 7% is noticed at 600°C with the 1.9 wt% K additive. Further doping caused a significant reduction in conversion. No stability tests were conducted with any of the doped catalysts.

High temperature RWGS experiments using a Cu-Ni bimetallic mixture has been researched by one group [63]. The main topic of the paper was to examine the effect of the Cu:Ni ratio on selectivity and CO_2 conversion for the RWGS reaction. 20 wt% of metal was deposited on γ-Al_2O_3 and tested at 500°C and 600°C. The Cu/(Cu+Ni) ratios used were 0.75, 0.50, 0.25 and 0.17. A gas hourly space velocity (GHSV) of 1000h^{-1} was used with the reactants fed stoichiometrially according to the RWGS reaction. Their results are given in form of conversion and selectivity shown in Eq 2.6 and 2.7 respectively.

$$CO_2 \text{ conversion } (\%) = \frac{CO_2(feed) - CO_2(out)}{CO_2(feed)} \text{ x } 100\% \quad (2.6)$$

$$\text{CO selectivity } (\%) = \frac{CO(Out)}{CO_2(feed) - CO_2(out)} \text{ x } 100\% \quad (2.7)$$

The researchers noticed a decrease in CO selectivity and conversion when the Cu/(Cu+Ni) ratio was below 0.75. Conversion of 28.7% at 600°C was observed with CO selectivity of 79.7% using that ratio. The conversion and selectivity drop to 27.1% and 71.8% respectively when the ratio is decreased (higher Ni content). Consequently, the selectivity towards CH_4 is increased. The CO yield, calculated using Eq 2.8, is 19.5% at higher Ni loadings compared to 22.9% at lower Ni loadings.

$$\text{CO yield } (\%) = \frac{\text{CO(out)}}{\text{CO}_2\text{(feed)}} \text{ x } 100\% \quad (2.8)$$

The group concluded that high Ni contents yielded increased formation of CH_4 while high Cu content generated more CO.

2.3.4 Ni for RWGS Reaction

Nickel is another transition metal with good hydrogenation behaviour. Its stability at high temperatures is similar to that of Fe with a melting point of 1455°C [66]. However Ni is known for its capability to further hydrogenate CO to CH_4 [31], [75]–[77] making it a lesser candidate for the RWGS reaction. Hydrogenating CO is an undesired step because it inhibits the application of the Fischer-Trospch process which utilizes a syngas mixture to make long chain hydrocarbons or alcohols.

Nickel remains a candidate as a catalyst for the RWGS reaction despite its high CH_4 selectivity. This is in large part caused by the high operating temperatures used in the RWGS reaction. According to Gibbs equilibrium calculations, the CO methanation reaction is strongly favourable at lower temperatures (below 350°C) [35]. At the high operating temperatures the methanation reaction is somewhat less favourable which accounts for the use of Ni as a possible catalyst for the RWGS reaction.

Still, a lot of research has gone into the methanation of CO_2 using Ni as a catalyst [75]–[80]. This reaction uses lower operating temperatures in the goal of making a closed loop carbon cycle using renewable energy to make H_2. High H_2 requirements combined with natural gas' low cost would make for an unprofitable venture.

Other work consists of hydrogenating CO_2 to produce formic acid and/or methanol. Peng et al. [81] studied the mechanism over Ni(111) and Bermudez et al. [82] studied methanol synthesis over a Ni/γ-Al_2O_3 catalyst. The latter used coke oven gas as a feed source of CO_2.

Low temperature (270°C) RWGS reaction was done using Ni/C compared to Co/C by Guerrero-Ruiz et al in the mid 1980's [83]. Their work examined the conversion of CO_2 into either CH_4 or CO. They found similar conversions and both formed CH_4 and CO. However, they found Ni to be slightly more selective to CO than Co at the low operating temperatures.

High temperature RWGS experiments using Ni/CeO_2 were performed by Wang et al. in order to examine the preparation method [84] and the metal loading [85] effect on the RWGS reaction. They operated at high temperatures (400-750°C) and low reactant flow rates (50 mL/min) fed stoichiometrically according to the RWGS reaction. In their work, they found that both the preparation method and the metal loading influenced the results for the RWGS reaction. First, they noticed that the Ni particles formed deficiencies within ceria's crystal lattice creating oxygen vacancies which increased conversion. They also found that 2wt% loading had the best conversion amongst a range of 0 to 20 wt%. Their catalyst showed high CO formation and some CH_4 yields.

Other groups [86], [87] studied the reaction kinetics on Ni providing in depth analyses of the production of formates on Ni surfaces. The group claims that formate species are a "dead-end spectator molecule." As mentioned in section 2.3.1, Goguet et al. [49] also suggested that formate species did not actively participate in the reaction. Instead, the reaction pathway would go through a Eley-Rideal mechanism [86], [87].

A lot of research has gone into doping Ni in order to examine its effect on selectivity and conversion. The following section is devoted specifically to that research.

2.3.5 Doped-Ni for the RWGS Reaction

The doping effect is often examined in the hopes of enhancing a certain negative aspect of a metal without eliminating whatever advantage the metal had in the first place. Research on dopants for Ni catalysts has been done either in hopes of increasing CO selectivity or in order to examine reaction mechanisms on different surfaces.

Potassium (K) was amongst the first dopants used with Ni for the RWGS reaction. Campbell et al. [88] looked into adding different weight loadings of K to a Ni/SiO_2 catalyst. The researchers operated at low temperatures (280°C) and increased H_2:CO_2 ratios (3.3:1). They noticed an increase in the CO turnover number and a decrease in the CH_4 turnover number with loadings of up to 0.81wt% K. Their work showed that doping Ni with K can increase CO selectivity.

Other researchers [89] further tested K-doped Ni deposited on Al_2O_3 for the RWGS reaction at 500°C. They discovered the formation of coke on top of their Ni-K particles. In fact, the coking mechanism was strongly dependant on the K loading. The resulting coke was in the form of nanofibers. Results showed that the coking was a direct result of CO_2 reduction to carbon.

Rare earth metals such as Ce and La have also been used as doping agents for the RWGS reaction using a Ni catalyst. Barrault et al. [79] tested different weight loadings of La and Ce over carbon supported Ni. Their first tests had approximately 1 wt% of La and Ce over 5 wt% of Ni. They noticed a dramatic increase in CH_4 formation with the addition as well as overall catalytic activity. CO selectivity was reduced from 58% (only Ni) to 1.5% with 1 wt% La. Similarly, 19.5% selectivity towards CO was observed with 1 wt% Ce. Further doping increased

the selectivity towards CH_4 above 95% for both dopants. These results are most likely caused by the fact that CO_2 adsorbs strongly on the surface of rare earth oxides [79].

As mentioned in section 2.3.2, a Cu-Ni bimetallic metal was tested for the RWGS reaction [63]. Cu-Ni bimetallic compounds were also tested for the WGS reaction by Lin [6]. The researcher noticed increased activity towards the WGS reaction when an equimassic ratio of Cu-Ni was used when deposited on Al_2O_3.

2.4 Support Interaction

The interaction between metal catalyst and the support on which it is deposited has been demonstrated for thousands of reactions and continues to be a corner stone in the catalysis world. It is a well proven fact that catalysts generally perform better under a metal/support configuration rather than strictly metal. In addition, aspects such as support reducibility [46], [90]–[92], conductivity [93]–[95], surface area [96] and oxygen vacancies [97], [98] can impact how catalytically active the support is and can even participate in the reaction.

Metal-support interaction using reducible supports is a well-known process in catalysis. Gases can either be reduced or oxidized because the support is capable of exchanging ions with adsorbed specie. This mechanism has been successfully proven for the WGS reaction [45], [64], [92], [99] where the support can increase selectivity and conversion of the WGS reaction.

Support conductivity is a phenomenon developed by Vayenas and Stoukides [100] in the early 1980's when they applied a potential to their Yttria-stabilized Zirconia (YSZ) pellet. Ionic conductivity has been exploited for the RWGS reaction by Pekridis et al. [34] as seen in section 2.3.1. This phenomenon was later proven without electrical current. Vernoux et al. [101] recently

claimed that the conductivity through the YSZ support can also be thermally induced without the presence of an electrical current.

Oxygen vacancies can also actively participate in the WGS/RWGS reaction mechanisms. Chen et al. [53] studied the impact of oxygen vacancies using different morphologies of ZrO_2 with a Cu metal catalyst. They were able to synthesize ZrO_2 having varying oxygen vacancy contents and compare the different supports for the WGS reaction. They noticed an increase in conversion with increasing oxygen vacancy content. Higher synergistic interaction was observed between the Cu particles and the oxygen vacancies causing the increased catalytic activity.

Wang et al. [84] tested Ni-CeO_2 varying the catalyst's preparation method. Results obtained showed that Ni was inserted within the crystal lattice generating oxygen vacancies. The group concluded that those vacancies are the principle reason for the increased conversion that they observed.

Daza et al. [102] recently examined the use of perovskite-type oxides for use in the RWGS reaction. Their work consisted of synthesizing different perovskite-type oxides and examining them for high temperature RWGS reaction. The catalysts had different oxygen vacancy contents and were seen as oxygen carriers. This aspect permitted the oxides to interact with gases providing increasing CO_2 conversion.

The work conducted in this report was done using supports having varying oxygen vacancy contents. Those supports were: gamma-alumina, γ-Al_2O_3, carbon black, C, yttria-stabilized zirconium, YSZ, and samarium-doped ceria, SDC. Both C and γ-Al_2O_3 were considered to contain no theoretical oxygen vacancies. YSZ and SDC have 0.074 and 0.1 oxygen vacancies per cation respectively according to stoichiometry. Carbon black and gamma-alumina

have been thoroughly researched in both the WGS and RWGS reaction [31], [35], [82], [83], [103]. However, YSZ and SDC have very limited research for their use in both reactions.

Firstly, alumina has been used extensively as a support for the WGS reaction [35]. It has shown signs of deactivation at high temperatures when used for the RWGS reaction [65]. However, some have claimed that the support can be used extensively at high temperatures (800°C) for long periods of time (50 hours) and experience no deactivation [82].

YSZ is best known for its use as a solid electrolyte for solid oxide fuel cells (SOFC) [104]–[106]. It is also used as a ceramic insulation inside high temperature furnaces making it a suitable support for high operating temperatures. However, YSZ has a relatively low surface area, as seen in the experimental procedure section. YSZ must therefore depend on its oxygen vacancies to provide increased catalytic activity.

Researchers have already shown that this support is capable of increased catalytic activity for different reactions in comparison to both C and γ-Al_2O_3 [24], [41]. Few Researchers have used YSZ as support for the RWGS reaction. As mentioned, Pekridis et al [34] was among the first to use it in a SOFC using the RWGS reaction.

In addition, Ismail [107] studied the support alone without the addition of a metal catalyst for the RWGS reaction. In his work, YSZ was exposed to different H_2:CO_2 ratios at temperatures ranging from 650°C to 750°C. He noticed CO_2 conversion at all conditions. YSZ had a 19% conversion of CO_2 at 700°C using a stoichiometric ratio of H_2:CO_2. The researcher does not discuss whether the support is selective to CO or other by-products. The support's activity without the presence of a metal catalyst makes it a strong candidate for the RWGS reaction.

SDC is another support used for SOFC [108], [109]. Its high ionic conductivity and thermal stability makes it a good candidate for its use as a solid electrolyte for SOFC. In addition, SDC has more theoretical oxygen vacancies giving it potential to be a better support. SDC is also among the least reducible ceria-doped powders available [108]. Therefore, the impact of oxygen vacancies can be examined with less concern for the support reduction mechanism.

Ismail [107] also researched SDC for its use as a support for the RWGS reaction. Like YSZ, SDC was exposed to high operating temperatures (650-750°C) with different H_2:CO_2 ratios. He observed high CO_2 conversions at all temperatures and H_2:CO_2 ratios. SDC obtained 30% conversion of CO_2 at 700°C and a 1:1 H_2:CO_2 ratio.

Both YSZ and SDC have shown considerable CO_2 conversion without the presence of a metal catalyst for the RWGS reaction. Experiments detailed in this report will demonstrate the impact these materials have on the RWGS reaction in comparison to more traditional supports containing no theoretical oxygen vacancies.

2.5 References:

[1] G. Schon and U. Simon, "A fascinating new field in colloid science: small ligand-stabilized metal clusters and their possible application in microelectronics," *Colloid Polym. Sci.*, vol. 273, no. 3, pp. 202–218, Mar. 1995.

[2] J. M. Thomas, "Colloidal metals: past, present and future," *Pure Appl. Chem.*, vol. 60, no. 10, pp. 1517–1528, Jan. 1988.

[3] P.-A. Brugger, P. Cuendet, and M. Gratzel, "Ultrafine and Specific Catalysts Affording Efficient Hydrogen Evolution from Water under Visible Light Illumination," *J. Am. Chem. Soc.*, vol. 103, pp. 2923–2927, 1981.

[4] A. T. Bell, "The impact of nanoscience on heterogeneous catalysis.," *Am. Assoc. Adv. Sci.*, vol. 299, pp. 1688–91, Mar. 2003.

[5] F. E. Kruis, H. Fissan, and A. Peled, “Synthesis of nanoparticles in the gas phase for electronic, optical and magnetic applications—a review,” *J. Aerosol Sci.*, vol. 29, no. 5–6, pp. 511–535, Jun. 1998.

[6] J. Lin, “Supported Copper, Nickel and Copper-Nickel nanoparticle Catalyst for Low Temperature WGS reaction,” University of Cincinnati, 2012.

[7] A. Corma and H. Garcia, “Supported gold nanoparticles as catalysts for organic reactions.,” *Chem. Soc. Rev.*, vol. 37, no. 9, pp. 2096–126, Sep. 2008.

[8] M. Grzelczak, J. Pérez-Juste, P. Mulvaney, and L. M. Liz-Marzán, “Shape control in gold nanoparticle synthesis.,” *Chem. Soc. Rev.*, vol. 37, no. 9, pp. 1783–91, Sep. 2008.

[9] A. V. Kabashin and M. Meunier, “Synthesis of colloidal nanoparticles during femtosecond laser ablation of gold in water,” *J. Appl. Phys.*, vol. 94, no. 12, p. 7941, 2003.

[10] S. Eliezer, N. Eliaz, E. Grossman, D. Fisher, I. Gouzman, Z. Henis, S. Pecker, Y. Horovitz, M. Fraenkel, S. Maman, and Y. Lereah, “Synthesis of nanoparticles with femtosecond laser pulses,” *Phys. Rev. B*, vol. 69, no. 14, p. 144119, Apr. 2004.

[11] S. Komarneni, D. Li, and B. Newalkar, “Microwave - Polyol Process for Pt and Ag Nanoparticles,” *Langmuir*, vol. 18, no. 15, pp. 5959–5962, 2002.

[12] K. Patel, S. Kapoor, D. P. Dave, and T. Mukherjee, “Synthesis of Pt, Pd, Pt/Ag and Pd/Ag nanoparticles by microwave-polyol method,” *J. Chem. Sci.*, vol. 117, no. 4, pp. 311–316, Jul. 2005.

[13] F. Bonet, S. Grugeon, L. Dupont, R. Herrera Urbina, C. Guéry, and J. M. Tarascon, “Synthesis and characterization of bimetallic Ni–Cu particles,” *J. Solid State Chem.*, vol. 172, no. 1, pp. 111–115, Apr. 2003.

[14] S. Mudah and N. Nanozarah, “Synthesis of Nickel Nanoparticles Via Non-Aqueous Polyol Method : Effect of Reaction Time,” *Sains Malaysiana*, vol. 41, no. 8, pp. 1037–1042, 2012.

[15] K. Nagaveni, A. Gayen, G. N. Subbanna, and M. S. Hegde, “Pd-coated Ni nanoparticles by the polyol method: an efficient hydrogenation catalyst,” *J. Mater. Chem.*, vol. 12, no. 10, pp. 3147–3151, Sep. 2002.

[16] K. J. Carroll, J. U. Reveles, M. D. Shultz, S. N. Khanna, and E. E. Carpenter, “Preparation of Elemental Cu and Ni Nanoparticles by the Polyol Method: An Experimental and Theoretical Approach,” *J. Phys. Chem. C*, vol. 115, no. 6, pp. 2656–2664, Feb. 2011.

[17] T. Sakurai, T. Hasizume, A. Jimbo, A. Sakai, and S. Hyodo, “New Results in Surface Segregation of Ni-Cu Binary Alloys,” *Phys. Rev. Lett.*, vol. 55, no. 5, pp. 514–517, 1985.

[18] P. van der Plank and W. M. H. Sachtler, “Surface Composition of Equilibrated Copper-Nickel Alloy Films,” *J. Catal.*, vol. 7, no. 3, pp. 300–303, 1967.

[19] K. Watanabe, M. Hashiba, and T. Yamashina, “A Quantitative Analysis of Surface Segragation and In-Depth Profile of Copper-Nickel Alloys,” *Surf. Sci.*, vol. 61, pp. 483–490, 1976.

[20] Y. Sun and Y. Xia, “Shape-controlled synthesis of gold and silver nanoparticles.,” *Am. Assoc. Adv. Sci.*, vol. 298, pp. 2176–9, Dec. 2002.

[21] Y. Li, E. Boone, and M. A. El-sayed, “Size Effects of PVP - Pd Nanoparticles on the Catalytic Suzuki Reactions in Aqueous Solution,” *Langmuir*, vol. 18, pp. 4921–4925, 2002.

[22] B. T. Meshesha, N. Barrabés, F. Medina, and J. E. Sueiras, “Polyol mediated synthesis & characterization of Cu nanoparticles : Effect of 1-hexadecylamine as stabilizing agent,” in *Nanotechnology*, 2009, pp. 87–91.

[23] R. J. Isaifan, H. A. E. Dole, E. Obeid, L. Lizarraga, E. A. Baranova, and P. Vernoux, “Catalytic CO Oxidation over Pt nanoparticles prepared from the Polyol Reduction Method supported on Yttria-Stabilized Zirconia .,” *Electrochem. Soc.*, vol. 35, no. 28, pp. 43–57, 2011.

[24] H. A. E. Dole, R. J. Isaifan, F. M. Sapountzi, L. Lizarraga, D. Aubert, A. Princivalle, P. Vernoux, and E. A. Baranova, “Low Temperature Toluene Oxidation Over Pt Nanoparticles Supported on Yttria Stabilized-Zirconia,” *Catal. Letters*, vol. 143, no. 10, pp. 996–1002, Jul. 2013.

[25] X. Yan and K. Yong, “Size control of polymer-stabilized ruthenium nanoparticles by polyol reduction,” *J. Mater. Chem.*, vol. 11, pp. 3387–3391, 2001.

[26] C. Bock, C. Paquet, M. Couillard, G. A. Botton, and B. R. MacDougall, “Size-selected synthesis of PtRu nano-catalysts: reaction and size control mechanism.,” *J. Am. Chem. Soc.*, vol. 126, pp. 8028–37, Jun. 2004.

[27] R. J. Isaifan, S. Ntais, and E. A. Baranova, “Particle size effect on catalytic activity of carbon-supported Pt nanoparticles for complete ethylene oxidation,” *Appl. Catal. A Gen.*, vol. 464–465, pp. 87–94, Aug. 2013.

[28] K. Chou and K. Huang, “Studies on the chemical synthesis of nanosized nickel powder and its stability,” *J. Nanoparticle Res.*, vol. 3, pp. 127–132, 2001.

[29] C. Liu, X. Wu, T. Klemmer, N. Shukla, X. Yang, D. Weller, A. G. Roy, M. Tanase, and D. Laughlin, “Polyol Process Synthesis of Monodispersed FePt Nanoparticles.,” *J. Phys. Chem. B*, vol. 108, no. 20, pp. 6121–3, May 2004.

[30] A. V. Zeigarnik, C. Callaghan, R. Datta, I. Fishtik, and E. Shustorovich, "Prediction of Comparative Catalytic Activity in the Series of Single Crystalline Surfaces in a Water-Gas Shift Reaction," *Kinet. Catal.*, vol. 46, no. 4, pp. 509–515, Jul. 2005.

[31] W. Wang, S. Wang, X. Ma, and J. Gong, "Recent advances in catalytic hydrogenation of carbon dioxide.," *Chem. Soc. Rev.*, vol. 40, no. 7, pp. 3703–27, Jul. 2011.

[32] S. S. Kim, H. H. Lee, and S. C. Hong, "A study on the effect of support's reducibility on the reverse water-gas shift reaction over Pt catalysts," *Appl. Catal. A Gen.*, vol. 423–424, pp. 100–107, May 2012.

[33] S. S. Kim, K. H. Park, and S. C. Hong, "A study of the selectivity of the reverse water–gas-shift reaction over Pt/TiO2 catalysts," *Fuel Process. Technol.*, vol. 108, pp. 47–54, Apr. 2013.

[34] G. Pekridis, K. Kalimeri, N. Kaklidis, E. Vakouftsi, E. F. Iliopoulou, C. Athanasiou, and G. E. Marnellos, "Study of the reverse water gas shift (RWGS) reaction over Pt in a solid oxide fuel cell (SOFC) operating under open and closed-circuit conditions," *Catal. Today*, vol. 127, no. 1–4, pp. 337–346, Sep. 2007.

[35] C. Ratnasamy and J. P. Wagner, "Water Gas Shift Catalysis," *Catal. Rev.*, vol. 51, no. 3, pp. 325–440, Sep. 2009.

[36] D. Theleritis, S. Souentie, A. Siokou, A. Katsaounis, and C. G. Vayenas, "Hydrogenation of CO2 over Ru/YSZ Electropromoted Catalysts," *ACS Catal.*, vol. 2, no. 5, pp. 770–780, May 2012.

[37] J. Tsai and K. M. Nicholas, "Rhodium-Catalyzed Hydrogenation of Carbon Dioxide to Formic Acid," *J. Am. Chem. Soc.*, vol. 114, pp. 5117–5124, 1992.

[38] R. A. Dagle, A. Platon, D. R. Palo, A. K. Datye, J. M. Vohs, and Y. Wang, "PdZnAl catalysts for the reactions of water-gas-shift, methanol steam reforming, and reverse-water-gas-shift," *Appl. Catal. A Gen.*, vol. 342, no. 1–2, pp. 63–68, Jun. 2008.

[39] J. Wambach, A. Baiker, and A. Wokaun, "CO2 hydrogenation over metal/zirconia catalysts," *Phys. Chem. Chem. Phys.*, vol. 1, no. 22, pp. 5071–5080, 1999.

[40] A. Baikera, M. Kilob, M. M. S. Menzia, and A. Wokaunb, "Hydrogenation of CO2 Over Copper, Silver and Gold/Zirconia Catalysts: Comparative Study of Catalys Properties and Reaction Pathways," in *10th International Congress on Catalysis*, 1992, pp. 1257–1272.

[41] R. J. Isaifan, H. A. E. Dole, E. Obeid, L. Lizarraga, P. Vernoux, and E. A. Baranova, "Metal-Support Interaction of Pt Nanoparticles with Ionically and Non-Ionically Conductive Supports for CO Oxidation," *Electrochem. Solid-State Lett.*, vol. 15, no. 3, p. E14, 2012.

[42] E. Xue, M. O'Keeffe, and J. R. H. Ross, "Water-gas shift conversion using a feed with a low steam to carbon monoxide ratio and containing sulphur," *Catal. Today*, vol. 30, no. 1–3, pp. 107–118, Jun. 1996.

[43] A. Basinska, T. P. Maniecki, and W. K. Jozwiak, "Catalytic Activity in Water-Gas Shift Reaction of Platinum Group Metals Supported on Iron Oxides," *React. Kinet. Catal. Lett.*, vol. 89, no. 2, pp. 319–324, 2006.

[44] A. Luengnaruemitchai, S. Osuwan, and E. Gulari, "Comparative studies of low-temperature water–gas shift reaction over Pt/CeO2, Au/CeO2, and Au/Fe2O3 catalysts," *Catal. Commun.*, vol. 4, no. 5, pp. 215–221, May 2003.

[45] C. M. Kalamaras, P. Panagiotopoulou, D. I. Kondarides, and A. M. Efstathiou, "Kinetic and mechanistic studies of the water–gas shift reaction on Pt/TiO2 catalyst," *J. Catal.*, vol. 264, no. 2, pp. 117–129, Jun. 2009.

[46] S. S. Kim, H. H. Lee, and S. C. Hong, "A study on the effect of support's reducibility on the reverse water-gas shift reaction over Pt catalysts," *Appl. Catal. A Gen.*, vol. 423–424, pp. 100–107, May 2012.

[47] B. Tidona, A. Urakawa, and P. Rudolf von Rohr, "High pressure plant for heterogeneous catalytic CO2 hydrogenation reactions in a continuous flow microreactor," *Chem. Eng. Process. Process Intensif.*, vol. 65, pp. 53–57, Mar. 2013.

[48] R. W. Dorner, D. R. Hardy, F. W. Williams, B. H. Davis, and H. D. Willauer, "Influence of Gas Feed Composition and Pressure on the Catalytic Conversion of CO2 to Hydrocarbons Using a Traditional Cobalt-Based Fischer-Tropsch Catalyst," *Energy & Fuels*, vol. 23, no. August 2008, pp. 4190–4195, 2009.

[49] A. Goguet, F. C. Meunier, D. Tibiletti, J. P. Breen, and R. Burch, "Spectrokinetic Investigation of Reverse Water-Gas-Shift Reaction Intermediates over a Pt/CeO2 Catalyst," *Phys. Chem.*, vol. 108, pp. 20240–20246, 2004.

[50] A. Goguet, F. Meunier, J. Breen, R. Burch, M. Petch, and A. Faurghenciu, "Study of the origin of the deactivation of a Pt/CeO catalyst during reverse water gas shift (RWGS) reaction," *J. Catal.*, vol. 226, no. 2, pp. 382–392, Sep. 2004.

[51] D. Tibiletti, A. Goguet, F. C. Meunier, J. P. Breen, and R. Burch, "On the importance of steady-state isotopic techniques for the investigation of the mechanism of the reverse water-gas-shift reaction.," *Chem. Commun. (Camb).*, no. 14, pp. 1636–7, Jul. 2004.

[52] D.-W. Jeong, W.-J. Jang, J.-O. Shim, W.-B. Han, H.-S. Roh, U. H. Jung, and W. L. Yoon, "Low-temperature water–gas shift reaction over supported Cu catalysts," *Renew. Energy*, vol. 65, pp. 102–107, May 2014.

[53] C. Chen, C. Ruan, Y. Zhan, X. Lin, Q. Zheng, and K. Wei, "The significant role of oxygen vacancy in Cu/ZrO2 catalyst for enhancing water–gas-shift performance," *Int. J. Hydrogen Energy*, vol. 39, no. 1, pp. 317–324, Jan. 2014.

[54] Y. Zhang, C. Chen, X. Lin, D. Li, X. Chen, Y. Zhan, and Q. Zheng, "CuO/ZrO2 catalysts for water–gas shift reaction: Nature of catalytically active copper species," *Int. J. Hydrogen Energy*, vol. 39, no. 8, pp. 3746–3754, Mar. 2014.

[55] G. Centi and S. Perathoner, "Opportunities and prospects in the chemical recycling of carbon dioxide to fuels," *Catal. Today*, vol. 148, no. 3–4, pp. 191–205, Nov. 2009.

[56] M. J. . Ginés, A. J. Marchi, and C. R. Apestegufa, "Kinetic study of the reverse water-gas shift reaction," *Appl. Catal. A Gen.*, vol. 154, no. 96, pp. 155–171, 1997.

[57] S.-I. Fujita, M. Usui, and N. Takezawa, "Mechanism of the reverse water gas shift reaction over Cu/ZnO catalyst*1," *J. Catal.*, vol. 134, no. 1, pp. 220–225, Mar. 1992.

[58] C. T. Campbell and K. Ernst, *Forward and Reverse Water — Gas Shift Reactions on Model Copper Catalysts Kinetics and Elementary Steps*. 1992, pp. 131–142.

[59] K.-H. Ernst, C. T. Campbell, and G. Moretti, "Kinetics of the Reverse Water-Gas Shift Reaction over Cu (110)," *J. Catal.*, vol. 134, pp. 66–74, 1992.

[60] C. Chen, W. Cheng, and S. Lin, "Mechanism of CO formation in reverse water – gas shift reaction over Cu/Al2O3 catalyst," *Catal. Letters*, vol. 68, pp. 45–48, 2000.

[61] C. Chen and W. Cheng, "Study on the mechanism of CO formation in reverse water gas shift reaction over Cu/SiO2 catalyst by pulse reaction , TPD and TPR," *Catal. Letters*, vol. 83, no. November, pp. 121–126, 2002.

[62] C. Chen, W. Cheng, and S. Lin, "Study of reverse water gas shift reaction by TPD , TPR and CO2 hydrogenation over potassium-promoted Cu/SiO2 catalyst," *Appl. Catal. A Gen.*, vol. 238, pp. 55–67, 2003.

[63] Y. Liu and D. Liu, "Study of bimetallic Cu-Ni/ gamma Al2O3 catalysts for carbon dioxide hydrogenation," *J. Hydrog. Energy*, vol. 24, pp. 351–354, 1999.

[64] X. Qi and M. Flytzani-stephanopoulos, "Activity and Stability of Cu-CeO2 Catalysts in High-Temperature Water - Gas Shift for Fuel-Cell Applications," *Ind. Eng. Chem. Res.*, vol. 43, pp. 3055–3062, 2004.

[65] C. Chen, W.-H. Cheng, and S.-S. Lin, "Study of iron-promoted Cu/SiO2 catalyst on high temperature reverse water gas shift reaction," *Appl. Catal. A Gen.*, vol. 257, no. 1, pp. 97–106, Jan. 2004.

[66] M. V. Twigg and M. S. Spencer, “Deactivation of supported copper metal catalysts for hydrogenation reactions,” *Appl. Catal. A Gen.*, vol. 212, no. 1–2, pp. 161–174, Apr. 2001.

[67] C. S. Chen, J. H. Lin, J. H. You, and C. R. Chen, “Properties of Cu as a precursor to prepare Cu/SiO2 catalyst using the atomic layer epitaxy technique.,” *J. Am. Chem. Soc.*, vol. 128, no. 50, pp. 15950–1, Dec. 2006.

[68] M. A. Edwards, D. M. Whittle, C. Rhodes, A. M. Ward, D. Rohan, M. D. Shannon, G. J. Hutchings, and C. J. Kiely, “Microstructural studies of the copper promoted iron oxide/chromia water-gas shift catalyst,” *Phys. Chem. Chem. Phys.*, vol. 4, no. 15, pp. 3902–3908, Jul. 2002.

[69] R. Hughes, “Deactivation of Catalysts,” in *Academic Press*, 1994.

[70] S. Natesakhawat, X. Wang, L. Zhang, and U. S. Ozkan, “Development of chromium-free iron-based catalysts for high-temperature water-gas shift reaction,” *J. Mol. Catal. A Chem.*, vol. 260, no. 1–2, pp. 82–94, Dec. 2006.

[71] I. L. Júnior, J.-M. M. Millet, M. Aouine, and M. do Carmo Rangel, “The role of vanadium on the properties of iron based catalysts for the water gas shift reaction,” *Appl. Catal. A Gen.*, vol. 283, no. 1–2, pp. 91–98, Apr. 2005.

[72] A. F. Ghenciu, “Review of fuel processing catalysts for hydrogen production in PEM fuel cell systems,” *Solid State Mater. Sci.*, vol. 6, pp. 389–399, 2002.

[73] C.-S. Chen, W.-H. Cheng, and S.-S. Lin, “Enhanced activity and stability of a Cu/SiO2 catalyst for the reverse water gas shift reaction by an iron promoter,” *Chem. Commun.*, no. 18, pp. 1770–1771, 2001.

[74] F. S. Stone and D. Waller, “Cu-ZnO and Cu–ZnO/Al2O3 catalysts for the reverse water-gas shift reaction . The effect of the Cu/Zn ratio on precursor characteristics and on the activity of the derived catalysts,” *Top. Catal.*, vol. 22, no. April, pp. 305–318, 2003.

[75] N. Takezawa, T. Hiroyuki, M. Shimokawabe, and H. Kobayashi, “Methanation of Carbon Dioxide: Preperation of Ni/MgO Catalysts and Their Performance,” *Appl. Catal. A Gen.*, vol. 23, pp. 291–298, 1986.

[76] K. B. Kester, E. Zagli, and J. L. Falconer, “Methanation of Carbon Monoxide and Carbon Dioxide on Ni/Al2O3 Catalysts: Effect of Nickel Loading,” *Appl. Catal.*, vol. 22, pp. 311–319, 1986.

[77] C. Schild, A. Wokaun, R. A. Koeppel, and A. Baiker, “CO2 Hydrogenation over Nickel / Zirconia Catalysts from Amorphous Precursors : On the Mechanism of Methane Formation,” *J. Phys. Chem.*, vol. 95, pp. 6341–6346, 1991.

[78] A. E. Arksoylu and Z. I. Onsan, “Hydrogenation of carbon oxides using coprecipitated and impregnated Ni/Al203 catalysts,” *Appl. Catal. A Gen.*, vol. 164, pp. 1–11, 1997.

[79] J. Barrault and A. Chafik, “Conversion of carbon oxide(s) on carbon-supported nickel-rare earth catalysts,” *Appl. Catal.*, vol. 67, pp. 257–268, 1991.

[80] G. D. Weatherbee and C. H. Bartholomew, “Hydrogenation of CO2 on Group VIII Metals,” *J. Catal.*, vol. 77, pp. 460–472, 1982.

[81] G. Peng, S. J. Sibener, G. C. Schatz, S. T. Ceyer, and M. Mavrikakis, “CO2 Hydrogenation to Formic Acid on Ni (111),” *J. Phys. Chem. C*, vol. 116, pp. 3001–3006, 2012.

[82] J. M. Bermúdez, B. Fidalgo, a. Arenillas, and J. a. Menéndez, “CO2 reforming of coke oven gas over a Ni/γAl2O3 catalyst to produce syngas for methanol synthesis,” *Fuel*, vol. 94, pp. 197–203, Apr. 2012.

[83] A. Guerrero-ruiz and I. Rodriguez-Ramos, “Hydrogenation of CO2 on Carbon-Supported Nickel and Cobalt,” *React. Kinet. Catal. Lett.*, vol. 29, no. 1, pp. 93–99, 1985.

[84] L. Wang, H. Liu, Y. Liu, Y. Chen, and S. Yang, “Influence of preparation method on performance of Ni-CeO2 catalysts for reverse water-gas shift reaction,” *J. Rare Earths*, vol. 31, no. 6, pp. 559–564, Jun. 2013.

[85] L. Wang, S. Zhang, and Y. Liu, “Reverse water gas shift reaction over Co-precipitated Ni-CeO2 catalysts,” *J. Rare Earths*, vol. 26, pp. 66–70, 2008.

[86] E. Vesselli, M. Rizzi, L. De Rogatis, X. Ding, A. Baraldi, G. Comelli, L. Savio, L. Vattuone, M. Rocca, P. Fornasiero, A. Baldereschi, and M. Peressi, “Hydrogen-Assisted Transformation of CO2 on Nickel: The Role of Formate and Carbon Monoxide,” *J. Phys. Chem. Lett.*, vol. 1, no. 1, pp. 402–406, Jan. 2010.

[87] E. Vesselli, J. Schweicher, A. Bundhoo, A. Frennet, and N. Kruse, “Catalytic CO2 Hydrogenation on Nickel : Novel Insight by Chemical Transient Kinetics,” *J. Phys. Chem. CJournal Phys. Chem. C*, vol. 115, pp. 1255–1260, 2011.

[88] T. K. Campbell and J. L. Falconer, “Carbon dioxide hydrogenation on potassium-promoted nickel catalysts,” *Appl. Catal.*, vol. 50, no. 1, pp. 189–197, May 1989.

[89] C. S. Chen, J. H. Lin, J. H. You, and K. H. Yang, “Effects of potassium on Ni-K/Al2O3 catalysts in the synthesis of carbon nanofibers by catalytic hydrogenation of CO2.,” *J. Phys. Chem. A*, vol. 114, no. 11, pp. 3773–81, Mar. 2010.

[90] R. D. Green, “Carbon Dioxide Reduction on Gadolina Doped Ceria Cathodes,” Case Wester Reserve University, 2009.

[91] F. B. Noronha, E. C. Fendley, R. R. Soares, W. E. Alvarez, and D. E. Resasco, "Correlation between catalytic activity and support reducibility in the CO2 reforming of methane over Pt/CexZr(1−x)O2 catalysts," *Chem. Eng. J.*, vol. 82, pp. 21–31, 2001.

[92] P. Panagiotopoulou and D. I. Kondarides, "Effect of the nature of the support on the catalytic performance of noble metal catalysts for the water–gas shift reaction," *Catal. Today*, vol. 112, no. 1–4, pp. 49–52, Mar. 2006.

[93] P. Vernoux, L. Lizarraga, M. N. Tsampas, F. M. Sapountzi, A. De Lucas-consuegra, J. Valverde, S. Souentie, C. G. Vayenas, D. Tsiplakides, S. Balomenou, and E. A. Baranova, "Ionically Conducting Ceramics as Active Catalyst Supports," *Chem. Rev.*, 2013.

[94] P. Gellings and H. J. . Bouwmeester, "Ion and mixed conducting oxides as catalysts," *Catal. Today*, vol. 12, pp. 1–105, 1992.

[95] H. Yahiro, Y. Eguchi, K. Eguchi, and H. Arai, "Oxygen ion conductivity of the ceria-samarium oxide system with fluorite structure," *J. Appl. Electrochem.*, vol. 18, no. 4, pp. 527–531, Jul. 1988.

[96] M. Machida, K. Eguchi, and H. Arai, "Effect of additives on the surface area of oxide supports for catalytic combustion," *J. Catal.*, vol. 103, pp. 385–393, Feb. 1987.

[97] W. Dow and T. Huang, "Effects of oxygen vacancy of yttria-stabilized zirconia support on carbon monoxide oxidation over copper catalyst," *J. Catal.*, 1994.

[98] M. G. Sanchez and J. L. Gazquez, "Oxygen Vacancy Model in Strong Metal-Support Interaction," *J. Catal.*, vol. 104, pp. 120–135, 1987.

[99] P. Panagiotopoulou and D. I. Kondarides, "Effect of morphological characteristics of TiO2-supported noble metal catalysts on their activity for the water?gas shift reaction," *J. Catal.*, vol. 225, no. 2, pp. 327–336, Jul. 2004.

[100] M. Stoukides and G. Vayenas, "The Effect of Electrochemical Oxygen Pumping on the Rate and Selectivity of Ethylene Oxidation on Polycrystalline Silver," *J. Catal.*, vol. 70, pp. 137–146, 1981.

[101] P. Vernoux, M. Guth, and X. Li, "Ionically Conducting Ceramics as Alternative Catalyst Supports," *Electrochem. Solid-State Lett.*, vol. 12, no. 7, p. E9, 2009.

[102] Y. A. Daza, R. A. Kent, M. M. Yung, and J. N. Kuhn, "Carbon Dioxide Conversion by Reverse Water–Gas Shift Chemical Looping on Perovskite-Type Oxides," *Ind. Eng. Chem. Res.*, vol. 53, no. 14, pp. 5828–5837, Apr. 2014.

[103] S. Yin and Q. Ge, "Selective CO2 hydrogenation on the γ-Al2O3 supported bimetallic Co–Cu catalyst," *Catal. Today*, vol. 194, no. 1, pp. 30–37, Oct. 2012.

[104] C. Zhang, C.-J. Li, G. Zhang, X.-J. Ning, C.-X. Li, H. Liao, and C. Coddet, "Ionic conductivity and its temperature dependence of atmospheric plasma-sprayed yttria stabilized zirconia electrolyte," *Mater. Sci. Eng. B*, vol. 137, no. 1–3, pp. 24–30, Feb. 2007.

[105] X. . Chen, K. . Khor, S. . Chan, and L. . Yu, "Overcoming the effect of contaminant in solid oxide fuel cell (SOFC) electrolyte: spark plasma sintering (SPS) of 0.5wt.% silica-doped yttria-stabilized zirconia (YSZ)," *Mater. Sci. Eng. A*, vol. 374, no. 1–2, pp. 64–71, Jun. 2004.

[106] C.-J. Li, X.-J. Ning, and C.-X. Li, "Effect of densification processes on the properties of plasma-sprayed YSZ electrolyte coatings for solid oxide fuel cells," *Surf. Coatings Technol.*, vol. 190, no. 1, pp. 60–64, Jan. 2005.

[107] M. Ismail, "Model Development and Validation of Samaria Doped Ceria (SDC) Based Solid Oxide Fuel Cell Operating with Practical Fuels," Univiersity of Waterloo, 2013.

[108] K. Eguchi, T. Setoguchi, T. Inoue, and H. Arai, "Electrical Properties of Ceria-Based Oxide and their Application to Solid Oxide Fuel Cells," *Solid State Ionics*, vol. 52, pp. 165–172, 1992.

[109] Z. Zhan, T. Wen, H. Tu, and Z. Lu, "AC Impedance Investigation of Samarium-Doped Ceria," *J. Electrochem. Soc.*, vol. 148, no. 5, pp. 427–432, 2001.

Chapter 3 – Synthesis of CuNi/C and CuNi/γ-Al2O3 Catalysts for the Reverse Water Gas Shift Reaction

Abstract

A new polyol synthesis method is described in which CuNi nanoparticles of different Cu/Ni atomic ratios were supported on both carbon and on gamma alumina and compared with Pt catalysts using the reverse water gas shift, RWGS, reaction. All catalysts were highly selective for CO formation. The concentration of CH_4 was less than the detection limit. Cu was the most abundant metal on the CuNi alloy surfaces, as determined by X-ray photo electron spectroscopy, XPS, measurements. Only one CuNi alloy catalyst, $Cu_{50}Ni_{50}$/C, appeared to be as thermally stable as the Pt/C catalysts. After three temperature cycles, from 400–700°C, the CO yield at 700°C obtained using the $Cu_{50}Ni_{50}$/C catalyst was comparable to that obtained using a Pt/C catalyst.

3.1 Introduction

The carbon dioxide hydrogenation reaction has been proposed for use with carbon capture technologies for the production of industrially viable chemicals, such as long chain hydrocarbons, methanol, formic acid and carbon monoxide [1], [2]. When co-feeding CO_2 and H_2 over a hydrogenation catalyst, there are two main hydrogenation processes that can take place, the reverse water gas shift reaction

$$CO_2 + H_2 = CO + H_2O \tag{3.1}$$

and the subsequent hydrogenation of CO to either hydrocarbons or alcohols, depending on the values of x, y, and z in Equation 3. 2.

$$x\ CO + (x\text{-}z+y/2)\ H_2 = C_XH_YO_Z + (x\text{-}z)\ H_2O \tag{3.2}$$

One of the reactions in Equation 3.2, the hydrogenation of CO to methane, is of particular interest in this study.

$$CO + 2\ H_2 = CH_4 + H_2O \tag{3.3}$$

When CO is selectively formed via Equation 3.1 and mixed with H_2, the resulting syngas can be a feed-stock for the Fischer Tropsch process [2] that produces liquid fuels. In contrast CH_4 formed via Equation 3.3 is an undesirable by-product that is not convertible to liquid fuels in a Fischer Tropsch process.

Wang et al. [1] have recently reviewed catalysts for the RWGS reaction. They reported that noble metals have been studied and shown to be among the best catalysts for the RWGS reaction because they generally promote H_2 dissociation. Among noble metals used for the RWGS reaction, platinum (Pt) has received considerable attention. It was found to produce high CO yields [3]–[5]. In addition, Pekridis et al. [6] tested the electro-kinetics of the RWGS reaction in solid oxide fuel cells containing a Pt/YSZ catalyst. The Pt/YSZ catalyst was found to be stable

at high temperatures and the cell achieved a maximum power density of 9 mW/cm^2 [6]. In spite of the recognized performance of noble metals as catalysts for the RWGS reaction, their main drawback is their high cost that limits their commercial application.

Transition metals such as copper (Cu), nickel (Ni), and iron (Fe) are promising alternatives to noble metal catalysts for the RWGS reaction. Both copper and nickel based catalysts have shown good conversion for the WGS reaction as well as the RWGS reaction [7]–[12]. Chen et al. [7] investigated Cu nanoparticles ranging in size from 2.4 – 3.4 nm and found that the catalyst becomes unstable at higher temperatures [13]. These researchers [14] also added Fe to Cu in an attempt to stabilize the catalyst. Although Fe alone had poor conversions, Fe stabilized the Cu catalyst for 120 h and caused an increase in conversion of approximately 7% at 600°C. On the other hand, the Cu catalyst without the iron stabilizer deactivated rapidly and reached zero conversion after 120 hours.

Similar research was performed by Chen et al [15] using Ni catalysts. Ni alone showed high selectivity towards methane. When they added potassium to a Ni/ γ-Al_2O_3 catalyst they reported higher selectivity towards CO even though they did not notice an increase in CO_2 conversion. However with the potassium promoter they noticed the formation of coke.

Liu and Liu [16] studied a Ni-Cu catalyst that was prepared by immersing gamma-alumina (γ-Al_2O_3) in an aqua ammonia solution of nickel nitrate and copper nitrate. Their catalysts were not selective in that they reported large yields of both CH_4 and CO. They interpreted their results as CO_2 being adsorbed on Cu and H_2 being adsorbed on Ni.

The polyol synthesis method has been used extensively in the past for the synthesis of metal particles from a metal salt precursor [$Cu(NO_3)_2$ or $Ni(NO_3)_2$ represented here as

$Me(NO_3)_2$]. Bonet et al. [17], [18] indicated that the overall reactions at 180°C included the following reactions to form acetic acid, glycolaldehyde, and glycolic acid:

$$(CH_2OH)–(CH_2OH) + Me(NO_3)_2 \rightarrow CH_3COOH + 2\,HNO_3 + Me^0 \quad (3.4)$$

$$(CH_2OH)–(CH_2OH) + Me(NO_3)_2 \rightarrow (CH_2OH)–(CHO) + 2\,HNO_3 + Me^0 \quad (3.5)$$

$$(CH_2OH)–(CH_2OH) + H_2O + 2\,Me(NO_3)_2 \rightarrow (CH_2OH)–(COOH) + 4\,HNO_3 + 2\,Me^0 \quad (3.6)$$

Bock et al. [19] found that oxalic acid, HOOC–COOH, is also formed and suggested that the majority of the metal is formed by the oxidation of ethylene glycol to glycolic acid. At the boiling point of ethylene glycol, 196°C, Bonet et al. [17] indicated that the overall reactions included the formation of diacetyl:

$$2\,(CH_2OH)–(CH_2OH) + Me(NO_3)_2 \rightarrow (CH_3CO)–(CH_3CO) + 2\,H_2O + 2\,HNO_3 + Me^0 \quad (3.7)$$

where Me^0 represents either copper or nickel in the metallic state. Bonet et al. [17] also commented on the reaction mechanism and indicated that intermediate solid phases (metal glycolates) precipitate before the metal powder is formed. Bock et al. [18] indicated that oxidation products containing carboxylic acids act as stabilizers for metal colloid particles. Specifically they indicated that glycolate anions, the deprotonated form of glycolic acid, are good stabilizers for colloidal metal particles and that their concentration increases when the pH is greater than 6. In their work, they increased the pH by the addition of NaOH and reported that PtRu bimetallic nanoparticle sizes decreased when the pH was increased. Their explanation of glycolate anions on the exterior of the metal particles preventing metal colloid agglomeration seems to be consistent with their nanoparticle size results. The polyol synthesis method has become known for its simplicity and accurate control of particle size [17], [18]. The addition of

NaOH during the polyol synthesis has been used to synthesize Pt nanoparticles of narrow size distribution [20]–[23].

Other researchers [16], [18], [24] have also used the polyol synthesis method to obtain bi-metallic particles. When alloying two metals together, the resulting reaction properties can often be enhanced compared to the pure metal. In the past both Cu and Ni have been alloyed with other metals to form alloys. For instance, Viau et al. [24] prepared Co-Ni and Fe-Ni particles using the polyol synthesis method.

Bonet et al. [18] used a polyol synthesis method to obtain Cu-Ni particles. When nickel carbonate and copper carbonate were used at 140°C they obtained a Cu-Ni powder composed of both a Ni rich Cu-Ni solid solution and a Cu rich Cu-Ni solid solution. When the carbonates were used at 196°C they obtained a Cu-Ni powder composed of a Cu rich Cu-Ni solid solution and a solid Ni metal phase. They noted that the reduction temperature for Cu is less than for Ni. Their particles had a particle size of 140 nm. They did not report any reaction results.

In this work base metal Cu-Ni nano-particle catalysts were prepared by a new synthesis technique. Cu was chosen because it is selective for the formation of CO [16], although it is unstable (sinters) at the higher temperatures where the equilibrium for the RWGS reaction is more favourable. Ni was chosen because it also produces CO [15] although it also can form unwanted by-products, CH_4 and coke. One of the purposes of the investigations was to determine if sintering of pure Cu could be prevented by the addition of Ni in the same way that it was prevented by the addition of Fe [14]. The resulting CuNi catalysts are compared to results obtained with Pt nano-particle catalysts that were synthesized and tested using a variety of reactions: ethylene oxidation [21], CO oxidation [20] and toluene oxidation [23]. These Pt catalysts are considered to be among the best catalysts for the RWGS reaction because they

achieve reaction equilibrium at some conditions. We report Cu-Ni catalyst compositions that promote CO formation and inhibit CH_4 formation at specific reaction conditions.

3.2 Experimental

3.2.1 Catalyst preparation

The synthesis of CuNi nanoparticles was achieved using a modified polyol technique. First, 314.5 mg of nickel nitrate ($Ni(NO_3)_2$) (hexahydrate 99.999% metal basis, Alfa Aesar) was dissolved in 30 mL of ethylene glycol (anhydrous 99.8%, SigmaAldrich) to obtain a green solution. That solution's pH was then increased to 11 via the addition of 199 mg of sodium hydroxide (NaOH) pellets (EM Science, ACS grade) to obtain Solution 1. This caused the solution to slightly darken. In a separate beaker, 321.8 mg of copper nitrate ($Cu(NO_3)_2$) (hexahydrate 99.999% metal basis, Alfa Aesar) was dissolved in 30 mL of ethylene glycol to obtain a blue solution. Its pH was also increased to 11 using 199 mg of NaOH pellets to obtain Solution 2. Solution 2 also darkened. Following this, Solution 1 was poured into a round bottom flask, refluxed and stirred at 196˚C. Once the temperature reached 196 ˚C, Solution 2, at room temperature, was poured into the hot round bottom flask. The combined solution was refluxed at 196 ˚C for 30 minutes and then cooled. The combined solution gradually became dark brown in colour. Once cooled, the colloidal particles were stored in the ethylene glycol solution. The final pH of the combined solution was 7.

The colloidal particles were then deposited on supports, C and γ-Al_2O_3, using a wet impregnation technique. A powdered support was placed into a beaker and subsequently an amount of the combined solution was poured into the powder. The amount of combined solution was chosen to result in 10 wt% CuNi and 90 wt% support. The solution/support was sonicated for 1 hour and stirred for 24 hours. The supported metal was then centrifuged at 6000 rpm and

washed with 20 mL of deionized water 10 times to remove the salts remaining after the synthesis procedure. The supports used were carbon black (Vulcan XC-72R, Cabot Corp. specific surface area of 254 m^2/g) and gamma-alumina (Alfa-Aesar, specific surface area 120 m^2/g). The catalyst was then dried using a freeze dryer for 24 h. Prior to any experiments, the catalyst was crushed to a fine powder using a mortar and pestle.

CuNi particles of three different compositions were prepared. The combined solution for each composition was prepared with a different ratio of Solution 1 to Solution 2. The ratio was selected to obtain CuNi colloidal particles of 80 wt % Cu / 20 wt % Ni (nominally $Cu_{80}Ni_{20}$), 50 wt % Cu / 50 wt % Ni (nominally $Cu_{50}Ni_{50}$), and 20 wt % Cu / 80 wt % Ni (nominally $Cu_{20}Ni_{80}$).

Pt nanoparticles were synthesized using a modified polyol method as described elsewhere [20]. It involved diluting $PtCl_4$ in a 0.06M NaOH solution of ethylene glycol. The mixture was then refluxed at 160°C for 3 hours. Once synthesized, the nanoparticles were deposited on carbon black and gamma-alumina using the deposition technique described above. 1 wt% of Pt was deposited on the support.

3.2.2 Physical Characterization

Transmission electron microscopy (TEM) of supported Pt nanoparticles was performed using a JEOL JEM 2100F FETEM operating at 200 kV. Image J software was used to determine the particle size distribution. Details of the Pt nanoparticle characterization have been described elsewhere [20].

Scanning electron microscopy (SEM) of CuNi particles supported on carbon was performed using a JEOL model JSM-7500F Field emission scanning electron microscope, FESEM, in both lower-secondary electron image, LEI, and compositional, COMPO, modes set at a distance of 8 mm with an acceleration voltage of 5 kV. An energy-dispersive X-ray

spectroscope (EDS) attached to the SEM machine was used to quantify the amount of Cu and Ni found in the bulk CuNi particles.

X-ray diffraction (XRD) measurements were made on the CuNi colloidal particles using a RigakuUltima IV difractometer which used a Cu Kα X-ray (40 ma, 44 kV) operating with focused beam geometry and a divergence slit of 2/3 degree, a scan speed of 0.17 deg min^{-1} and a scan step of 0.06 degrees were used while operating between 35° and 55°. The crystal sizes determined by XRD are shown in Table 3.1.

Table 3.1: Carbon Catalyst physical characteristics

Catalyst	Metal loading (wt%)	XRD Crystalline size (nm)	Typical particle size (nm)
Pt / C	1	3.8	2.8
Pt / γ-Al_2O_3			N/A
$Cu_{80}Ni_{20}$ / C	10	30.2	64.4
$Cu_{80}Ni_{20}$ / γ-Al_2O_3			N/A
$Cu_{50}Ni_{50}$ / C	10	24	53.4
$Cu_{50}Ni_{50}$ / γ-Al_2O_3			N/A
$Cu_{20}Ni_{80}$ / C	10	16.7	41.1
$Cu_{20}Ni_{80}$ / γ-Al_2O_3			N/A

X-ray photoelectron spectroscopy (XPS) measurements were made on CuNi / C catalysts using a KRATOS Axis Ultra DLD XPS in hybrid lens mode. The data were analyzed using the XPS Peak program. The results are summarized in Table 3.2. XPS measurements were also made on both Cu and Ni wires in order to compare the pure metal results to those for the CuNi catalysts.

Table 3.2: Cu-Ni surface ratios obtained from XPS measurements

	Theoretical bulk Cu/Ni ratio from nominal composition	Actual Surface Cu/Ni ratio from XPS	Percentage Increase
$Cu_{20}Ni_{80}$	0.25	1.2	380%
$Cu_{50}Ni_{50}$	1	2	100%
$Cu_{80}Ni_{20}$	4	4.2	5%

3.2.3 Reaction Experiments

The performances of the supported CuNi catalysts were evaluated using the RWGS reaction. 50 mg of powdered catalyst was placed on a fritted quartz bed within a 35 mL quartz tube to act as a fixed bed reactor. A gas mixture of 1 kPa H_2 (Grade 4.0, Linde), 1 kPa CO_2 (Grade 3.0, Linde) and the balance He (Grade 4.7 Linde) flowed through the reactor at a total flow rate of 510 mL/min. The reaction was performed at atmospheric pressure using three consecutive temperature cycles. Each temperature cycle consisted of a series of experiments over the temperature range from 400°C – 700°C. Before each experiment, the temperature was held constant for 30 min. Although the same mass of catalyst was used in each experiment, the gas hourly space velocity (GHSV) was different because the supports had different bulk densities (288 g/L for the carbon support and 461 g/L for the alumina support). The GHSV values were 176000 h^{-1} and 282000 h^{-1} respectively for CuNi/C and CuNi/Al_2O_3 catalysts. The effluent was dehumidified by flowing through an adsorbent and was analyzed by flowing through a mass spectrometer (Ametek Proline DM 100) and a non-dispersive infra-red CO gas analyzer (Horiba VIA-510). Each set of experiments was repeated three times (24 hrs total) in order to examine reproducibility and stability. The yield of CO was calculated using the following formula:

$$\text{Yield of CO (\%)} = [CO]_{OUT} / [CO_2]_{IN} \times 100\% \quad (3.8)$$

The mass spectrometer identified any by-products that were formed via side reactions such as CO methanation. The mass spectrometer indicated the presence of gases with a molecular weight of up to 50 atomic units and had a detection limit of 50 ppm.

3.3 Results and Discussion

The X-ray diffraction spectra of the CuNi nanoparticles are shown in Figure 3.1. The positions of the peaks for both pure Cu (2θ = 43.2, ICSD Collection Code: 53246) and pure Ni (2θ = 44.6, ICSD Collection Code: 43397) are shown as straight vertical lines in Figure 3.1. They are the X-ray reflections from the 111 crystal lattice planes. The smaller peaks near 2θ values of 50.4 and 51.5 are the reflections from the 200 crystal lattice planes of Cu and Ni respectively. No species other than Cu and Ni were identified. There is a slight difference between the peak positions for the pure metals and the metals in the catalysts. Deviations exist because the catalysts are bimetallic solid solutions rather than pure metals. The catalyst that is nominally $Cu_{80}Ni_{20}$ in Figure 3.1c had a 2θ peak position of 43.345 that is slightly greater than the one for pure Cu. The catalyst that is nominally $C_{20}Ni_{80}$ in Figure 3.1a had a 2θ peak position of 44.412 for Ni, that is slightly less than the one for pure Ni. This suggests that the two peaks represent a Cu rich solid solution and a Ni rich solid solution.

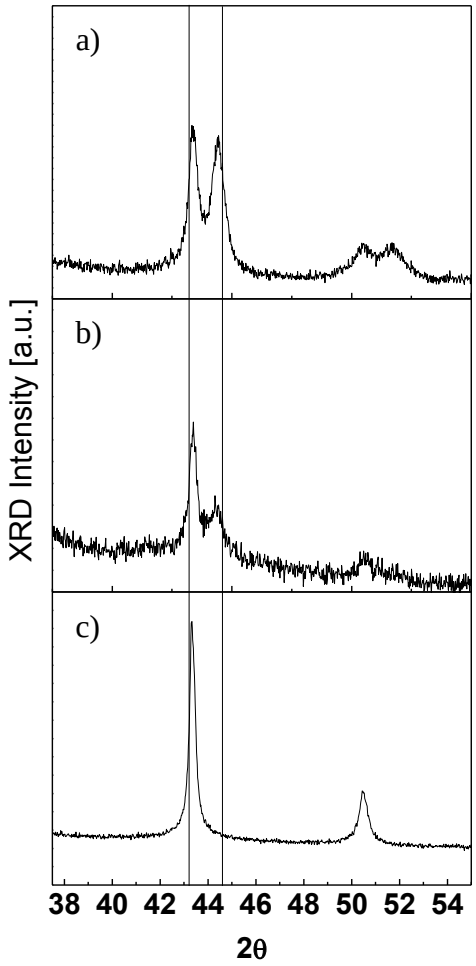

Figure 3.1: XRD Spectra of colloidal: **a)** $Cu_{20}Ni_{80}$ **b)** $Cu_{50}Ni_{50}$ and **c)** $Cu_{80}Ni_{20}$

There is only one peak for the $Cu_{80}Ni_{20}$ catalyst in Figure 3.1c. That means that all of the Ni was soluble in the Cu lattice. The single peak in Figure 3.1c is experimental evidence for a copper rich CuNi solid solution in which the spacing between planes of the catalyst lattice is close to that of pure copper.

There are two peaks for the $Cu_{20}Ni_{80}$ catalyst in Figure 3.1a. Because the first peak has a 2θ value at 43.394, close to that for pure Cu, the spacing between its planes will be similar to pure copper. Because the second peak has a 2θ value at 44.412, close to that for pure Ni, the spacing between its planes will be similar to pure nickel. Even though there is a large disparity between the bulk Cu content and the bulk Ni content of the catalyst, the two peaks appear to

have similar areas. Therefore a substantial amount of Ni must be dissolved in the first Cu-like peak, and the first peak must represent a CuNi solid solution. Since the second peak has a 2θ value slightly different from pure Ni it will contain some Cu and that would make it a Ni rich NiCu solid solution.

The observation of solid solutions is consistent with other work reported in the literature. Bonet et al. [18] synthesized Cu-Ni particles using a similar technique. In their work they refluxed copper and nickel carbonates starting materials in ethylene glycol. After 39 hours at 140°C they observed the presence of a copper-rich solid solution, $Cu_{81}Ni_{19}$, and a Ni rich solid solution, $Ni_{86}Cu_{14}$.

The crystalline size of the synthesized nanoparticles increases with Cu content. A summary of their diameters (15 – 65 nm) can be found in Table 3.1. They were calculated from the XRD data using Scherrer's formula. The CuNi particles described by Bonet et al. [17] had diameters of 250 – 400 nm. It is possible that the longer refluxing times and the absence of NaOH may have provided more opportunity for agglomeration.

TEM images of supported Pt / C nanoparticles were taken and a sample image is shown in Figure 3.2. The particles are shown to be mainly spherical with a reasonably narrow size distribution. The dispersion also appears to be relatively high. Numerical data derived from several TEM images indicated that a typical particle size for the Pt/C particles was 2.8 nm (Table 3.1). Furthermore, the typical particle size from TEM analysis, 2.8 nm, is close to the bulk crystalline size obtained from the XRD spectra, 3.8 nm.

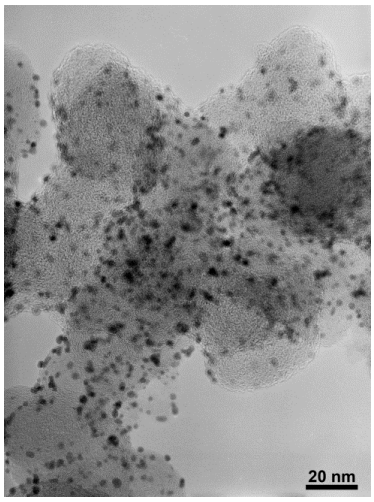

Figure 3.2: TEM image of Pt/C

An SEM image for the $Cu_{50}Ni_{50}$/C catalyst is shown in Figure 3.3. The particles appear to be generally spherical and to vary in size from 4 nm to 100 nm. This variation is mainly due to visible signs of agglomeration.

Typical particle sizes for all of the CuNi catalysts measured by SEM are listed in Table 3.1. In general the CuNi particle sizes are an order of magnitude larger than the Pt particle size. Since the CuNi metal loading, eg. 10 wt%, is an order of magnitude larger than the Pt loading, eg.1 wt%, a greater extent of metal particle agglomeration might be expected for the CuNi particles.

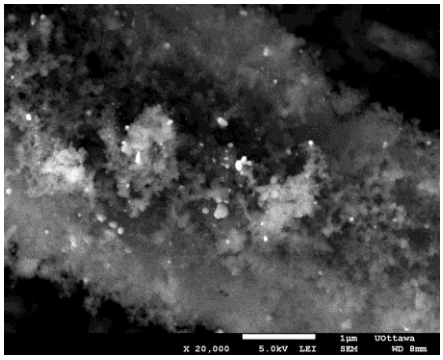

Figure 3.3: SEM image of a $Cu_{50}Ni_{50}$/C catalyst

An Energy-dispersive x-ray spectroscopy, EDS, analysis was also performed on the catalyst. For example, the $Cu_{80}Ni_{20}$ / C catalyst had a measured composition of 82.7 wt% Cu and

17.3 wt% Ni. The EDS measurement was repeated at two different sites on the catalyst's surface with reproducible results. The EDS results were consistent with the $Cu_{80}Ni_{20}$ nominal composition of the synthesized particles. This indicates the synthesis method was successful in obtaining the nominal Cu:Ni ratio that was intended.

XPS measurements were performed on the CuNi / C catalysts to determine their surface compositions. The results in Table 3.2 show that the Cu surface concentration was greater than that of the Cu bulk concentrations for all three of the CuNi / C catalysts. Furthermore, the surface concentration of the Cu always exceeded the surface concentration of the Ni, even for the nominal $Cu_{20}Ni_{80}$/C catalyst. That result is consistent with the literature. An early report by van der Plank and Sachtler [25] indicated that Cu was the dominant species on the surface of CuNi alloys. Subsequently Watanabee et al. [26] provided definitive experimental data for the phenomenon. Later Sakurai et al. stated that the phenomenon had been conclusively shown [27].

In order to examine the physical changes of the catalyst, $Cu_{50}Ni_{50}$/C was examined by SEM before and after exposure to high temperature and reactants. There were no visible signs of additional agglomeration or any other physical changes to the metal in comparison to the unreacted catalyst. In addition, an XPS analysis of the before and after catalysts was also performed and showed no differences in the surface composition. This suggests that the catalyst is compositionally stable at temperatures of at least 700°C.

The reverse water gas shift reaction was performed using eight different catalysts. These results can be seen in Figures 3.4 – 3.11. In each figure the results for the 3 consecutive temperature cycles, over the temperature range from 400°C to 700°C, are shown. Some of the CuNi catalysts showed slight deactivation between the first and second cycle and also between the second and third cycle.

The only observable components in the gas stream entering the mass spectrometer were CO_2, H_2, CO, trace amounts of H_2O and the carrier gas, He. These results indicate that CO was the main product having a typical concentration of 2000 ppm. Other products including CH_4 had concentrations of less than the detection limit of the spectrometer, 50 ppm.

The absence of CH_4 in the products was a highly desirable result, since CH_4 is an undesirable by-product if syngas for a Fischer Tropsch process is the goal. Cu is known to favour CO production while CH_4 is known to form on Ni catalysts [1]. Since some of the catalysts used in this work contained 80 wt% Ni the absence of CH_4 might be considered to be inconsistent with the literature [1]. The advantage of the CuNi alloys made using this particular polyol synthesis method is that more than one-half of the surface was composed of Cu, even for catalysts having consisting of 80 % Ni in bulk metal, as was shown by our XPS results. Perhaps the presence of sufficient Cu on the surface may allow CO to desorb before additional hydrogenation occurs to form CH_4.

The catalysts supported on carbon are shown in Figures 3.4 – 3.7. During the first temperature cycle, the $Cu_{80}Ni_{20}$ metal carbon supported catalyst produced a slightly greater CO yield than the Pt metal carbon supported catalyst. In addition, it was the only CuNi metal carbon supported catalyst that produced a CO yield at 400°C during the first cycle. The yields of CO at 700°C using all the CuNi carbon supported catalysts differed from those using Pt by no more than 3 %.

Deactivation was observed between the first and second temperature cycles for all of the CuNi catalysts supported on carbon. Virtually no deactivation was observed when using the Pt metal carbon supported catalyst. This suggests that the deactivation observed with the CuNi carbon supported catalyst may have been related to the CuNi metal and not to the catalyst

support. The $Cu_{50}Ni_{50}$/C catalyst in Figure 3.5 was different from the $Cu_{20}Ni_{80}$/C and $Cu_{80}Ni_{20}$/C catalysts in that no deactivation occurred between the second and third temperature cycles. This suggests that after sufficient time-on-stream the performance of the $Cu_{50}Ni_{50}$/C may become invariant with time, and that it may become a thermally stable catalyst.

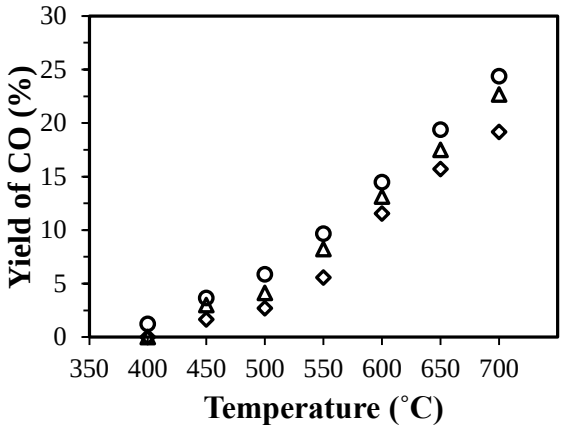

Figure 3.4: RWGS reaction at 1atm, $P_{H2} = P_{CO2} = 1$ kPa, balance He, GHSV = 176000 h^{-1}, 50 mg of catalyst: $Cu_{80}Ni_{20}$/C, 10 wt% where ○ = 1st cycle, △ = 2nd cycle and ◇ = 3rd cycle

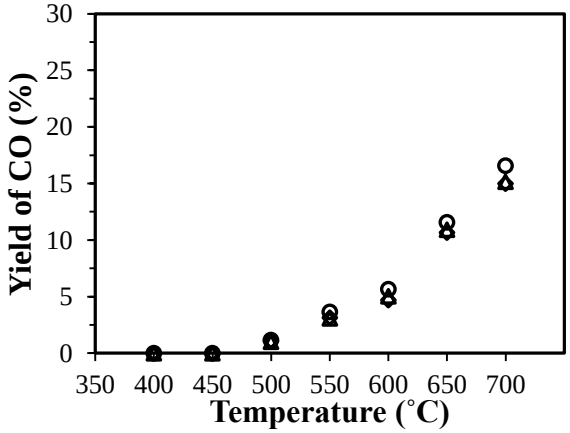

Figure 3.5: RWGS reaction at 1atm, $P_{H2} = P_{CO2} = 1$ kPa, balance He, GHSV = 176000 h^{-1}, 50 mg of catalyst: $Cu_{50}Ni_{50}$/C, 10 wt% where ○ = 1st cycle, △ = 2nd cycle and ◇ = 3rd cycle

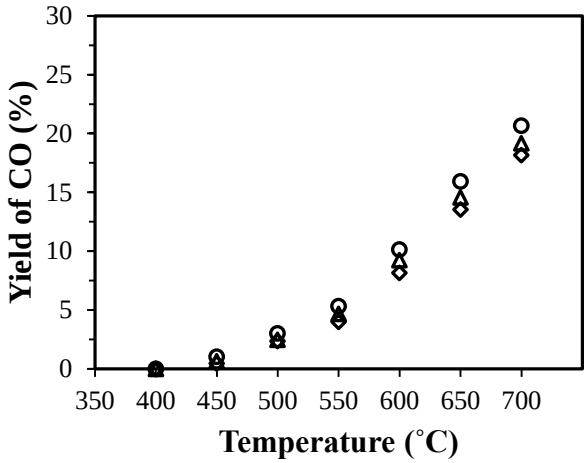

Figure 3.6: RWGS reaction at 1atm, $P_{H2} = P_{CO2} = 1$ kPa, balance He, GHSV = 176000 h^{-1}, 50 mg of catalyst: $Cu_{20}Ni_{80}$/C, 10 wt% where ○ = 1st cycle, △ = 2nd cycle and ◇ = 3rd cycle

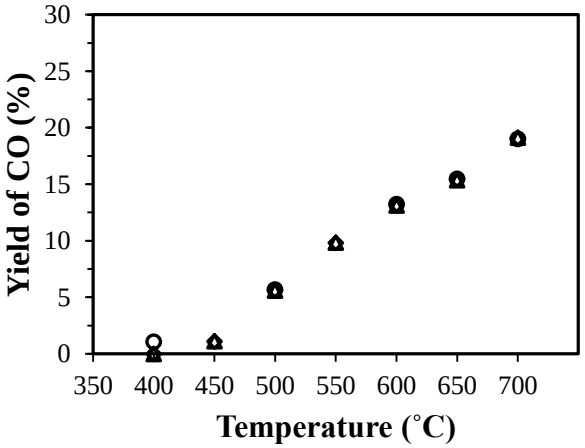

Figure 3.7: RWGS reaction at 1atm, $P_{H2} = P_{CO2} = 1$kPa, balance He, GHSV = 176000 h^{-1}, 50 mg of catalyst: Pt/C, 1 wt% where ○ = 1st cycle, △ = 2nd cycle and ◇ = 3rd cycle

The catalysts supported on gamma alumina, γ-Al_2O_3, are shown in Figures 3.8 – 3.11. In general the CO yields on the γ-Al_2O_3 supported catalyst were slightly greater than those on the carbon supported catalysts in Figures 3.4 – 3.7. For the first temperature cycle the CuNi metal γ-Al_2O_3 supported catalysts produced CO yields at 700°C that was 2 – 4 % less than those produced by the Pt metal γ-Al_2O_3 supported catalyst. In addition, only the Pt metal γ-Al_2O_3 supported catalyst produced a non-zero CO yield at 400°C during the first cycle.

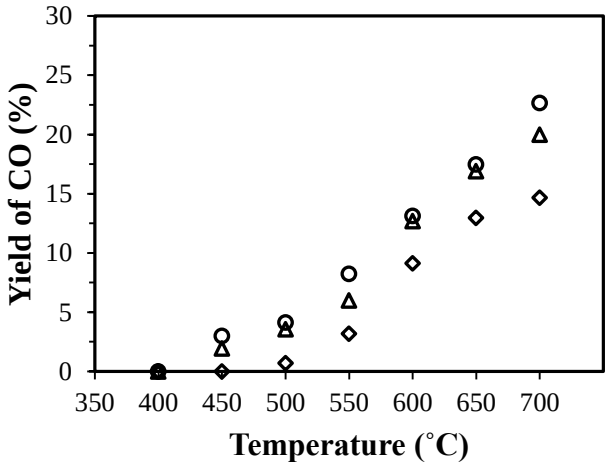

Figure 3.8: RWGS reaction at 1atm, P_{H2} = P_{CO2} = 1kPa, balance He, GHSV = 282000 h^{-1}, 50 mg of catalyst: $Cu_{80}Ni_{20}/\gamma\text{-}Al_2O_3$, 10 wt% where ○ = 1st cycle, △ = 2nd cycle and ◇ = 3rd cycle

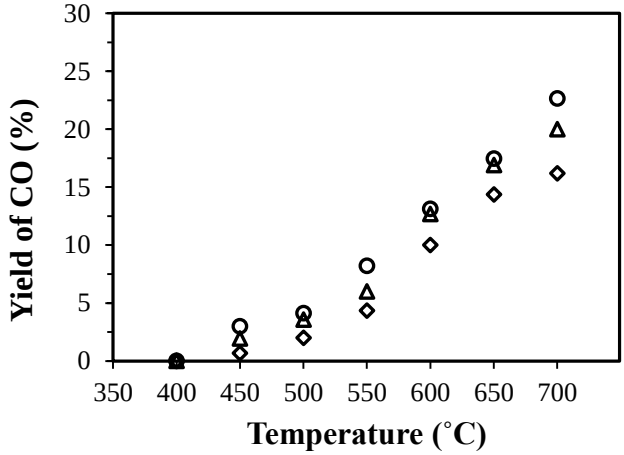

Figure 3.9: RWGS reaction at 1atm, P_{H2} = P_{CO2} = 1 kPa, balance He, GHSV = 282000 h^{-1}, 50 mg of catalyst: $Cu_{50}Ni_{50}/\gamma\text{-}Al_2O_3$, 10 wt% where ○ = 1st cycle, △ = 2nd cycle and ◇ = 3rd cycle

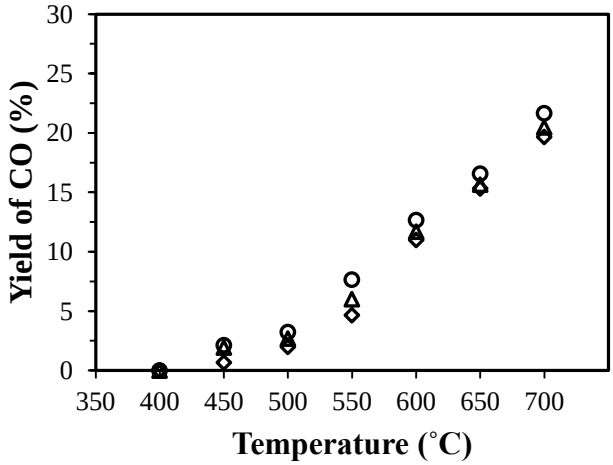

Figure 3.10: RWGS reaction at 1atm, P_{H2} = P_{CO2} = 1 kPa, balance He, GHSV = 282000 h^{-1}, 50 mg of catalyst: $Cu_{20}Ni_{80}/\ \gamma\text{-}Al_2O_3$, 10 wt% where ○ = 1st cycle, △ = 2nd cycle and ◇ = 3rd cycle

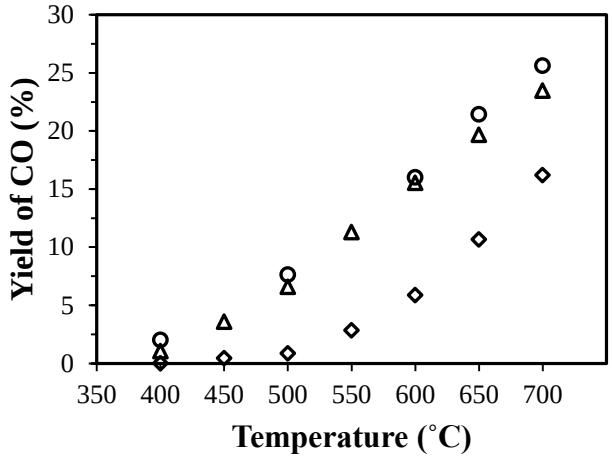

Figure 3.11: RWGS reaction at 1atm, $P_{H2} = P_{CO2} = 1$ kPa, balance He, GHSV = 282000 h^{-1}, 50 mg of catalyst: Pt/ γ-Al_2O_3, 1 wt% where ○ = 1st cycle, △ = 2nd cycle and ◇ = 3rd cycle

Deactivation was observed between the first and third temperature cycles for all the γ-Al_2O_3 supported catalysts, both for CuNi and Pt. The smallest extent of deactivation, 2 %, was observed with the $Cu_{20}Ni_{80}$ γ-Al_2O_3 supported catalyst. It is the CuNi catalyst with the smallest Cu content. In contrast the CO yields at 700°C for $Cu_{80}Ni_{20}$ and Pt γ-Al_2O_3 supported catalysts decreased by over 8% between the first and third temperature cycles. In contrast, no deactivation was observed for Pt metal carbon supported catalysts. This suggests that the γ-Al_2O_3 support may contribute to the deactivation. It is known [28] that as the temperature is increased above 500°C, gamma alumina can be converted to other phases such as delta alumina, theta alumina, and alpha alumina. Alpha alumina has a much smaller surface area than gamma alumina. The tendency of the γ-Al_2O_3 support to deactivate at high temperatures is consistent with literature data [14], [29].

Liu and Liu [16] tested a similar catalyst having $C_{50}Ni_{50}/\gamma$-Al_2O_3 at a maximum temperature of 600°C. They used twice the metal content (20 wt%) and much smaller GHSVs (much greater residence times in the reactor) and obtained CO_2 conversions that exceeded the

ones being reported here. They used a catalyst preparation method that was different than the one used here. Perhaps that may explain why the CH_4 selectivity (eg. 28.2%) in their work was much greater than in this work. Even though their CO_2 conversions were greater than the ones reported here, their finite selectivity to CH_4 caused their CO yields to be similar to the ones reported here. Liu and Liu [16] noticed an increase in CH_4 when the Ni content of the CuNi catalysts was increased.

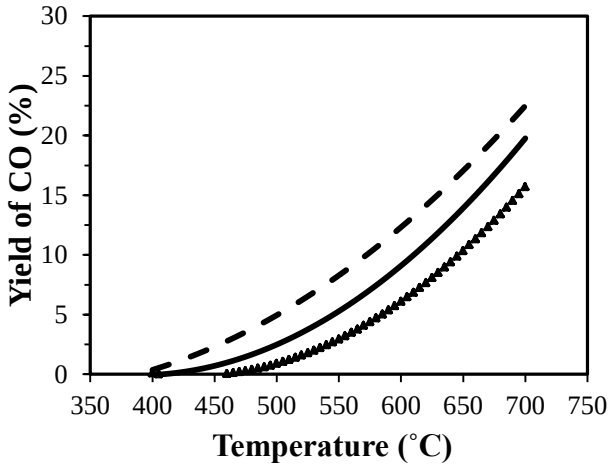

Figure 3.12: Average yield of CO for the Reverse water gas shift reaction at 1atm, $P_{H2} = P_{CO2}$ = 1 kPa, balance He, GHSV = 176000 h^{-1}, 50 mg of Cu_xNi_{1-x}/C catalyst: The solid line represents $Cu_{20}Ni_{80}$/C catalysts, the triangles represent $Cu_{50}Ni_{50}$/C catalysts, and the dashed line represents $Cu_{80}Ni_{20}$/C catalysts.

A comparison of the average CO yields for the carbon supported catalysts are shown in Figure 3.12. The CO yields obtained with $Cu_{50}Ni_{50}$/C catalyst are smaller than those obtained with the other two CuNi catalysts. The $Cu_{50}Ni_{50}$/C catalyst was the one that appeared to be compositionally stable according to the XPS results discussed previously. It was also the one that appeared to be the most thermally stable in Figure 3.5. Perhaps there is an association between minimum CO yield and thermal stability. In other words, perhaps the reaction sites on CuNi catalysts with the largest turnover frequencies are the ones that are the most thermally unstable.

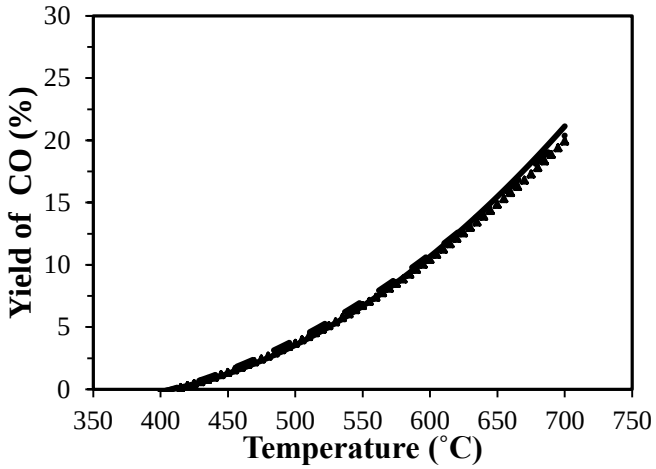

Figure 3.13: Average yield of CO for the Reverse water gas shift reaction at 1atm, $P_{H2} = P_{CO2}$ = 1 kPa, balance He, GHSV = 282000 h^{-1}, 50 mg of $Cu_xNi_{1-x}/\gamma\text{-}Al_2O_3$ catalyst: The solid line represents $Cu_{20}Ni_{80}/\ \gamma\text{-}Al_2O_3$ catalysts, the triangles represent $Cu_{50}Ni_{50}/\ \gamma\text{-}Al_2O_3$ catalysts, and the dashed line represents $Cu_{80}Ni_{20}/\ \gamma\text{-}Al_2O_3$ catalysts.

A comparison of the average CO yields for the alumina supported catalysts shown in Figure 3.13 are almost identical regardless of catalyst composition. Nevertheless substantial catalyst deactivation was evident in Figures 3.8–3.11. That suggests that the deactivation caused by thermal transitions in alumina (loss of surface area, spinel formation) may have had more influence on catalyst performance than variations in CuNi catalyst composition. In spite of the similarity of the results in Figure 3.13, the CO yields for the $Cu_{50}Ni_{50}/\ \gamma\text{-}Al_2O_3$ catalyst appear to be slightly less than the other two catalyst compositions. That is consistent with the observation in Figure 3.12 that the $Cu_{50}Ni_{50}$/C catalyst also produced smaller yields than the other two CuNi catalysts.

As discussed above, some deactivation occurs when CuNi metal is supported on either carbon or $\gamma\text{-}Al_2O_3$. As a result, most catalysts composed of CuNi metal supported on either carbon or $\gamma\text{-}Al_2O_3$ will not satisfy one of the main objectives of this research, namely obtaining a thermally stable catalyst capable of operating under high temperatures. The one exception

discussed here is the $Cu_{50}Ni_{50}$/C catalyst. Unless deactivation can be mitigated CuNi catalysts will not meet the requirements for an efficient, industrially viable catalyst.

3.4 Conclusion

The results of this investigation can be summarized by the following statements: The new polyol synthesis method permits both Cu and Ni metal salts to be reduced at the same time and at the same temperature, by first heating the Ni salt solution to 196°C and then adding the Cu salt solution that was at room temperature. In the past [18] a Ni rich surface was obtained because $Cu(NO_3)_2$ was reduced first at temperatures as low as 140°C followed by $Ni(NO_3)_2$ reduction as the solution continued to be heated to 196°C. The CuNi alloy catalysts investigated in this work are similar to pure Cu catalysts in that they show selectivity for CO formation and the absence of CH_4 formation. The selectivity to CO was attributed to Cu being the most abundant metallic species on the surface of the catalyst, as determined by XPS measurements. Although the CuNi alloys show some deactivation, they are not nearly as thermally unstable as pure Cu (sintering) at the higher temperatures that are necessary for the equilibrium of the RWGS reaction to be thermodynamically favorable. Deactivation was observed in each case that an alumina catalyst support was used. With one carbon supported catalyst, $Cu_{50}Ni_{50}$/C, there was little deactivation between the second and third temperature cycles and it appeared to be compositionally stable. Finally, CO yields at 700°C during the third temperature cycle with the $Cu_{50}Ni_{50}$/C catalyst (16.6 %) were comparable to those with the Pt/C catalyst (16.3 %).

In conclusion, considering the difference in cost between CuNi alloys and Pt metal, these results suggest more studies are warranted on the use of CuNi alloy catalysts for the RWGS reaction.

3.5 Acknowledgements

The Natural Science and Engineering Research Council (NSERC) and Phoenix Canada Oil Company Limited are gratefully acknowledged for their financial support.

3.6 References

[1] W. Wang, S. Wang, X. Ma, and J. Gong, "Recent advances in catalytic hydrogenation of carbon dioxide.," *Chem. Soc. Rev.*, vol. 40, no. 7, pp. 3703–27, Jul. 2011.

[2] P. Vibhatavata, J.-M. Borgard, M. Tabarant, D. Bianchi, and C. Mansilla, "Chemical recycling of carbon dioxide emissions from a cement plant into dimethyl ether, a case study of an integrated process in France using a Reverse Water Gas Shift (RWGS) step," *Int. J. Hydrogen Energy*, vol. 38, no. 15, pp. 6397–6405, May 2013.

[3] S. S. Kim, K. H. Park, and S. C. Hong, "A study of the selectivity of the reverse water–gas-shift reaction over Pt/TiO2 catalysts," *Fuel Process. Technol.*, vol. 108, pp. 47–54, Apr. 2013.

[4] S. S. Kim, H. H. Lee, and S. C. Hong, "A study on the effect of support's reducibility on the reverse water-gas shift reaction over Pt catalysts," *Appl. Catal. A Gen.*, vol. 423–424, pp. 100–107, May 2012.

[5] S. S. Kim, H. H. Lee, and S. C. Hong, "Applied Catalysis B : Environmental The effect of the morphological characteristics of TiO2 supports on the reverse water – gas shift reaction over Pt/TiO2 catalysts," *"Applied Catal. B, Environ.*, vol. 119–120, pp. 100–108, 2012.

[6] G. Pekridis, K. Kalimeri, N. Kaklidis, E. Vakouftsi, E. F. Iliopoulou, C. Athanasiou, and G. E. Marnellos, "Study of the reverse water gas shift (RWGS) reaction over Pt in a solid oxide fuel cell (SOFC) operating under open and closed-circuit conditions," *Catal. Today*, vol. 127, no. 1–4, pp. 337–346, Sep. 2007.

[7] C. S. Chen, J. H. Wu, and T. W. Lai, "Carbon Dioxide Hydrogenation on Cu Nanoparticles," *J. Phys. Chem. C*, pp. 15021–15028, Aug. 2010.

[8] C. Chen, W. Cheng, and S. Lin, "Mechanism of CO formation in reverse water – gas shift reaction over Cu/Al2O3 catalyst," *Catal. Letters*, vol. 68, pp. 45–48, 2000.

[9] L. Wang, S. Zhang, and Y. Liu, "Reverse water gas shift reaction over Co-precipitated Ni-CeO2 catalysts," *J. Rare Earths*, vol. 26, pp. 66–70, 2008.

[10] F. S. Stone and D. Waller, “Cu-ZnO and Cu–ZnO/Al2O3 catalysts for the reverse water-gas shift reaction . The effect of the Cu/Zn ratio on precursor characteristics and on the activity of the derived catalysts,” *Top. Catal.*, vol. 22, no. April, pp. 305–318, 2003.

[11] J. Lin, “Supported Copper, Nickel and Copper-Nickel nanoparticle Catalyst for Low Temperature WGS reaction,” University of Cincinnati, 2012.

[12] C. Chen, C. Ruan, Y. Zhan, X. Lin, Q. Zheng, and K. Wei, “The significant role of oxygen vacancy in Cu/ZrO2 catalyst for enhancing water–gas-shift performance,” *Int. J. Hydrogen Energy*, vol. 39, no. 1, pp. 317–324, Jan. 2014.

[13] C. Chen, W. Cheng, and S. Lin, “Study of reverse water gas shift reaction by TPD , TPR and CO2 hydrogenation over potassium-promoted Cu/SiO2 catalyst,” *Appl. Catal. A Gen.*, vol. 238, pp. 55–67, 2003.

[14] C. Chen, W.-H. Cheng, and S.-S. Lin, “Study of iron-promoted Cu/SiO2 catalyst on high temperature reverse water gas shift reaction,” *Appl. Catal. A Gen.*, vol. 257, no. 1, pp. 97–106, Jan. 2004.

[15] C. S. Chen, J. H. Lin, J. H. You, and K. H. Yang, “Effects of potassium on Ni-K/Al2O3 catalysts in the synthesis of carbon nanofibers by catalytic hydrogenation of CO2.,” *J. Phys. Chem. A*, vol. 114, no. 11, pp. 3773–81, Mar. 2010.

[16] Y. Liu and D. Liu, “Study of bimetallic Cu-Ni/ gamma Al2O3 catalysts for carbon dioxide hydrogenation,” *J. Hydrog. Energy*, vol. 24, pp. 351–354, 1999.

[17] L. Poul, N. Jouini, and F. Fie, “Layered Hydroxide Metal Acetates (Metal) Zinc , Cobalt , and Nickel): Elaboration via Hydrolysis in Polyol Medium and Comparative Study,” *Chem. Mater.*, vol. 12, no. 10, pp. 3123–3132, 2000.

[18] F. Bonet, S. Grugeon, L. Dupont, R. Herrera Urbina, C. Guéry, and J. M. Tarascon, “Synthesis and characterization of bimetallic Ni–Cu particles,” *J. Solid State Chem.*, vol. 172, no. 1, pp. 111–115, Apr. 2003.

[19] C. Bock, C. Paquet, M. Couillard, G. A. Botton, and B. R. MacDougall, “Size-selected synthesis of PtRu nano-catalysts: reaction and size control mechanism.,” *J. Am. Chem. Soc.*, vol. 126, pp. 8028–37, Jun. 2004.

[20] R. J. Isaifan, H. A. E. Dole, E. Obeid, L. Lizarraga, E. A. Baranova, and P. Vernoux, “Catalytic CO Oxidation over Pt nanoparticles prepared from the Polyol Reduction Method supported on Yttria-Stabilized Zirconia .,” *Electrochem. Soc.*, vol. 35, no. 28, pp. 43–57, 2011.

[21] R. J. Isaifan, S. Ntais, and E. A. Baranova, “Particle size effect on catalytic activity of carbon-supported Pt nanoparticles for complete ethylene oxidation,” *Appl. Catal. A Gen.*, vol. 464–465, pp. 87–94, Aug. 2013.

[22] R. J. Isaifan, H. A. E. Dole, E. Obeid, L. Lizarraga, P. Vernoux, and E. A. Baranova, "Metal-Support Interaction of Pt Nanoparticles with Ionically and Non-Ionically Conductive Supports for CO Oxidation," *Electrochem. Solid-State Lett.*, vol. 15, no. 3, p. E14, 2012.

[23] H. A. E. Dole, R. J. Isaifan, F. M. Sapountzi, L. Lizarraga, D. Aubert, A. Princivalle, P. Vernoux, and E. A. Baranova, "Low Temperature Toluene Oxidation Over Pt Nanoparticles Supported on Yttria Stabilized-Zirconia," *Catal. Letters*, vol. 143, no. 10, pp. 996–1002, Jul. 2013.

[24] G. Viau, F. Fiévet, and F. Fiévet-Vincent, "Nucleation and Growth of Bimetallic CoNi and FeNi Monodisperse Particles Prepared in Polyols," *Sol*, vol. 84, pp. 259–270, 1996.

[25] P. van der Plank and W. M. H. Sachtler, "Surface Composition of Equilibrated Copper-Nickel Alloy Films," *J. Catal.*, vol. 7, no. 3, pp. 300–303, 1967.

[26] K. Watanabe, M. Hashiba, and T. Yamashina, "A Quantitative Analysis of Surface Segragation and In-Depth Profile of Copper-Nickel Alloys," *Surf. Sci.*, vol. 61, pp. 483–490, 1976.

[27] T. Sakurai, T. Hasizume, A. Jimbo, A. Sakai, and S. Hyodo, "New Results in Surface Segregation of Ni-Cu Binary Alloys," *Phys. Rev. Lett.*, vol. 55, no. 5, pp. 514–517, 1985.

[28] R. K. Oberlander, "Aluminas for Catalysts: Their preparation and properties," *Appl. Industiral Catal.*, vol. 3, p. 67, 1984.

[29] J. Hu, K. P. Brooks, J. D. Holladay, D. T. Howe, and T. M. Simon, "Catalyst development for microchannel reactors for martian in situ propellant production," *Catal. Today*, vol. 125, no. 1–2, pp. 103–110, Jul. 2007.

Chapter 4 – Synthesis of CuNi/YSZ and CuNi/SDC for the Reverse Water Gas Shift Reaction

Abstract

$Cu_{50}Ni_{50}$ nanoparticles were synthesized using a modified polyol method and deposited on samarium-doped ceria, SDC, and yttria-stabilized zirconia, YSZ, supports to form reverse water-gas shift, RWGS, catalysts. The best CO yields, obtained with the $Cu_{50}Ni_{50}$/SDC catalyst, were about 90% of the equilibrium CO yields. In contrast CO yields using Pt/SDC catalysts were equal to equilibrium CO yields at 700°C. Catalyst selectivity to CO was 100% at hydrogen partial pressures equal to CO_2 partial pressures, 1 kPa, and decreased as methane was formed when the hydrogen partial pressure was 2 kPa or greater. The reaction results were explained using a combination of Eley-Rideal and Langmuir-Hinshelwood mechanisms that involved adsorption on the metal surface and the concentration of oxygen vacancies in the support. Finally the $Cu_{50}Ni_{50}$/SDC catalyst was found to be thermally stable for 48 hours at 600/700°C.

4.1 Introduction

The emission of carbon dioxide into the environment is viewed by many as a major contributor to global warming [1]. In spite of the current fossil fuel energy prices, the use of fossil fuels continues to increase resulting in more carbon dioxide emissions. Those emissions affect the state of the atmosphere and the state of the oceans.

Carbon capture and storage technologies are one means of diminishing CO_2 emissions. Unfortunately, storing CO_2 in underground caverns is not sustainable because all the caverns will eventually be filled. An alternative to carbon storage would be the reaction of CO_2 with another chemical to obtain a useful product.

This work describes the reaction of carbon dioxide with hydrogen obtained from a renewable source. By hydrogenating CO_2 [2], [3], it is possible to obtain syngas via Equation 4.1 or alcohols and hydrocarbons (using the Fischer-Tropsch process), via Equation 4.2.

$$CO_2 + H_2 \leftrightarrow CO + H_2O \tag{4.1}$$

$$x\ CO_2 + (2x\text{-}z+y/2)\ H_2 \leftrightarrow C_xH_yO_z + (2x\text{-}z)\ H_2O \tag{4.2}$$

Equation 4.1 is the reverse water-gas shift reaction (RWGS). Equation 4.2 is a synthesis reaction that is practiced on an industrial scale, the Fischer-Tropsch process. In Equation 4.2 when $x = 1$, $y = 4$ and $z = 0$, methane (CH_4) is formed. It is a common by-product of the RWGS reaction. When $x = 1$, $y = 4$ and $z = 1$, the product is methanol (CH_3OH). When $z = 0$ and $5 < x < 20$, a highly valued liquid hydrocarbon product is obtained.

An appropriate catalyst must satisfy several criteria. Because the equilibrium yield of CO from the RWGS reaction increases with temperature, thermal stability of the catalyst is one criterion. Others are rapid kinetics and selectivity to CO rather than to CH_4.

Noble metals such as platinum (Pt) have been studied and proven to be among the best RWGS catalysts because they have the ability to dissociate H_2 [2]. Also, Pt is stable at high temperatures and produces both high CO selectivity and CO_2 conversion [4]–[6]. However, noble metals such as Pt have a high cost.

Copper (Cu) and nickel (Ni) transition metals may be promising alternative catalysts to Pt noble metals. One indication is that both of these metals have produced promising results with the water gas shift, WGS, reaction [2], [7] that is shown in Equation 4.3.

$$CO + H_2O \leftrightarrow CO_2 + H_2 \tag{4.3}$$

Good results were also obtained when they were tested individually on catalyst supports [4]–[6] using the RWGS reaction.

Metallic pure Cu catalysts have shown a tendency to deactivate over time when exposed to high temperatures [8]–[10]. Stabilizers have been used in an attempt to improve copper's thermal stability. Chen et al [11] reported that an iron (Fe) additive stabilized Cu at 600°C for up to 120 h. It also increased CO_2 conversion by 7%. In contrast, Cu without Fe deactivated quickly reaching 0% conversion after 120 h. Other additives include potassium [12] and zinc oxide [9].

Chen et al. [13] showed that a Ni catalyst used for the RWGS reaction enhanced the formation of CH_4 which is undesirable. They also investigated a Ni catalyst that was promoted with a potassium (K) additive. Although K increased the selectivity toward CO, it also caused the formation of coke.

Liu et al. [14] made a bimetallic Ni and Cu catalyst and used it for the RWGS reaction. Their research was aimed at examining the effect of both metals on selectivity for the RWGS reaction. They found that an increase in catalyst Ni content generated greater CH_4 yields while increased Cu contents generated greater CO selectivity.

Catalysts are often supported on materials such as γ-Al_2O_3, SiO_2, and C. Yttria-stabilized zirconia, YSZ, and samariam-doped ceria, SDC, are two less common supports that have shown potential for the RWGS reaction [15], [16]. Both contain oxygen vacancies.

Yttria-stabilized zirconia, $Y_{0.15}Zr_{0.85}O_{1.925}$, is a combination of 0.15* Y_2O_3 and 0.85 ZrO_2. It is a conductive ceramic which has been used in solid oxide fuel cells and sensor technologies [17]. It is also used for the electrochemical promotion of catalysts, EPOC [18]. The purpose for doping ZrO_2 with Y_2O_3 is twofold: (1) Y_2O_3 stabilizes the cubic fluorite structure eliminating volumetric variations caused by phase transformations, and (2) Y_2O_3 creates oxygen vacancies within the ZrO_2 lattice [19], [20]. Oxygen vacancies are important for all of the YSZ applications mentioned above. In addition oxygen vacancies in ZrO_2 have been shown to affect the WGS reaction [7].

Similarly, adding dopants to ceria, CeO_2, increases the oxygen vacancies within the crystal lattice [8]. Doping with cations having an ionic radius and electronegativity close to CeO_2 are considered to be the most appropriate [21]. Samarium showed the greatest resistance to reduction of the CeO_2 support [22] among the doping agents investigated. Since the intent of the work was to examine the effect of oxygen vacancies and not the reducibility of the support, samarium was chosen as the dopant. $Sm_{0.2}Ce_{0.8}O_{1.9}$ (SDC) is a combination of 0.2*Sm_2O_3 and 0.8*CeO_2.

YSZ and SDC have different oxygen vacancy contents. Samarium doped ceria, $Sm_{0.2}Ce_{0.8}O_{1.9}$, has 0.1 oxygen vacancies per cation when compared to CeO_2. In contrast, yttria-stabilized zirconia, $Y_{0.15}Zr_{0.85}O_{1.926}$, has 0.074 oxygen vacancies per cation when compared to ZrO_2. Both of these materials have been tested by themselves without the addition of other metals and have demonstrated thermal stability and CO_2 conversion [15].

In the present work, $Cu_{50}Ni_{50}$ nanoparticles were synthesized using a modified polyol technique and deposited on SDC and YSZ supports. The SDC and YSZ supported catalysts were compared to catalysts containing Pt nanoparticles deposited on the same supports at the same reaction conditions. The $Cu_{50}Ni_{50}$ catalyst with the best performance was examined at a variety of partial pressures. In addition thermal stability experiments were performed in which the temperature was maintained between 600 and 700°C for 48 h.

4.2 Experimental

4.2.1 Catalyst preparation

The synthesis of CuNi nanoparticles was achieved using a modified polyol technique. First, 314.5 mg of nickel nitrate ($Ni(NO_3)_2$) (hexahydrate 99.999% metal basis, Alfa Aesar) was dissolved in 30 mL of ethylene glycol (anhydrous 99.8%, SigmaAldrich) to obtain a green solution. That solution's pH was then increased to 11 via the addition of 199 mg of sodium hydroxide (NaOH) pellets (EM Science, ACS grade) to obtain Solution 1. This caused the solution to slightly darken. In a separate beaker, 321.8 mg of copper nitrate ($Cu(NO_3)_2$) (hexahydrate 99.999% metal basis, Alfa Aesar) was dissolved in 30 mL of ethylene glycol to obtain a blue solution. Its pH was also increased to 11 using 199 mg of NaOH pellets to obtain Solution 2. Solution 2 also darkened. Following this, Solution 1 was poured into a round bottom flask, refluxed and stirred at 196˚C. Once the temperature reached 196 ˚C, Solution 2, at room temperature, was added to the round bottom flask. The ratio of Solution 1 to Solution 2 was selected to obtain CuNi colloidal particles of 50 wt % Cu / 50 wt % Ni (nominally $Cu_{50}Ni_{50}$). The combined solution was refluxed at 196 ˚C for 30 minutes and then cooled. The combined solution gradually became dark brown in colour. Once cooled, the colloidal particles were stored in the ethylene glycol solution. The final pH of the combined solution was 7.

The colloidal particles were then deposited on supports using a wet impregnation technique. A powdered support was placed into a beaker and subsequently an amount of the combined solution was poured unto the powder. The amount of combined solution was chosen to result in nominally 10 wt% of CuNi when deposited on the supports, which corresponds to a $Cu_{50}Ni_{50}$ metal/support ratio of 1 to 9. The solution/support was sonicated for 1 hour and stirred for 24 hours. The supported metal was then centrifuged and washed with deionized water several times to remove the salts remaining after the synthesis procedure. The supports were yttria-stabilized zirconia (Tosoh, BET surface area 14.8 $m^2 \cdot g^{-1}$) and samarium-doped ceria (FCM, BET surface area 31.0 $m^2 \cdot g^{-1}$). The catalyst was then dried using a freeze dryer. Prior to any experiments, the catalyst was crushed.

Pt nanoparticles were synthesized using a polyol method as described elsewhere [23]. It involved diluting $PtCl_4$ in a 0.06 M NaOH solution of ethylene glycol. The mixture was then refluxed at 160°C for 3 hours. The deposition technique was the same as that for $Cu_{50}Ni_{50}$ and the same supports were used. After deposition, each support contained 1 wt% of Pt nanoparticles.

4.2.2 Physical Characterization

X-ray diffraction (XRD) measurements were made on the CuNi colloidal particles using a RigakuUltima IV difractometer which used a Cu Kα X-ray (40 ma, 44 kV) operating with focused beam geometry and a divergence slit of 2/3 degree, a scan speed of 0.17 deg min^{-1} and a scan step of 0.06 degrees were used while operating between 35° and 55°.

Characterization of the CuNi metal particles by scanning electron microscopy, SEM, and X-ray photoelectron spectroscopy has been reported previously [24]. Characterization of the Pt metal particles by transmission electron microscopy, TEM, has also been reported previously [25]. The characterization measurements were made with the metal particles supported on

carbon, in order to avoid electrostatic charging that would occur when metals are supported on insulating materials.

4.2.3 Catalytic Performance

Catalytic reaction rates were measured on both $Cu_{50}Ni_{50}$ and Pt supported nanoparticles for the RWGS reaction. First, the dry metal/support catalyst was finely crushed. Then, 50 mg of the metal/support catalyst was placed on top of a fritted quartz bed located within a tubular, 35 mL quartz reactor. A gaseous mixture containing 1 kPa H_2 (Grade 4.0, Linde), 1 kPa CO_2 (Grade 3.0, Linde) with the balance being He (Grade 4.7 Linde) flowed through the reactor at a flow rate of 510 $mL \cdot min^{-1}$. The reaction was performed at a total pressure of 1 atm using three consecutive temperature cycles. Each temperature cycle consisted of a series of experiments over the temperature range from 400°C – 700°C. Before each experiment, the temperature was held constant for 30 min. The same mass of catalyst was used in each experiment, 50 mg, so that the weight hourly space velocity was constant at 612 L/(h g). Nevertheless, the gas hourly space velocity (GHSV) was different because the supports had different bulk densities (1187 g/L for the YSZ support and 1570 g/L for the SDC support). The GHSV values were 716000 h^{-1} and 960800 h^{-1} respectively for CuNi/YSZ and CuNi/SDC catalysts. The effluent was dehumidified by flowing through an adsorbent and was analyzed by flowing through a mass spectrometer (Ametek Proline DM 100) and a non-dispersive infra-red CO gas analyzer (Horiba VIA-510). Each set of experiments was repeated three times (24 hrs total) in order to examine reproducibility and stability.

A schematic of the experimental equipment is shown in Fig. 4.1.

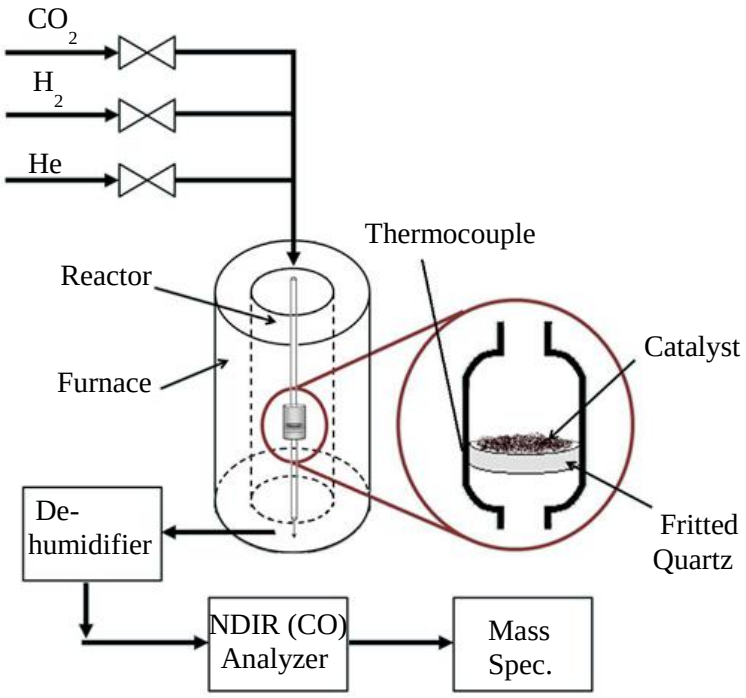

Figure 4.1: Schematic of experimental setup used for catalytic testing of the RWGS reaction

The yield of CO was calculated using the following formula:

$$\text{Yield of CO (\%)} = [CO]_{out} / [CO_2]_{in} \times 100\% \quad (4.4)$$

The quantitative measurements obtained using the NDIR CO analyzer were used to obtain the concentration of CO coming out of the reactor ($[CO]_{out}$). The mass spectrometer identified any by-products that were formed via side reactions such as CO methanation. The mass spectrometer indicated the presence of gases with a molecular weight of up to 50 atomic units and had a detection limit of 50 ppm.

The reactant partial pressures were also varied during experiments using the SDC supported $Cu_{50}Ni_{50}$ catalyst. First, the H_2 partial pressure was kept constant at 1 kPa while the CO_2 partial pressure was varied from 1 to 4 times the H_2 partial pressure. Then, the CO_2 partial pressure was kept constant at 1 kPa while the H_2 partial pressure varied from 1 to 4 times the CO

partial pressure. The total flow rate of the gaseous stream was kept constant at 510 mL·min^{-1}, by adjusting the He flow rate. The total gas pressure remained constant at 1 atm in all experiments.

Thermal stability experiments were performed on the $Cu_{50}Ni_{50}$/SDC catalyst by maintaining the temperature at 700°C for 24 hrs at a total pressure of 1 atm and a total flow rate of 510 mL·min^{-1}. The gas composition was 1 kPa H_2, 1 kPa CO_2 with the balance being He. Subsequently, the temperature was decreased to 600°C and maintained constant for another 24 hrs, for a total catalyst time-on-stream of 48 hrs.

Thermodynamic equilibrium calculations were performed using UniSim simulation software. A Gibbs reactor calculation was used to determine the equilibrium conversion at the operating conditions. Equilibrium conversions were compared with experimental results.

4.3 Results and Discussion

4.3.1 Physical Characterization of $Cu_{50}Ni_{50}$

X-ray diffraction spectra of $Cu_{50}Ni_{50}$ nanoparticles are shown in Figure 4.2. Ni and Cu were the major species and no nitrate salts were present. X-ray diffraction peaks having 2θ values of 43.39° and 44.41° were attributed respectively to reflections from the 111 plane of a Cu rich alloy and from the 111 plane of a Ni rich alloy as shown in [24]. The crystalline size was obtained using Scherrer's formula and gave 20.5 nm for the Cu rich (111) peak and 9.6 nm for the Ni rich (111) peak.

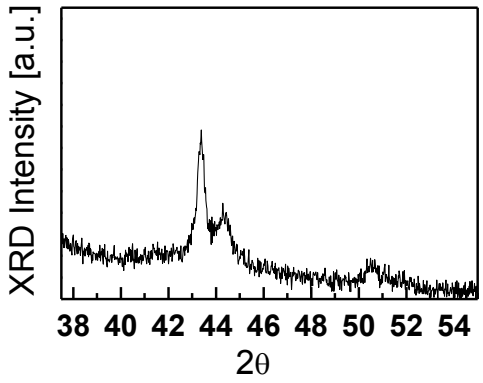

Figure 4.2: XRD of $Cu_{50}Ni_{50}$ colloidal solution

SEM images were used to measure particle size, shape and dispersion on a carbon support. A carbon support was used for SEM because carbon would have less electron static charging than YSZ or SDC. Two images are shown in Fig. 4.3 for both COMPO, composition, and LEI, lower secondary electron image, settings.

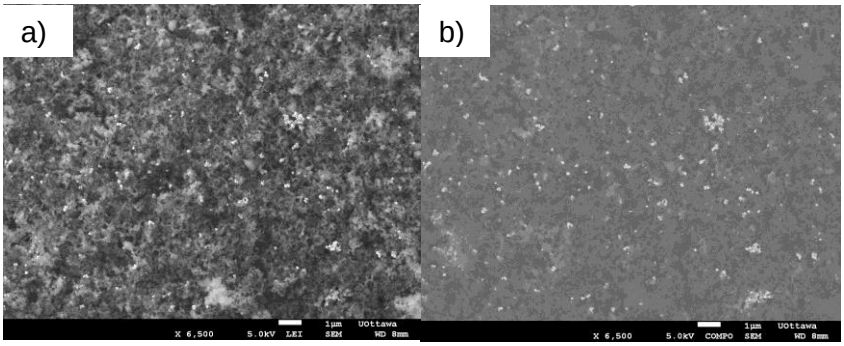

Figure 4.3: SEM of $Cu_{50}Ni_{50}$/C in a) LEI mode and b) COMPO mode

Light coloured regions are indicative of $Cu_{50}Ni_{50}$ particles and the darker coloured background represents the C support. These images show good dispersion of the metal on the support and also indicate agglomeration. Anti-agglomerating agents like polyvinylpyrrolidone (PVP) were not used to minimize the cost of the synthesis materials. A typical particle size observed in multiple SEM spectra was 30 nm.

4.3.2 Catalytic Performance

The only observable components in the gas stream entering the mass spectrometer were CO_2, H_2, CO, trace amounts of H_2O and the carrier gas, He. These results indicate that CO was the main product having a typical concentration of 2000 ppm. Other products including CH_4 had concentrations of less than the detection limit of the spectrometer, 50 ppm. These results with the CuNi/YSZ and CuNi/SDC catalysts were completely consistent with previous work using CuNi/C and CuNi/Al_2O_3 catalysts [24].

CO and CH_4 were the expected products with pure copper catalysts [9], [11], [14], [26] and pure nickel catalysts [14] respectively. The absence of CH_4 in this work might have been caused by the enhanced copper concentration on the catalyst surface. XPS analysis reported previously for $Cu_{50}Ni_{50}$/C catalysts [24] indicated that the surface atomic Cu/Ni was "2" , even though the bulk atomic Cu/Ni rate was "1". Perhaps any CO formed on Ni atom sites may have "spilled over" to Cu atom sites and desorbed prior to further hydrogenation to CH_4.

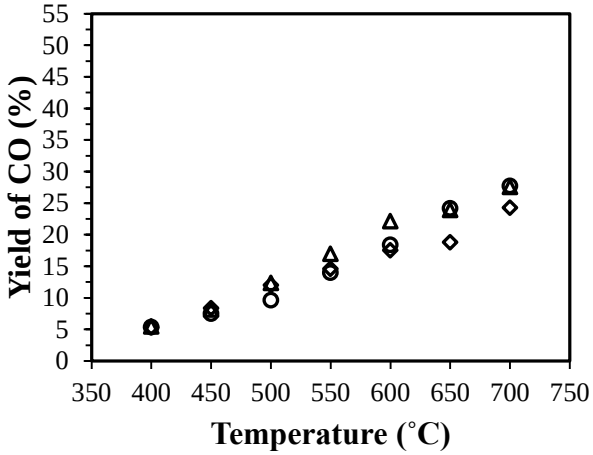

Figure 4.4: RWGS reaction at 1atm, $P_{H2} = P_{CO2} = 1$ kPa, balance He, GHSV = 716000 h^{-1}, 50 mg of catalyst: Pt/YSZ, 1 wt% catalyst where ○ = 1st cycle, △ = 2nd cycle and ◇ = 3rd cycle

The data in Figure 4.4 were obtained when the RWGS reaction was performed with a catalyst composed of platinum supported on a YSZ support. The CO yields obtained during all of the

cycles were similar at 400 and 450°C. In contrast the CO yields at 650 and 700°C for the third cycle were slightly less than those during the first and second cycles.

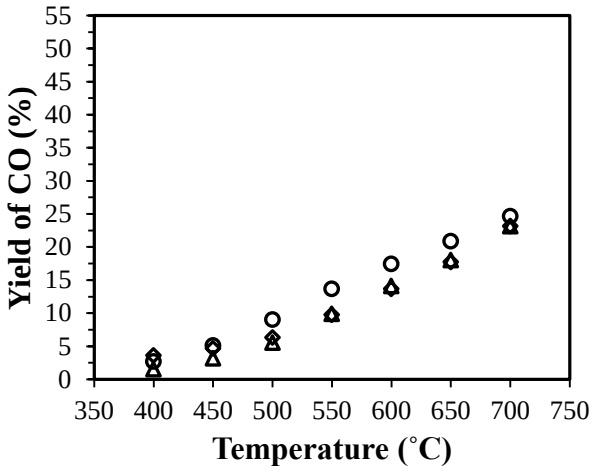

Figure 4.5: RWGS reaction at 1atm, $P_{H2} = P_{CO2} = 1$ kPa, balance He, GHSV = 716000 h^{-1}, 50 mg of catalyst: $Cu_{50}Ni_{50}$/YSZ, 10 wt% catalyst where ○ = 1st cycle, △ = 2nd cycle and ◇ = 3rd cycle

Figure 4.5 demonstrates the results obtained when the RWGS reaction was performed over a catalyst composed of CuNi nanoparticles supported on a YSZ support. The CO yields obtained during the second and third cycles were similar and were somewhat less than those obtained during the first cycle. It indicates that while some deactivation had occurred, the catalysts became thermally stable after the first cycle. Cu alone is known to be unstable at high temperatures [9], [11], [26]. It may be that the Ni in $Cu_{50}Ni_{50}$ stabilizes Cu so that the Ni provides the desired thermal stability and the Cu provides the desired CO yields.

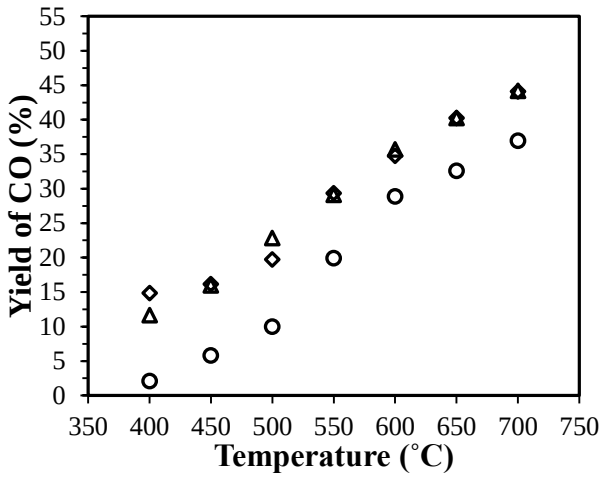

Figure 4.6: RWGS reaction at 1atm, $P_{H2} = P_{CO2} = 1$ kPa, balance He, GHSV = 960800 h^{-1}, 50 mg of catalyst: Pt/SDC, 1 wt% catalyst where ○ = 1st cycle, △ = 2nd cycle and ◇ = 3rd cycle

The data in Figure 4.6 shows the results obtained when Pt supported on a samarium-doped ceria support was used for the RWGS reaction. The CO yields obtained during the second and third cycles were superior to those obtained during the first cycle. This might be caused by a reduction of Pt oxide particles on the surface of the catalyst to metal Pt. Once reduced, its catalytic performance appears to be stable. The fact that similar CO yields were obtained during the second and third cycles indicates that no deactivation was apparent. The thermal stability shown by Pt was expected based on previous reports [16], [27]–[29]. The CO yields obtained with the Pt/SDC catalyst in Figure 4.6 were superior to those obtained with the Pt/YSZ catalyst in Figure 4.4.

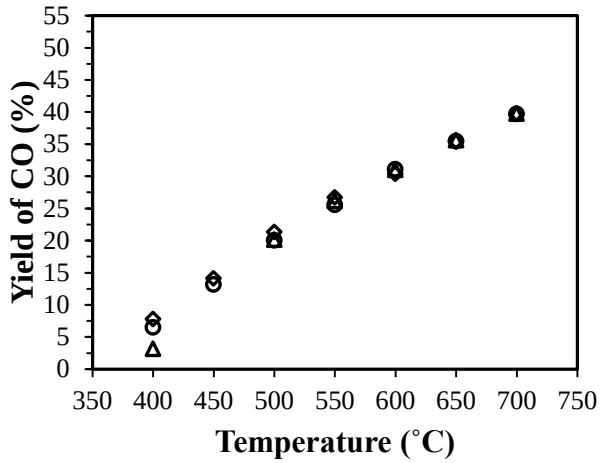

Figure 4.7: RWGS reaction at 1atm, $P_{H2} = P_{CO2} = 1$ kPa, balance He, GHSV = 960800 h^{-1}, 50 mg of catalyst: $Cu_{50}Ni_{50}$/SDC, 10 wt% catalyst where ○ = 1st cycle, △ = 2nd cycle and ◇ = 3rd cycle

The data in Figure 4.7 were obtained when CuNi nanoparticles supported on a samarium doped ceria support was used for the RWGS reaction. The CO yields obtained during all of the cycles were virtually the same, indicating that the catalyst was thermally stable and that there was no deactivation. The CO yields obtained with the $Cu_{50}Ni_{50}$ /SDC catalyst in Figure 4.7 were superior to those obtained with the $Cu_{50}Ni_{50}$/YSZ catalyst in Figure 4.5.

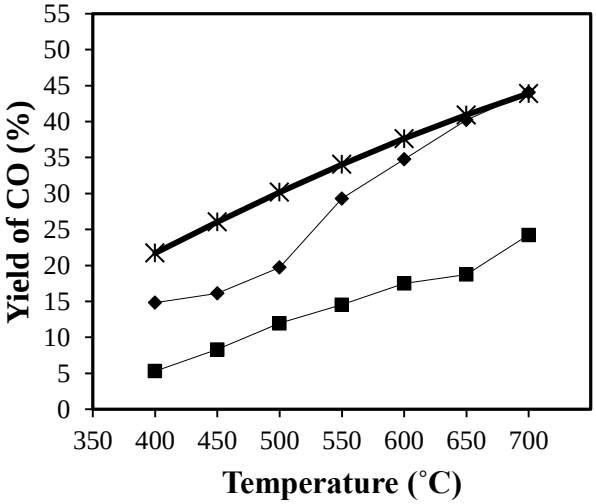

Figure 4.8: Average yield of CO for the RWGS reaction using Pt supported on SDC and YSZ at 1 atm. Total flow rate of 510mL·min^{-1}, $P_{CO2} = P_{H2} = 1$kPa, balance He. Where ✳ = equilibrium, ◆ = Pt/SDC and ■ = Pt/YSZ

The average yields of the two Pt catalysts are compared with the equilibrium CO yield in Figure 8. The CO yield with the Pt/SDC catalyst is better than that with the Pt/YSZ catalyst at all temperatures. The CO yield with the Pt/YSZ catalyst was always less than the equilibrium CO yield. Although the CO yield with the Pt/SDC catalyst was less than the equilibrium yield at lower temperatures, at 700°C the equilibrium CO yield was attained using the Pt/SDC catalyst.

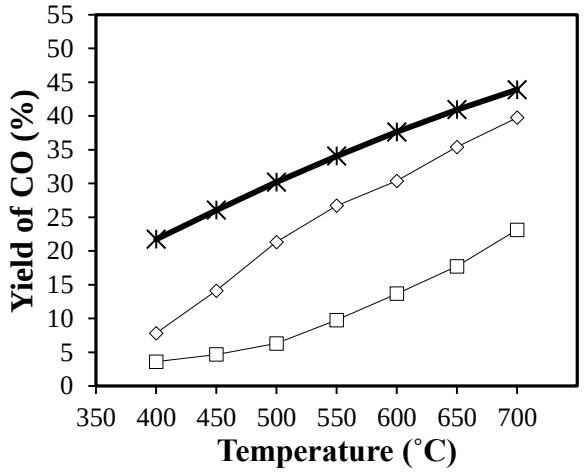

Figure 4.9: Average yield of CO for the RWGS reaction using $Cu_{50}Ni_{50}$ supported on SDC and YSZ at 1 atm. Total flow rate of 510 mL·min^{-1}, P_{CO2} = P_{H2} = 1kPa, balance He. Where ✳ = equilibrium, ◇ = $Cu_{50}Ni_{50}$ / SDC and □ = $Cu_{50}Ni_{50}$ / YSZ

The average yields of the two $Cu_{50}Ni_{50}$ catalysts are compared with the equilibrium yield in Figures 4.9. The CO yield with the $Cu_{50}Ni_{50}$/SDC catalyst is better than that with the $Cu_{50}Ni_{50}$/YSZ catalyst at all temperatures. In addition the CO yields with both catalysts are less than the equilibrium CO yields at all temperatures.

For both Pt and $Cu_{50}Ni_{50}$ catalysts the CO yields were greater with the SDC support than with the YSZ support. This is consistent with data reported by Ismail [19] for SDC and YSZ supports that did not contain $Cu_{50}Ni_{50}$. [15]. The CO yields may be related to the concentration of bulk phase oxygen vacancies in the two supports, 0.1 for SDC and 0.074 for YSZ.

Two supports having no bulk phase oxygen vacancies, C and γ-Al_2O_3, were investigated in previous work [24]. Their results with $Cu_{50}Ni_{50}$ nanoparticles were combined with the $Cu_{50}Ni_{50}$ nanoparticle results on YSZ and SDC supports and are shown in Figure 4.10. The CO yields in Figure 4.10 are definitely correlated with the oxygen vacancy content of the support. Other reaction results have also been correlated with oxygen vacancies. For example, the results Pekridis et al. [16] obtained using a solid oxide fuel cell (SOFC) at 650-800°C were explained in terms of oxygen vacancies.

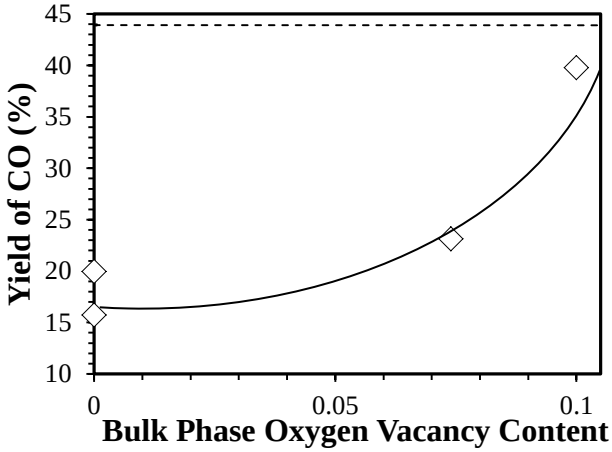

Figure 4.10: CO Yield versus bulk phase oxygen content in supports containing $Cu_{50}Ni_{50}$ nanoparticles at 700°C and 1 atm. Total flow rate of 510 mL·min^{-1}, $P_{CO2} = P_{H2}$ = 1kPa, balance He

The catalysts containing carbon and γ-Al_2O_3 supports had measurable CO yields even though they did not contain bulk phase oxygen vacancies. The surfaces of γ-Al_2O_3 contain oxygen vacancies. During the preparation of γ-Al_2O_3, hydroxyl groups are formed on the solid surface. When the solid is heated some of the hydroxyl groups combine to form a water molecule that enters the gas phase [30]. An oxygen anion and an oxygen vacancy are left behind on the solid alumina surface. The surfaces of carbon particles contain various oxygen groups including hydroxyls and carboxyls. When hydrogen is present at the reaction conditions of these experiments, water can be formed and enter the gas phase, leaving surface oxygen vacancies on

the surface. Although the carbon and γ-Al_2O_3 supports do not contain bulk phase oxygen vacancies, they do contain surface oxygen vacancies. The presence of surface oxygen vacancies would be consistent with the CO yields they obtained.

A diagram illustrating the bi-functional nature of the catalyst is shown in Figure 4.11. A catalytic mechanism can be suggested that involves the adsorption of hydrogen on the CuNi metal phases and the adsorption of carbon dioxide on the support. The amount of H_2 adsorbed on pure Ni is known to be five times greater than that adsorbed on pure Cu [31]. The amount of hydrogen adsorbed on CuNi alloys does not vary much with alloy composition and is approximately one-third of that adsorbed on pure Ni [31]. CO_2 adsorption on YSZ has been reported as a bicarbonate species [32]. Although we are not aware of any SDC data, CO_2 adsorption has also been reported on gallium doped ceria as a bicarbonate species [33].

Based on the above, the adsorption of the reactants can be expressed in the form of equations. CO_2 adsorbed on support oxygen vacancies, $V_o^x(S)$, might be represented as shown in

$$CO_2(g) + V_o^x(S) = CO_2(ads)\text{-}Sup \quad (4.5)$$

Equation 4.5. Hydrogen from the gas phase might be dissociatively adsorbed on the surface of the metal, where the electron on a dissociated hydrogen radical is shared with an empty orbital in the conduction band of the metal, $\square_{Me}$, as shown in Equation 4.6.

$$H_2(g) + 2\,\square_{Me} = 2\,H(ads)\text{-}Me \quad (4.6)$$

Eley-Rideal mechanisms might be operative in two ways. Hydrogen from the gas phase might react with adsorbed CO_2 as shown in Equations 4.7 and 4.8.

$$\tfrac{1}{2}\,H_2(g) + CO_2(ads)\text{-}Sup = OCOH(ads)\text{-}Sup \quad (4.7)$$

$$\tfrac{1}{2}\,H_2(g) + OCOH(ads)\text{-}Sup = CO(g) + H_2(g) + V_o^x(S) \quad (4.8)$$

Since the CO_2 adsorbed on the support reacts with hydrogen in the gas phase, it could reduce CO_2 to CO even if the catalyst did not contain metal particles, as was shown in other work reported by Ismail [15]. In his work, he described both YSZ and SDC catalysts that converted CO_2 to other products without a metallic component in the catalyst.

A second Eley-Rideal mechanism would occur if CO_2 in the gas phase reacted with adsorbed H_2 as shown in Equation 4.9. Vesselli et al [34], [35] has described the occurrence of the Eley-Rideal mechanism in RWGS reactions.

$$CO_2(g) + 2\,H(ads)\text{-}Me = CO(g) + H_2O(g) + 2\,\square_{Me} \quad (4.9)$$

A Langmuir-Hinshelwood mechanism might also be possible. The adsorbed hydrogen might react with the adsorbed CO_2 at the three-phase (metal-support-gas) boundary, as shown in Equations 4.10. Alternatively, the hydrogen adsorbed on the metal surface diffuses from the metal surface unto the support surface prior to reacting via Equation 4.10 (hydrogen spillover). The resulting species, OCOH(ads), might diffuse over a support surface by hopping from one oxygen vacancy to another until two OCOH(ads) species were adjacent to one another which

$$H(ads)\text{-}Me + CO_2(ads)\text{-}Sup = OCOH(ads)\text{-}Sup + \square_{Me} \quad (4.10)$$

might yield the reaction via Equation 4.11.

$$2\,OCOH(ads)\text{-}Sup = CO_2(ads)\text{-}Sup + V_o^x(S) + CO(g) + H_2O(g) \quad (4.11)$$

The rate of surface diffusion might be influenced by the concentration of oxygen vacancies on the support surface. In this case the reaction would occur on an extended region of the support surface surrounding the three-phase boundary. Pekridis et al. [5] proposed a similar Langmuir-Hinshelwood mechanism to explain results obtained with a solid oxide fuel cell.

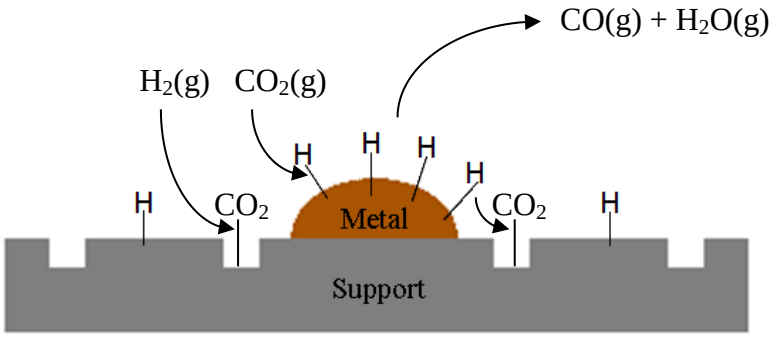

Figure 4.11: Diagram showing adsorbed species on the surface of a bifunctional catalyst operating through an Eley-Rideal and a Langmuir Hinshelwood mechanism

4.3.3. Partial Pressure Variation and Stability Measurements

The results of experiments in which the partial pressure of hydrogen was varied at constant CO_2 partial pressure are shown in Figure 4.12. Four different temperatures were used. At each temperature there was an increase in CO yield as the hydrogen partial pressure increased. The equilibrium constant, K_{RWGS}, shown in Equation 4.12, will be a different constant at each temperature.

$$K_{RWGS} = [CO][H_2O] / [CO_2]\,[H_2] \qquad (4.12)$$

Both the equilibrium CO partial pressure and the equilibrium CO yield will increase as the hydrogen partial pressure increases. Since the hydrogen partial pressure in the experiments increased by a factor four, the equilibrium CO yield would also be expected to increase by a factor of four, if the reaction was equilibrium limited. Since the increase in CO yield with H_2 partial pressure in Figure 12 is much less than a factor of four at all temperatures it can be suggested that the increase in CO yield may not entirely be caused by changes in equilibrium conditions.

Another possibility is that the reaction is kinetically limited. For a gas phase reaction, such as the Eley-Rideal mechanism, the rate might be expressed as shown in Equation 4.13. The

$$\text{Rate} = k * (p_{H2})^N \qquad (4.13)$$

data in Figure 4.13 are consistent with the notion that the increase in hydrogen partial pressure caused an increase in the kinetics of the reaction, because the CO yield increased as the hydrogen partial pressure increased.

CH_4 production was observed at H_2:CO_2 ratios greater than 2. CH_4 is undesirable for two reasons. The selling price of CH_4 is generally less than the cost of supplying the H_2 from which it is made. Furthermore, any increase in the amount of carbon used to make CH_4 means there is less carbon used to make CO that can be used in the Fischer-Tropsch process to make valuable hydrocarbons.

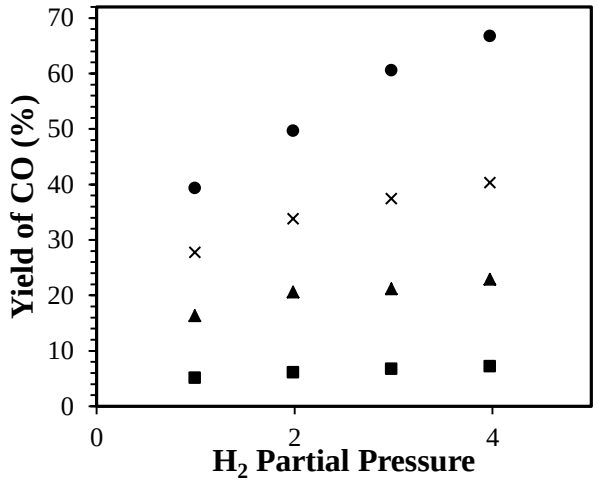

Figure 4.12: Partial pressure variation using $Cu_{50}Ni_{50}$/SDC at varying temperatures. GHSV = 960800 h^{-1}. P_{CO2} = cst. Total flow rate of 510 mL·min^{-1}. Where ● = 700°C, × = 600°C, ▲ = 500°C and ■ = 400°C

The results of experiments in which the partial pressure of carbon dioxide was varied at constant H_2 partial pressure are shown in Figure 4.13. Four different temperatures were used. At each temperature there was a decrease in CO yield as the CO_2 partial pressure increased. If the concentration of adsorbed CO_2 on the support surface increased with increasing CO_2 partial pressure, the surface concentration of oxygen vacancies would decrease. Fewer oxygen vacancies on the support surface would suggest that the rate of diffusion of OCOH(ads) species

might decrease. Therefore the decrease in CO yield observed in Figure 4.13 is consistent with the hypothesis that the concentration of oxygen vacancies on the support surface influences the rate of surface diffusion of OCOH(ads) reaction intermediate species.

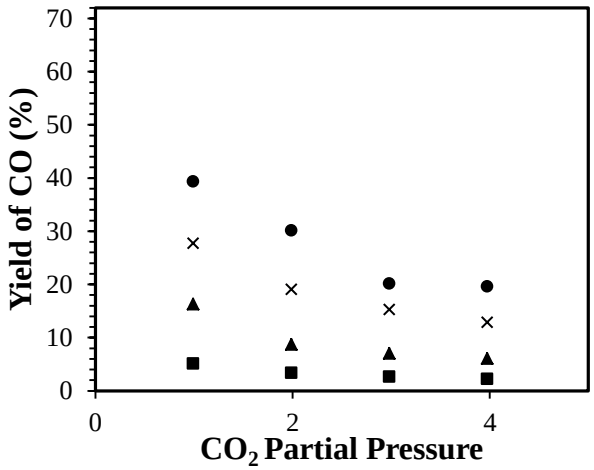

Figure 4.13: Partial pressure variation using $Cu_{50}Ni_{50}$/SDC at varying temperatures. GHSV = 960800 h^{-1}. P_{H2} = cst. Total flow rate of 510 mL·min^{-1}. Where ● = 700°C, × = 600°C, ▲= 500°C and ■ = 400°C

Time-on-stream experiments were performed in order to examine the catalyst's thermal stability over a 48-hour period, 24 hours at 700°C and subsequently another 24 hours at 600°C. The results are shown in Figure 4.14. No deactivation was apparent.

This is a significant achievement in the use of a Cu catalyst for the RWGS reaction. Previous studies suggested that Cu is inadequate for use at high temperatures because of its tendency to deactivate over time [11], [12]. However, the results in Figure 4.14 demonstrated CO yields that approached the equilibrium CO yield and the results in Figure 4.14 suggested long-term thermal stability.

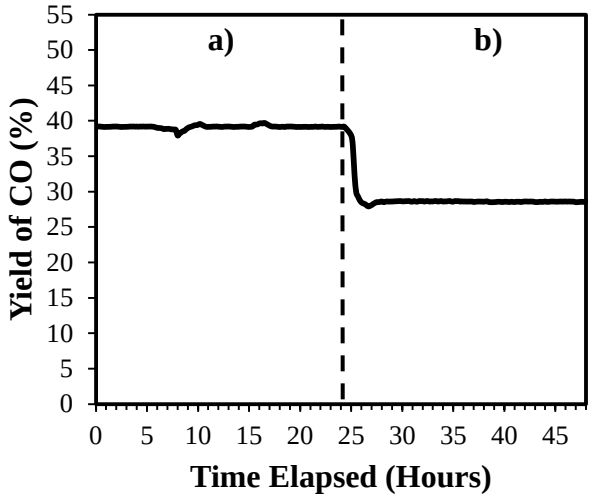

Figure 4.14: Stability measurements of $Cu_{50}Ni_{50}$/SDC for 2 consecutive days of testing at **a)** 700°C and **b)** 600°C. GHSV = 960800 h^{-1}. Total flow rate of 510 $mL \cdot min^{-1}$

The favorable results reported here can probably be attributed to Cu being used as a CuNi alloy catalyst. The Ni component is most likely responsible for the thermal stability. The 100 % selectivity to CO may be attributed to the CuNi alloy surface having a much greater concentration of Cu than the bulk CuNi alloy. A large surface concentration of Cu diminishes the tendency for CH_4 to be formed on Ni.

All of the results reported here were obtained at small partial pressures of hydrogen. The experiments performed at H_2 partial pressures of 2 kPa and greater showed that CH_4 was formed and that 100 % selectivity to CO was not obtained. There may be merit in performing future experiments at greater hydrogen partial pressures with CuNi alloy catalysts that have larger Cu/Ni ratios than the one used in this investigation, since it is known [24] that the surface Cu/Ni ratio increases non-linearly with the bulk Cu/Ni ratio.

4.4 Summary and Conclusion

$Cu_{50}Ni_{50}$ nanoparticles were successfully synthesized using a modified polyol method that caused both the copper and nickel compounds to be reduced simultaneously and thereby

form CuNi alloy nanoparticles. CO yields with Pt/SDC catalysts equaled equilibrium CO yields at 650 and 700°C. In contrast CO yields with $Cu_{50}Ni_{50}$/SDC catalysts were about 90% of the equilibrium CO yields at 650 and 700°C. Catalysts with YSZ supports had CO yields that were approximately 55% of the CO yields obtained with catalysts having SDC supports.

The catalyst selectivity to CO was essentially 100% for the experiments performed at a hydrogen partial pressure of 1 kPa. That may have been caused in part by the Cu content of the catalyst surface being substantially greater than that in the bulk catalyst. When experiments were performed using hydrogen partial pressures of 2 kPa or greater, an increase in the CO yield was observed but methane was observed in the product gas, thereby decreasing the selectivity to CO. When the partial pressure of CO_2 was increased the CO yield decreased. The reaction results were explained using a combination of Eley-Rideal and Langmuir-Hinshelwood mechanisms that involved adsorption on the metal surface and the concentration of oxygen vacancies in the support. Finally the $Cu_{50}Ni_{50}$/SDC catalyst was found to be thermally stable for 48 hours at 650/700°C.

Because the costs of Cu and Ni are substantially less than for Pt and because the performance of the $Cu_{50}Ni_{50}$/SDC catalysts approached the performance of Pt/SDC catalysts more extensive testing of supported CuNi catalysts is warranted.

4.5 Acknowledgements

Both the Natural Sciences and Engineering Research Council (NSERC) and Phoenix Canada Oil Company Limited are gratefully acknowledged for their financial support.

4.6 References

[1] T. F. Stocker, D. Qin, G.-K. Plattner, M. Tignor, S. K. Allen, J. Boschung, A. Nauels, Y. Xia, V. Bex, and P. M. Midgley, "Climate Change 2013: The Physical Science Basis Working Group I Contribution to the Fifth Assessment Report of the Intergovernmental Panel on Climate Change Edited by," *Cambridge University Press*, 2013.

[2] W. Wang, S. Wang, X. Ma, and J. Gong, "Recent advances in catalytic hydrogenation of carbon dioxide.," *Chem. Soc. Rev.*, vol. 40, no. 7, pp. 3703–27, Jul. 2011.

[3] P. Vibhatavata, J.-M. Borgard, M. Tabarant, D. Bianchi, and C. Mansilla, "Chemical recycling of carbon dioxide emissions from a cement plant into dimethyl ether, a case study of an integrated process in France using a Reverse Water Gas Shift (RWGS) step," *Int. J. Hydrogen Energy*, vol. 38, no. 15, pp. 6397–6405, May 2013.

[4] S. S. Kim, K. H. Park, and S. C. Hong, "A study of the selectivity of the reverse water–gas-shift reaction over Pt/TiO2 catalysts," *Fuel Process. Technol.*, vol. 108, pp. 47–54, Apr. 2013.

[5] S. S. Kim, H. H. Lee, and S. C. Hong, "A study on the effect of support's reducibility on the reverse water-gas shift reaction over Pt catalysts," *Appl. Catal. A Gen.*, vol. 423–424, pp. 100–107, May 2012.

[6] S. S. Kim, H. H. Lee, and S. C. Hong, "Applied Catalysis B : Environmental The effect of the morphological characteristics of TiO2 supports on the reverse water – gas shift reaction over Pt/TiO2 catalysts," *"Applied Catal. B, Environ.*, vol. 119–120, pp. 100–108, 2012.

[7] C. Chen, C. Ruan, Y. Zhan, X. Lin, Q. Zheng, and K. Wei, "The significant role of oxygen vacancy in Cu/ZrO2 catalyst for enhancing water–gas-shift performance," *Int. J. Hydrogen Energy*, vol. 39, no. 1, pp. 317–324, Jan. 2014.

[8] J. Papavasiliou, G. Avgouropoulos, and T. Ioannides, "Effect of dopants on the performance of CuO–CeO2 catalysts in methanol steam reforming," *Appl. Catal. B Environ.*, vol. 69, no. 3–4, pp. 226–234, Jan. 2007.

[9] F. S. Stone and D. Waller, "Cu-ZnO and Cu–ZnO/Al2O3 catalysts for the reverse water-gas shift reaction . The effect of the Cu/Zn ratio on precursor characteristics and on the activity of the derived catalysts," *Top. Catal.*, vol. 22, no. April, pp. 305–318, 2003.

[10] C. S. Chen, J. H. Wu, and T. W. Lai, "Carbon Dioxide Hydrogenation on Cu Nanoparticles," *J. Phys. Chem. C*, pp. 15021–15028, Aug. 2010.

[11] C. Chen, W.-H. Cheng, and S.-S. Lin, "Study of iron-promoted Cu/SiO2 catalyst on high temperature reverse water gas shift reaction," *Appl. Catal. A Gen.*, vol. 257, no. 1, pp. 97–106, Jan. 2004.

[12] C. Chen, W. Cheng, and S. Lin, “Study of reverse water gas shift reaction by TPD , TPR and CO2 hydrogenation over potassium-promoted Cu/SiO2 catalyst,” *Appl. Catal. A Gen.*, vol. 238, pp. 55–67, 2003.

[13] C. S. Chen, J. H. Lin, J. H. You, and K. H. Yang, “Effects of potassium on Ni-K/Al2O3 catalysts in the synthesis of carbon nanofibers by catalytic hydrogenation of CO2.,” *J. Phys. Chem. A*, vol. 114, no. 11, pp. 3773–81, Mar. 2010.

[14] Y. Liu and D. Liu, “Study of bimetallic Cu-Ni/ gamma Al2O3 catalysts for carbon dioxide hydrogenation,” *J. Hydrog. Energy*, vol. 24, pp. 351–354, 1999.

[15] M. Ismail, “Model Development and Validation of Samaria Doped Ceria (SDC) Based Solid Oxide Fuel Cell Operating with Practical Fuels,” Univiersity of Waterloo, 2013.

[16] G. Pekridis, K. Kalimeri, N. Kaklidis, E. Vakouftsi, E. F. Iliopoulou, C. Athanasiou, and G. E. Marnellos, “Study of the reverse water gas shift (RWGS) reaction over Pt in a solid oxide fuel cell (SOFC) operating under open and closed-circuit conditions,” *Catal. Today*, vol. 127, no. 1–4, pp. 337–346, Sep. 2007.

[17] T. H. Etsell and S. N. Flengas, “The Electrical Properties of Lanthanum Oxide-Calcium Oxide Solid Electrolytes,” *J. Electrochem. Soc.*, vol. 116, no. 6, p. 771, 1969.

[18] C. Zhang, C.-J. Li, G. Zhang, X.-J. Ning, C.-X. Li, H. Liao, and C. Coddet, “Ionic conductivity and its temperature dependence of atmospheric plasma-sprayed yttria stabilized zirconia electrolyte,” *Mater. Sci. Eng. B*, vol. 137, no. 1–3, pp. 24–30, Feb. 2007.

[19] W. Dow and T. Huang, “Effects of Oxygen Vancancy of Yttria-Stabilized Zirconia Support on Carbon Monoxide Oxidation over Copper Catalyst,” *J. Catal.*, vol. 147, pp. 322–332, 1994.

[20] W. Dow, Y. Wang, and T.-J. Huang, “Yttria-Stabilized Zirconia Supported Copper Oxide Catalyst,” *J. Catal.*, vol. 170, no. 0135, pp. 155–170, 1996.

[21] G. Avgouropoulos, M. Manzoli, F. Boccuzzi, T. Tabakova, J. Papavasiliou, T. Ioannides, and V. Idakiev, “Catalytic performance and characterization of Au/doped-ceria catalysts for the preferential CO oxidation reaction,” *J. Catal.*, vol. 256, no. 2, pp. 237–247, Jun. 2008.

[22] H. Yahiro, K. Eguchi, and H. Arai, “Electrical properties and reducibilities of ceria-rare earth oxide systems and their application to solid oxide fuel cell,” *Solid State Ionics*, vol. 36, no. 1–2, pp. 71–75, Oct. 1989.

[23] R. J. Isaifan, H. A. E. Dole, E. Obeid, L. Lizarraga, E. A. Baranova, and P. Vernoux, “Catalytic CO Oxidation over Pt nanoparticles prepared from the Polyol Reduction

Method supported on Yttria-Stabilized Zirconia .," *Electrochem. Soc.*, vol. 35, no. 28, pp. 43–57, 2011.

[24] M. Lortie, "M.A.Sc. Dissertation,University of Ottawa, Chapter 3," University of Ottawa, 2014.

[25] R. J. Isaifan, S. Ntais, and E. A. Baranova, "Particle size effect on catalytic activity of carbon-supported Pt nanoparticles for complete ethylene oxidation," *Appl. Catal. A Gen.*, vol. 464–465, pp. 87–94, Aug. 2013.

[26] J. Papavasiliou, G. Avgouropoulos, and T. Ioannides, "Effect of dopants on the performance of CuO–CeO2 catalysts in methanol steam reforming," *Appl. Catal. B Environ.*, vol. 69, no. 3–4, pp. 226–234, Jan. 2007.

[27] A. Dauscher, L. Hilaire, F. Le Normand, W. Miiller, G. Maire, and A. Vasqwz, "Characterization by XPS and XAS of Supported Pt/TiO2-CeO2 Catalysts," vol. 16, pp. 341–346, 1990.

[28] C. M. Kalamaras, P. Panagiotopoulou, D. I. Kondarides, and A. M. Efstathiou, "Kinetic and mechanistic studies of the water–gas shift reaction on Pt/TiO2 catalyst," *J. Catal.*, vol. 264, no. 2, pp. 117–129, Jun. 2009.

[29] A. Goguet, F. C. Meunier, D. Tibiletti, J. P. Breen, and R. Burch, "Spectrokinetic Investigation of Reverse Water-Gas-Shift Reaction Intermediates over a Pt/CeO2 Catalyst," *Phys. Chem.*, vol. 108, pp. 20240–20246, 2004.

[30] J. B. Peri, "A Model for the Surface of Gamma-Alumina," *J. Phys. Chem.*, vol. 69, pp. 220–230, 1965.

[31] D. . Cadenhead and N. . Wagner, "Low-Temperature Hydrogen Adsorption on Copper-Nickel Alloys," *J. Phys. Chem.*, vol. 78, pp. 2775–2781, 1968.

[32] E. Kock, M. Kogler, T. Bielz, B. Klo, and S. Penner, "In Situ FT-IR spectroscopic study of CO2 and CO adsorption on Y2O3, ZrO2, and yttria-stabilized ZrO2," *J. Phys. Chem.*, 2013.

[33] G. Finos, S. Collins, G. Blanco, E. del Rio, J. M. Cíes, S. Bernal, and A. Bonivardi, "Infrared spectroscopic study of carbon dioxide adsorption on the surface of cerium–gallium mixed oxides," *Catal. Today*, vol. 180, pp. 9–18, Jan. 2012.

[34] E. Vesselli, J. Schweicher, A. Bundhoo, A. Frennet, and N. Kruse, "Catalytic CO2 Hydrogenation on Nickel : Novel Insight by Chemical Transient Kinetics," *J. Phys. Chem. CJournal Phys. Chem. C*, vol. 115, pp. 1255–1260, 2011.

[35] E. Vesselli, M. Rizzi, L. De Rogatis, X. Ding, A. Baraldi, G. Comelli, L. Savio, L. Vattuone, M. Rocca, P. Fornasiero, A. Baldereschi, and M. Peressi, "Hydrogen-Assisted

Transformation of CO2 on Nickel: The Role of Formate and Carbon Monoxide," *J. Phys. Chem. Lett.*, vol. 1, no. 1, pp. 402–406, Jan. 2010.

Chapter 5 – General Discussion

5.1 Introduction

The main goal of the Thesis was to identify a useful catalyst capable of being used industrially. This catalyst therefore needs to be relatively inexpensive to synthesize. The catalyst also needs to be selective to CO production, have high CO yields and be stable at high operating temperatures.

CuNi nanoparticles were chosen as a potential catalyst for the RWGS reaction. The main goal was to combine high CO selectivity achieved when using Cu nanoparticles [1], [2] and good stability at high temperatures when using Ni nanoparticles [3]–[5]. An alloy of the two compounds was considered to be a possible stable and selective catalyst capable of achieving high CO yields.

Finding a simple and efficient synthesis method for producing CuNi nanoparticles was one of the objectives of Chapter 3. These nanoparticles were then characterised using X-ray diffraction (XRD), scanning electron microscopy (SEM), energy dispersive x-ray spectroscope (EDS) and x-ray photoelectron spectroscopy (XPS) with the goal of identifying the size, content and morphology of the nanoparticles.

One batch of nanoparticles was synthesized and repeatedly used throughout the research. Because of this, the characterizations shown throughout Chapter 3 are applicable when analyzing results in Chapter 4. Using the same CuNi nanoparticles was necessary to study the effect of different supports on the RWGS reaction. In Chapter 3, the metal was supported on powders containing no stoichiometric oxygen vacancies (carbon and gamma-alumina). In Chapter 4, it

was deposited on supports containing stoichiometric oxygen vacancies (samarium-doped ceria, SDC, and yttria-stabilized zirconia, YSZ).

Another objective was to compare the performance of the CuNi nanocatalyst to a Pt nanocatalyst when both are deposited on the same supports. Pt was used as basis of comparison because Pt group metals (PGM) are usually good hydrogenation catalysts [2]. The Pt nanoparticles were already synthesized and characterised previously and had been shown to be a good working catalysts for other reactions [6]–[8].

Different Cu_xNi_{1-x} (x=20, 50, 80) ratios were used in Chapter 3. The best working Cu-Ni ratio was chosen for further testing which was described in Chapter 4 on supports containing stoichiometric oxygen vacancies.

5.2 Results and Discussion

The physical characterization of the CuNi nanoparticles produced several important results. XPS analysis done in Chapter 3 showed enriched Cu on the surface of the three Cu_xNi_{1-x} (x=20,50,80) metals. The XRD spectra showed shifts in both Cu (111) and Ni (111) peaks for all three CuNi ratios which indicated the presence of alloyed species.

Results obtained in Chapter 3 showed signs of stability at high temperatures. The $Cu_{50}Ni_{50}$/C catalyst was cycled 3 times for a total on-stream time of 24h showing no signs of deactivation after the second cycle. High selectivity towards CO was also observed since no CH_4 was measured during any of the experiments during Chapter 3.

The $Cu_{50}Ni_{50}$ metal catalyst was chosen in Chapter 4 due to its good yield and high stability. This catalyst was deposited on SDC and YSZ. Similar to the results obtained in Chapter 3, the CuNi catalysts showed no deactivation after the second cycle. In addition, the catalyst was

tested for a total of 48 h at 600 and 700°C showing no deactivation. This can be seen in Figure 5.1 below. CH_4 was not detected during any of the experiments when H_2 and CO_2 were fed stoichiometrically ($P_{H2}/P_{CO2} = 1$).

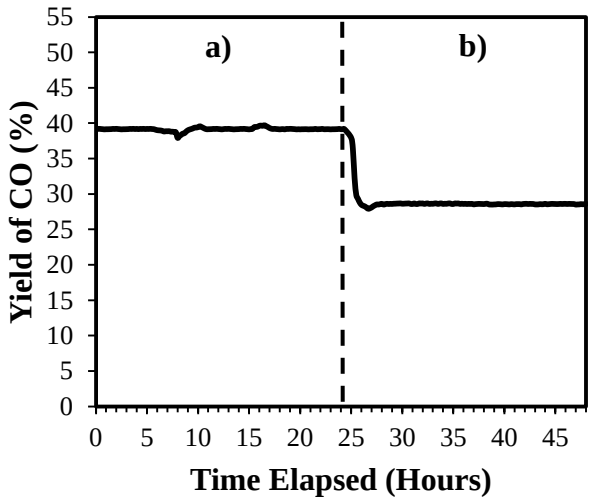

Figure 5.1: Stability measurements of $Cu_{50}Ni_{50}$/SDC for 2 consecutive days of testing at **a)** 700°C and **b)** 600°C. GHSV = 960800 h^{-1}. Total flow rate of 510 mL·min^{-1}

These results are explained using the physical characterization obtained in Chapter 3. It is hypothesized that CO selectivity is caused by the enrichment of Cu that was measured on the surface of the catalyst. In addition, it is hypothesized that the high stability of the catalyst may be caused by the presence of an alloyed metal. This was also reported in other research when Fe was used as stabilizer [9].

Support interaction has been shown to be an important aspect of catalysis. For example yield can be dependent on the support. The influence of catalyst-support interaction can be seen when comparing the data of Chapter 3 to the data in Chapter 4. Supports containing no stoichiometric oxygen vacancies were used in Chapter 3 (C and γ-Al_2O_3) while supports containing stoichiometric oxygen vacancies were used in Chapter 4 (YSZ and SDC). The effect of oxygen vacancies on CO yield from the RWGS reaction is evident in Figure 5.2. This is

consistent with other research reports which showed that the WGS reaction was accelerated using ZrO_2 containing oxygen vacancies [10]. Pt was also tested with the different supports. Similarly to CuNi, Pt showed increasing yield with supports containing oxygen vacancies as shown in Figure 5.2.

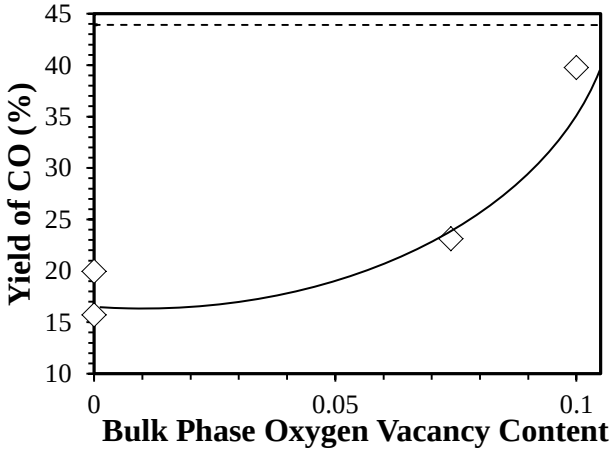

Figure 5.2: CO yield versus bulk phase oxygen content in supports containing $Cu_{50}Ni_{50}$ nanoparticles at 700°C and 1 atm. Total flow rate of 510 mL·min^{-1}, $P_{CO2} = P_{H2} = 1$kPa, balance He. Dashed line = equilibrium

A reaction mechanism was suggested in Chapter 4 which could explain the increased yield of CO obtained when using supports containing oxygen vacancies. Both Langmuir-Hinshelwood and Eley-Rideal mechanisms would be occurring in the reaction. A diagram shown in Figure 5.3 demonstrates how both pathways may be possible. It was hypothesized that CO_2 could adsorb on the surface of the support through its oxygen vacancy and subsequently could react with either gaseous H_2 or adsorbed H.

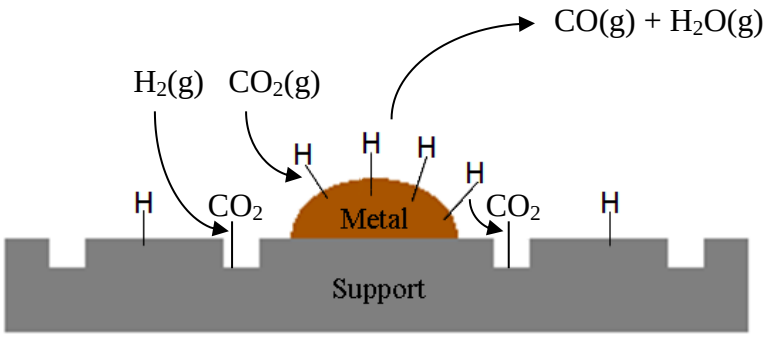

Figure 5.3: Diagram showing adsorbed species on the surface of a bifunctional catalyst operating through an Eley-Rideal and a Langmuir Hinshelwood mechanism

Both Chapters 3 and 4 compare results obtained using CuNi nanoparticle catalysts with Pt nanoparticle catalysts. In both cases, the yield of CO is comparable. Figure 5.4 compares CuNi to Pt when SDC is used as a support. Furthermore, it is speculated that CO yields might be increased to the equilibrium yield achieved with Pt that was obtained at 700°. Improving the synthesis method through the use of polyvinilpyrrolidone (PVP) or through pH and temperature variations might cause modifications to the physical properties of the nanoparticles making them different shapes or sizes [11]. These variations have been reported to be useful according to reports in literature [12]. Also, changing the metal loading of the catalyst may cause improved performance.

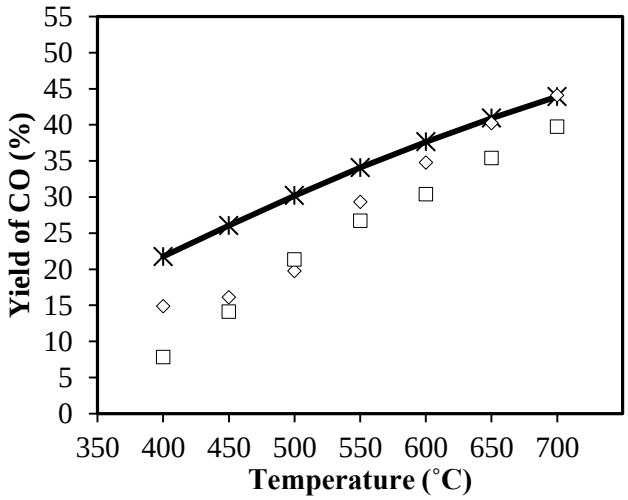

Figure 5.4: Average yield of CO for the RWGS reaction using $Cu_{50}Ni_{50}$ and Pt supported on SDC at 1 atm. Total flow rate of 510 mL·min^{-1}, $P_{CO2} = P_{H2}$ = 1kPa, balance He. Where ✳ = equilibrium, ◇ = Pt / SDC and □ = $Cu_{50}Ni_{50}$ / SDC

5.3 Conclusion

By combining the information in Chapters 3 and 4, several trends in the results were illustrated. They included high selectivity, stability and increased performance when using supports containing oxygen vacancies. A diagram was prepared to illustrate some possible reaction mechanisms that might occur in the RWGS reaction. In the future, the performance of a modified CuNi metal catalyst for the RWGS reaction might approach that of the Pt catalyst with all four supports (C, γ-Al_2O_3, YSZ and SDC). Finally, an important advantage of CuNi alloys is that they cost substantially less than Pt

5.4 References

[1] Y. Liu and D. Liu, "Study of bimetallic Cu-Ni/ gamma Al2O3 catalysts for carbon dioxide hydrogenation," *J. Hydrog. Energy*, vol. 24, pp. 351–354, 1999.

[2] W. Wang, S. Wang, X. Ma, and J. Gong, "Recent advances in catalytic hydrogenation of carbon dioxide.," *Chem. Soc. Rev.*, vol. 40, no. 7, pp. 3703–27, Jul. 2011.

[3] L. Wang, S. Zhang, and Y. Liu, "Reverse water gas shift reaction over Co-precipitated Ni-CeO2 catalysts," *J. Rare Earths*, vol. 26, pp. 66–70, 2008.

[4] J. M. Bermúdez, B. Fidalgo, a. Arenillas, and J. a. Menéndez, “CO2 reforming of coke oven gas over a Ni/γAl2O3 catalyst to produce syngas for methanol synthesis,” *Fuel*, vol. 94, pp. 197–203, Apr. 2012.

[5] C. Schild, A. Wokaun, R. A. Koeppel, and A. Baiker, “CO2 Hydrogenation over Nickel / Zirconia Catalysts from Amorphous Precursors : On the Mechanism of Methane Formation,” *J. Phys. Chem.*, vol. 95, pp. 6341–6346, 1991.

[6] R. J. Isaifan, H. A. E. Dole, E. Obeid, L. Lizarraga, P. Vernoux, and E. A. Baranova, “Metal-Support Interaction of Pt Nanoparticles with Ionically and Non-Ionically Conductive Supports for CO Oxidation,” *Electrochem. Solid-State Lett.*, vol. 15, no. 3, p. E14, 2012.

[7] H. A. E. Dole, R. J. Isaifan, F. M. Sapountzi, L. Lizarraga, D. Aubert, A. Princivalle, P. Vernoux, and E. A. Baranova, “Low Temperature Toluene Oxidation Over Pt Nanoparticles Supported on Yttria Stabilized-Zirconia,” *Catal. Letters*, vol. 143, no. 10, pp. 996–1002, Jul. 2013.

[8] R. J. Isaifan, H. A. E. Dole, E. Obeid, L. Lizarraga, E. A. Baranova, and P. Vernoux, “Catalytic CO Oxidation over Pt nanoparticles prepared from the Polyol Reduction Method supported on Yttria-Stabilized Zirconia .,” *Electrochem. Soc.*, vol. 35, no. 28, pp. 43–57, 2011.

[9] C. Chen, W.-H. Cheng, and S.-S. Lin, “Study of iron-promoted Cu/SiO2 catalyst on high temperature reverse water gas shift reaction,” *Appl. Catal. A Gen.*, vol. 257, no. 1, pp. 97–106, Jan. 2004.

[10] C. Chen, C. Ruan, Y. Zhan, X. Lin, Q. Zheng, and K. Wei, “The significant role of oxygen vacancy in Cu/ZrO2 catalyst for enhancing water–gas-shift performance,” *Int. J. Hydrogen Energy*, vol. 39, no. 1, pp. 317–324, Jan. 2014.

[11] K. J. Carroll, J. U. Reveles, M. D. Shultz, S. N. Khanna, and E. E. Carpenter, “Preparation of Elemental Cu and Ni Nanoparticles by the Polyol Method: An Experimental and Theoretical Approach,” *J. Phys. Chem. C*, vol. 115, no. 6, pp. 2656–2664, Feb. 2011.

[12] R. J. Isaifan, S. Ntais, and E. A. Baranova, “Particle size effect on catalytic activity of carbon-supported Pt nanoparticles for complete ethylene oxidation,” *Appl. Catal. A Gen.*, vol. 464–465, pp. 87–94, Aug. 2013.

Chapter 6: Conclusion

6.1 Summary of Results

The objectives of the Thesis were separated into four sections and each addressed throughout this work. The following section aims to summarize and conclude the findings achieved by completing the prescribed objectives. The objectives were as follows:

Objective 1: Develop a synthesis method producing Cu_xNi_{1-x} nanoparticles

Objective 2: Characterize the Cu_xNi_{1-x} catalysts

Objective 3: Establish a "best case scenario" using an established noble metal (Pt) based nanocatalyst

Objective 4: Investigate the performance of Cu_xNi_{1-x} nanoparticles deposited on supports having varying oxygen vacancy content for the RWGS reaction

6.1.1 Objective 1: Synthesis of Cu_xNi_{1-x} nanoparticles

CuNi nanoparticles were successfully synthesized using a novel polyol method. This method was simple, time efficient and yielded nanoparticles of a certain size distribution (4 nm - 100 nm) without the use of stabilizers such as PVP (polyvinylpyrrolidone). Cu and Ni nitrates were used as salt precursors dissolved in ethylene glycol. NaOH was used as pH adjuster increasing both solutions' pH to 11. The nickel nitrate solution was first refluxed at 196C and showed no signs of reduction to metallic nickel. The copper solution (room temperature) was then added resulting in the reduction of both species to metallic nanoparticles. Once cooled, the colloids were stored in their ethylene glycol solution.

The particles were deposited using an impregnation technique on a total of 4 supports: samarium-doped ceria, SDC, yttria-stabilized zirconia, YSZ, gamma-alumina, γ-Al_2O_3, and

carbon, C. The technique involved inserting a certain amount of the support in a beaker and injecting the colloids on top of the solution. The mixture was then sonicated and mixed for 24 hours. De-ionized water was then used to wash the powder removing impurities. The mixture was washed and centrifuged 10 times.

6.1.2 Objective 2: Characterization of the Cu_xNi_{1-x} catalysts

Characterization of the CuNi nanoparticles was done using several techniques including: scanning electron microscopy, SEM, energy-dispersive X-ray spectroscope, EDS, x-ray diffraction, XRD, and x-ray photoelectectron spectroscopy, XPS. Several findings were obtained using the aforementioned characterization techniques.

SEM micrographs of the carbon supported CuNi nanoparticles were taken in order to examine particle morphology and distribution. Spherical particles were the main shape observed in all micrographs. Typical SEM particle sizes observed are shown in Table. 6.1. Some agglomeration was observed principally due to the lack of stabilizer used during the synthesis. There were no observable differences between the particles before exposure to reaction conditions and after.

Table 6.1: Cu_xNi_{1-x} / Carbon physical characteristics

Catalyst	XRD Crystalline size (nm)	SEM Typical particle size (nm)
$Cu_{80}Ni_{20}$ / C	30.2	64.4
$Cu_{50}Ni_{50}$ / C	24	53.4
$Cu_{20}Ni_{80}$ / C	16.7	41.1

EDS was used to obtain the bulk composition of a small sample (2-5 nanoparticles) of the CuNi nanoparticles. There was a good agreement between the calculated ratios and those obtained through EDS measurements.

XRD spectra of the CuNi colloids were taken and analyzed with the goal of confirming the presence of both Cu and Ni metals as well as determine if the formation of an alloy was observed. Two distinct 111 peaks were obtained for the $Cu_{50}Ni_{50}$ and $Cu_{20}Ni_{80}$ particles and only one was observed for the $Cu_{80}Ni_{20}$ sample. All peaks were shifted inwards from pure Cu peak (43.2 ICSD Collection Code: 53246) and the pure Ni peak (44.6 ICSD Collection Code: 43397) suggesting that the particles contained a Cu rich solid solution and, for $Cu_{50}Ni_{50}$ and $Cu_{20}Ni_{80}$, a Ni rich solid solution in addition to the Cu rich solid solution. No salt was observed in any of the XRD spectra. Crystalline sizes were obtained using Scherer's' formula and are given in Table. 6.1 for all of the CuNi colloids.

An XPS analysis of the surface composition of each of the carbon supported CuNi catalysts was performed in order to identify to main specie found on the catalytic surface. All three catalysts were determined to have increased Cu concentrations on the surfaces than what was found in the bulk. This was consistent with literature [1]–[3].

6.1.3 Objective 3: Supported Pt Nanoparticles for the RWGS Reaction

Pt supported nanoparticles were previously synthesized using a synthesis method described elsewhere [4]. The supports were C, γ-Al_2O_3, YSZ and SDC. 50 mg of each catalyst was tested for the RWGS reaction under atmospheric pressure and with temperatures ranging from 400°C to 700°C. This was repeated for 3 cycles.

Gamma-alumina proved to be unstable at high temperatures. This was consistent with literature [5]. Otherwise, the catalysts showed signs of stability with all other supports during the 3 cycles for the temperature range used.

The C supported catalyst showed the lowest conversion of all supports used. There was a clear distinction between the traditional supports (C and γ-Al_2O_3) and the two other supports containing stoichiometric oxygen vacancies (YSZ and SDC). Pt/YSZ produced a good yield of CO at all temperatures but did not approach equilibrium. Pt/SDC reached the equilibrium yield to CO at 700°C (43.9%). The results are shown in Figure 6.1. There was no sign of CH_4 production during any of the experiments.

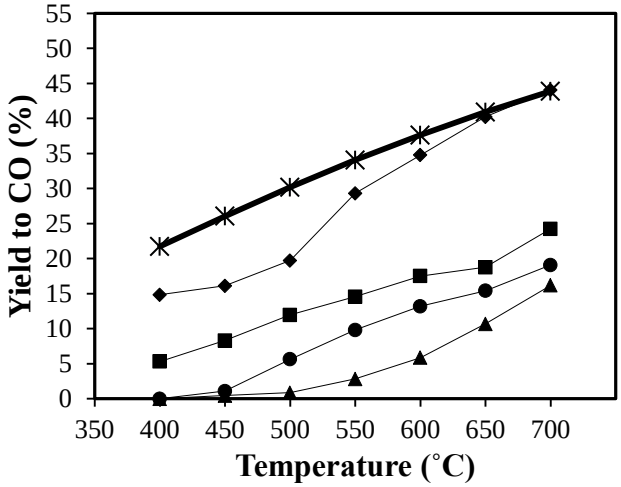

Figure 6.1: Average yield of CO for the RWGS reaction using Pt supported on C, γ-Al_2O_3, SDC and YSZ at 1 atm, $P_{H2} = P_{CO2}$ = 1kPa, balance He with 50 mg of catalyst. Total flow rate of mL·min-^{1}. Where ✳ = Equilibrium, ◆ = Pt/SDC, ■ = Pt/YSZ, ● = Pt/C, ▲ = Pt/ γ-Al_2O_3

Oxygen vacancies found on the surface of the two supports are suggested to be the main cause for the increased yields observed. A mechanism was also suggested in Chapter 4 which explains the interaction of the oxygen vacancies in the RWGS reaction.

6.1.4 Objective 4: Cu_xNi_{1-x} Nanoparticles Deposited on Supports Having Varying Oxygen Vacancy Contents for the RWGS Reaction

Similar to the work conducted with the supported Pt nanoparticles, CuNi nanoparticles were deposited on C, γ-Al_2O_3, YSZ and SDC. Three Cu_xNi_{1-x} catalysts were used: x = 20, 50, 80. 50 mg of each catalyst was tested for the RWGS reaction at atmospheric pressure and temperatures ranging from 400°C to 700°C each tested for 3 cycles.

Stability was one of the key components tested in these experiments. Once again, the γ-Al_2O_3 support showed a lack of stability for all metal catalysts. $Cu_{80}Ni_{20}$ and $Cu_{20}Ni_{80}$ also showed signs of instability when deposited on C. The only carbon supported CuNi catalyst to show consistent stability was the $Cu_{50}Ni_{50}$ catalyst. When YSZ and SDC were used as supports, both $Cu_{50}Ni_{50}$ and $Cu_{20}Ni_{80}$ showed good stability. In addition cyclic experiments were performed. $Cu_{50}Ni_{50}$/SDC was tested for 48 consecutive hours at 600°C and 700°C. There were no signs of deactivation during this period.

High CO yield was another important aspect for this research. There was no observable trend differentiating the CuNi ratios with most supports. There was however a clear distinction between each support. Higher stoichiometric oxygen vacancy content showed increased yields for all catalysts. This is shown in Figure 6.2. $Cu_{50}Ni_{50}$/SDC showed the highest yield to CO among CuNi catalyst achieving 39.8% at 700°C. This was less than 4% from equilibrium which was achieved by Pt/SDC.

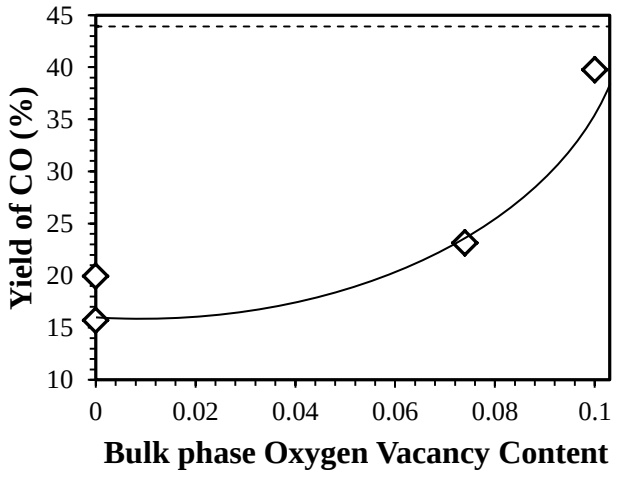

Figure 6.2: Effect of oxygen vacancy on yield of CO for the RWGS reaction using $Cu_{50}Ni_{50}$ metal at 1 atm, $P_{H2} = P_{CO2}$ = 1kPa, balance He, 50 mg of catalyst at 700°C. Total flow rate of mL·min-^{1}. Dotted line = equilibrium yield

Methane production was closely monitored during all experiments. CH_4 was expected when using a Ni containing catalyst since Ni has the tendency to hydrogenate CO to CH_4. There was no CH_4 observed during any of the experiments conducted. This was explained by the reduced Ni concentration on the surface of all CuNi catalysts. As shown by the XPS analysis, Cu is the dominant specie in all cases. Methane was observed when the partial pressure of H_2 was increased to 2 times that of CO_2. This is consistent with what is expected stoichiometrically and what is found in the literature [6]. Higher yields were also observed with higher H_2 partial pressures.

The $Cu_{50}Ni_{50}$/SDC catalyst was closest to achieving the equilibrium yield that was obtained with Pt/SDC. It was found that this catalyst operated very well for extended periods of time at high temperatures without generating CH_4 as a by-product. Some modifications suggested in section 6.2 describe how the $Cu_{50}Ni_{50}$/SDC catalyst could one day outperform the much more expensive Pt/SDC catalyst.

6.2 Recommendations

The catalysts synthesized via a novel synthesis method described in Chapter 3 achieved good yield, selectivity and in most cases, good stability. Nevertheless, improvements can be made to increase the yield of CO at lower temperatures and perhaps achieve equilibrium yield under certain conditions.

The suggested synthesis method is flexible and can be varied. NaOH concentrations can be varied in order to examine its effect on particle size and distribution. Smaller particles have already shown better conversion for other reactions [7]. Other additives could also be used in an

attempt to narrow the size distribution. For example, polyvinylpyrrolidone (PVP) is a polymer capable of preventing agglomeration and reducing particle size during synthesis.

Gas hourly space velocity (GHSV) varied from one support to the next depending on bulk density. Otherwise, the gas flowrate was not varied during the experiments. Lower GHSV values can increase yields. Investigating different reactant flow rates and/or concentrations is a method of achieving an ideal GHSV value for each catalyst. In addition, a relatively small amount of catalyst was used (50 mg). This can also be increased.

Reaction conditions were varied. Elements such as partial pressure and temperature were thoroughly examined. Reactor pressure remained constant. Varying operating pressures could be done in order to increase the yield of the gaseous reactions.

The research conducted showed increased yields when using supports containing stoichiometric oxygen vacancies. More supports containing varying oxygen vacancy contents could be tested in order to obtain an ideal amount for the reaction. A combination of high surface area and stoichiometric oxygen vacancy content could also be examined in hope of increasing yield of CO.

The CuNi nanoparticles were consistently deposited using 10 metal weight percent on the support. Examining the effect of varying this percentage could yield an ideal loading for the RWGS reaction.

Lastly, an alternative to CuNi would be to examine other bi-metallic catalysts for this reaction. Cu has shown to be a prominent catalyst throughout this research since it was capable of being stabilized. Other metals such as Sn or Fe could also be used as comparison to Ni in the goal of stabilizing Cu. Higher yields could be achieved with these alternatives.

6.3 Contributions to Knowledge

The RWGS reaction has been increasingly studied over the past two decades. Cu has shown to be a selective catalyst capable of high yields but is not stable at high temperatures [8]. While Ni has also shown high conversion, it does not contain the same selective nature shown by Cu. It does however remain stable at high temperatures [8]. Some [9] have researched Cu:Ni metals with different ratios for the RWGS reaction at high temperatures when supported on γ-Al_2O_3. That being said, stability measurements with the bimetallic catalyst were not done, nor were the characterization of the catalyst showing the presence of an alloyed compound.

1. Information pertaining to a new synthesis method capable of synthesizing CuNi nanoparticles containing two different solid solutions was given. This insight has shown a route for synthesizing a Cu rich CuNi solid solution on the surface of the catalyst while also having a Ni rich CuNi solid solution present. A Cu rich surface is important because of the possibility of methanation caused by Ni [9]. The synthesis was repeated for 3 different Cu_xNi_{1-x} (x = 20, 50, 80) ratios. Characterization for the CuNi nanoparticles was also provided.

2. The research also shows the absence of CH_4 during all experiments when the partial pressure of the reactants was kept at or below the stoichiometric ratio ($P_{H2} = P_{CO2}$). This had not been shown previously when Ni was involved in the RWGS reaction. Cu was also successfully stabilized using Ni as stabilizer.

3. High yields comparable to that of noble metals (Pt) which achieved equilibrium conversion at 700°C were obtained with the CuNi catalyst for the first time. More specifically, the yield with the CuNi/SDC catalyst was only 4% less than the equilibrium yield at 700°C (43.9%).

4. In the past Samarium-doped ceria (SDC) and yttria-stabilized zirconia (YSZ) have had limited testing for the RWGS reaction [10], [11]. In fact, SDC had only been tested without the presence of a metallic catalyst. This research showed the effectiveness of this support when it was combined with a metal catalyst. This research demonstrated the importance of oxygen vacancies generated when samarium is inserted in the crystal lattice of ceria.

6.4 References

[1] K. Watanabe, M. Hashiba, and T. Yamashina, "A Quantitative Analysis of Surface Segragation and In-Depth Profile of Copper-Nickel Alloys," *Surf. Sci.*, vol. 61, pp. 483–490, 1976.

[2] T. Sakurai, T. Hasizume, A. Jimbo, A. Sakai, and S. Hyodo, "New Results in Surface Segregation of Ni-Cu Binary Alloys," *Phys. Rev. Lett.*, vol. 55, no. 5, pp. 514–517, 1985.

[3] P. van der Plank and W. M. H. Sachtler, "Surface Composition of Equilibrated Copper-Nickel Alloy Films," *J. Catal.*, vol. 7, no. 3, pp. 300–303, 1967.

[4] C. Bock, C. Paquet, M. Couillard, G. A. Botton, and B. R. MacDougall, "Size-selected synthesis of PtRu nano-catalysts: reaction and size control mechanism.," *J. Am. Chem. Soc.*, vol. 126, pp. 8028–37, Jun. 2004.

[5] R. K. Oberlander, "Aluminas for Catalysts: Their preparation and properties," *Appl. Industiral Catal.*, vol. 3, p. 67, 1984.

[6] S. S. Kim, K. H. Park, and S. C. Hong, "A study of the selectivity of the reverse water–gas-shift reaction over Pt/TiO2 catalysts," *Fuel Process. Technol.*, vol. 108, pp. 47–54, Apr. 2013.

[7] R. J. Isaifan, S. Ntais, and E. A. Baranova, "Particle size effect on catalytic activity of carbon-supported Pt nanoparticles for complete ethylene oxidation," *Appl. Catal. A Gen.*, vol. 464–465, pp. 87–94, Aug. 2013.

[8] W. Wang, S. Wang, X. Ma, and J. Gong, "Recent advances in catalytic hydrogenation of carbon dioxide.," *Chem. Soc. Rev.*, vol. 40, no. 7, pp. 3703–27, Jul. 2011.

[9] Y. Liu and D. Liu, "Study of bimetallic Cu-Ni/ gamma Al2O3 catalysts for carbon dioxide hydrogenation," *J. Hydrog. Energy*, vol. 24, pp. 351–354, 1999.

[10] M. Ismail, "Model Development and Validation of Samaria Doped Ceria (SDC) Based Solid Oxide Fuel Cell Operating with Practical Fuels," Univiersity of Waterloo, 2013.

[11] G. Pekridis, K. Kalimeri, N. Kaklidis, E. Vakouftsi, E. F. Iliopoulou, C. Athanasiou, and G. E. Marnellos, "Study of the reverse water gas shift (RWGS) reaction over Pt in a solid oxide fuel cell (SOFC) operating under open and closed-circuit conditions," *Catal. Today*, vol. 127, no. 1–4, pp. 337–346, Sep. 2007.

Appendices:

This section compliments the discussion found in Chapters 3 and 4. All information pertinent to the Thesis that is not contained in either Chapter 3 or 4 will be discussed here. Both equipment and experimental methodologies were kept constant throughout all experiments and can be found in Chapters 3 and 4.

A.1 Yttria-Stabilized Zirconia for the RWGS reaction using Cu_xNi_{1-x} (x = 20, 50 and 80) nanoparticles

Yttria-stabilized Zirconia (YSZ) was used as support containing stoichiometric oxygen vacancies for all 3 Cu_xNi_{1-x} (x = 20, 50, 80) catalysts and tested for the RWGS reaction between 400°C and 700°C. In comparison to ZrO_2, YSZ has 0.074 oxygen vacancies per cation. Results obtained in Chapter 4 demonstrated that the increase in oxygen vacancy content may contribute to a higher yield of CO.

The results shown in Figure A.1 represent the 3rd cycle of each catalyst. Both the Ni rich and the Cu rich catalysts showed higher yield of CO than the equimassic ratio. This observation is consistent with what was observed in Chapter 3 when the same metal was deposited on Carbon. The Cu rich catalyst also showed the best yield of CO up until 700°C at which the deactivation of the catalyst caused it to drop below that of the Ni rich ratio, as shown in Figure A.1.

The Ni rich catalyst remains a good working catalyst despite its high Ni content. This aspect is discussed in Chapter 3. XPS measurements demonstrated high Cu concentrations on the surface of each catalyst. In fact, the Cu surface concentration is over 4 times what it should be theoretically for the bulk $Cu_{20}Ni_{80}$ metal. This is shown in Table A.1. In addition, there were no

sign of CH_4 formation during any of the experiments which would have normally been favourable with Ni rich surfaces [1], [2] that did not contain Cu.

There were small signs of deactivation for the Cu rich catalyst ($Cu_{80}Ni_{20}$) as seen in Figure A.2 a. Otherwise, $Cu_{50}Ni_{50}$/YSZ and $Cu_{20}Ni_{80}$/YSZ showed constant yield of CO after the first cycle.

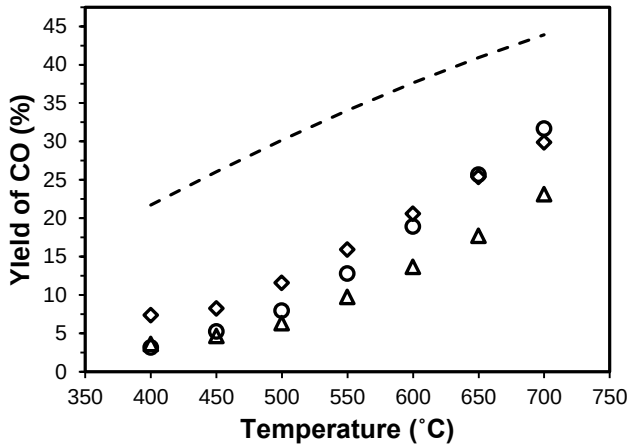

Figure A.1: RWGS reaction at 1atm, $P_{H2} = P_{CO2} = 1$ kPa, balance He, GHSV = 716000h^{-1} , 50 mg of catalyst: ○ = $Cu_{80}Ni_{20}$/YSZ, △ = $Cu_{50}Ni_{50}$/YSZ and ◇ = $Cu_{20}Ni_{80}$/YSZ. Dotted line is equilibrium yield

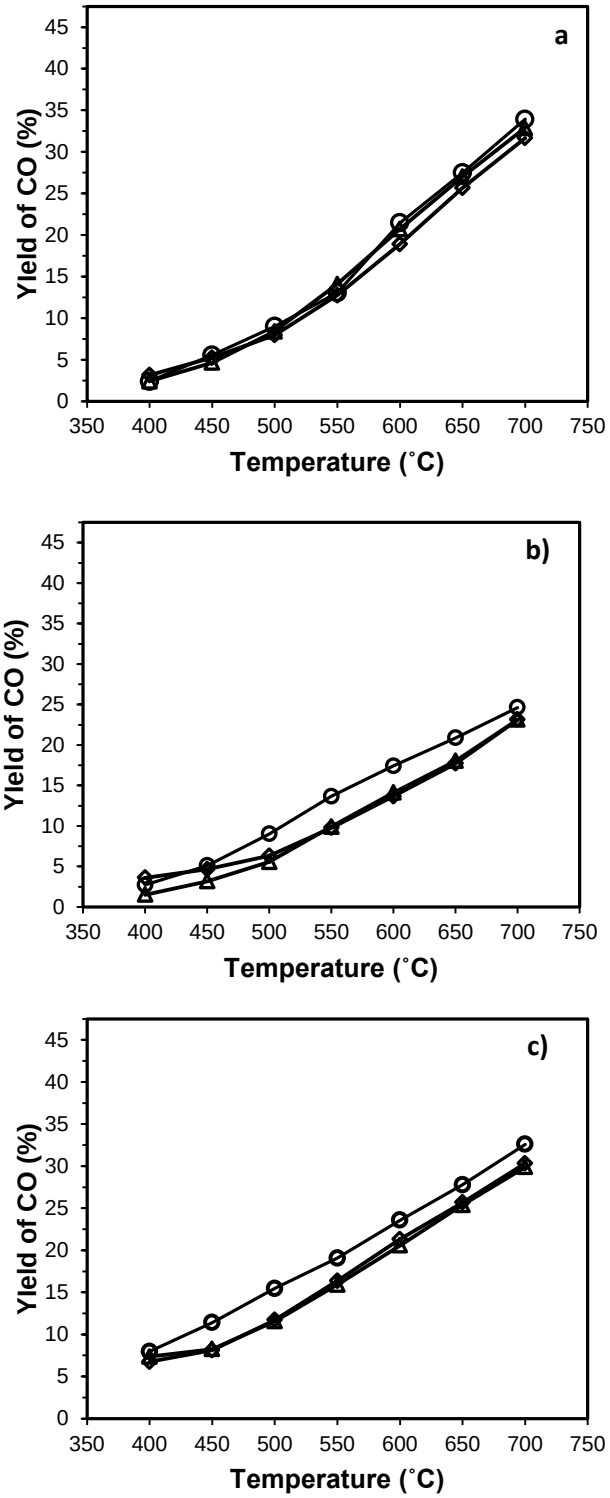

Figure A.2 : RWGS reaction at 1atm, $P_{H2} = P_{CO2} = 1$ kPa, balance He, GHSV = 716000 h^{-1} over **a)** $Cu_{80}Ni_{20}$/YSZ **b)** $Cu_{50}Ni_{50}$/YSZ **c)** $Cu_{20}Ni_{80}$/YSZ, where ○ = 1st cycle, △ = 2nd cycle and ◇ = 3rd cycle

Table A.1: Cu-Ni surface ratio measurements using XPS

	Theoretical Cu/Ni ratio	Actual Surface Cu/Ni ratio	Percentage Increase
$Cu_{20}Ni_{80}$	0.25	1.2	380%
$Cu_{50}Ni_{50}$	1	2	100%
$Cu_{80}Ni_{20}$	4	4.2	5%

YSZ showed good, stable yield of CO at high temperatures for all three Cu_xNi_{1-x} catalysts. Oxygen vacancies found within the crystal lattice of YSZ is thought to be the main contributor to this increase in yield and is further discussed in Chapter 4. Cu rich surfaces are also believed to cause the high CO yield as well as be the main reason why no CH_4 was observed. Ni is believed to be used as a stabilizing agent permitting the use of the $Cu_{20}Ni_{80}$/YSZ and the $Cu_{50}Ni_{50}$/YSZ catalysts at high temperatures (700°C).

A.2 Samarium-Doped Ceria for the RWGS reaction using Cu_xNi_{1-x} nanoparticles

Samarium-doped Ceria (SDC) was used as a support containing more stoichiometric oxygen vacancies than YSZ (0.074 per cation). In comparison to CeO_2, SDC has 0.1 oxygen vacancy per cation. The data in Chapter 4 illustrated the increase in yield of CO when SDC was used as the support.

Figure A.3 compares the 3^{RD} cycle of all 3 Cu_xNi_{1-x} / SDC (x = 20, 50, 80) catalysts used between 400°C and 700°C. All 3 Cu_xNi_{1-x} catalysts exhibit high CO yield at 700°C. Both $Cu_{50}Ni_{50}$/SDC and $Cu_{20}Ni_{80}$/SDC are found within 5% of the equilibrium yield. A maximum of 39.8% yield of CO is observed using the equi-massic mixture. The copper rich catalyst ($Cu_{80}Ni_{20}$/SDC) and the Ni rich catalysts have slightly less yield of CO at the same temperature (35.2% and 38.4% respectively).

Once again, slight deactivation was observed using the Cu rich ($Cu_{80}Ni_{20}$) metal catalyst over three cycles. Other Cu_xNi_{1-x} catalysts ($Cu_{50}Ni_{50}$ and $Cu_{20}Ni_{80}$) were stable at higher temperatures during all 3 cycles. These results are demonstrated in Figure A.4.

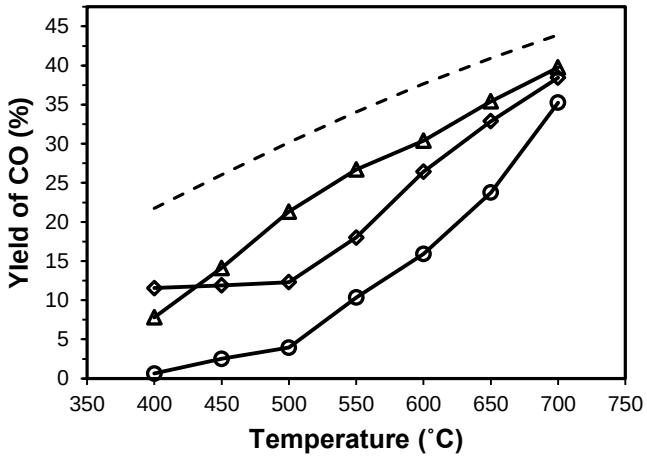

Figure A.3: RWGS reaction at 1atm, $P_{H2} = P_{CO2} = 1$ kPa, balance He, GHSV = 960800h^{-1} , 50 mg of catalyst: O = $Cu_{80}Ni_{20}$/SDC, Δ = $Cu_{50}Ni_{50}$/SDC and ◇ = $Cu_{20}Ni_{80}$/SDC. Dotted line is equilibrium yield

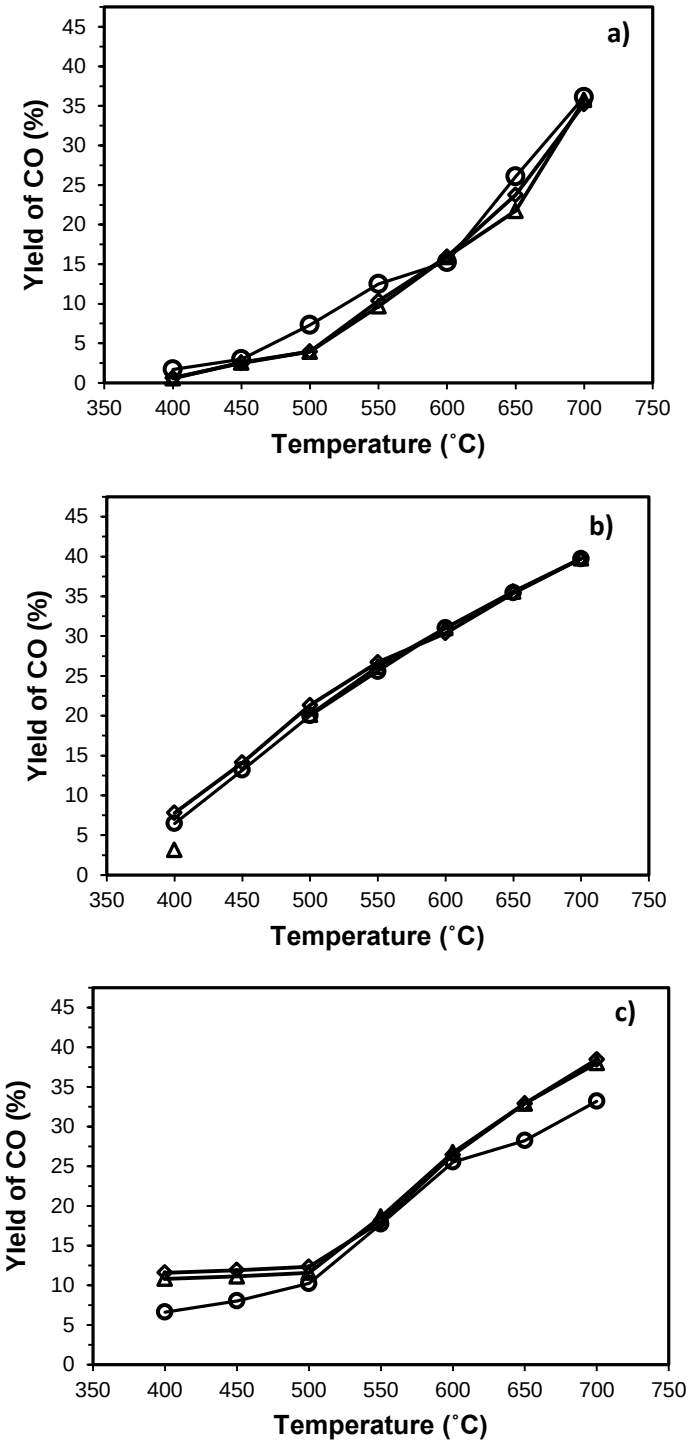

Figure A.4: RWGS reaction at 1atm, $P_{H2} = P_{CO2} = 1$ kPa, balance He, GHSV = 960800 h^{-1} over **a)** $Cu_{80}Ni_{20}$/SDC **b)** $Cu_{50}Ni_{50}$/SDC **c)** $Cu_{20}Ni_{80}$/SDC, where ○ = 1st cycle, △ = 2nd cycle and ◇ = 3rd cycle

The high yield of CO observed with high Ni content is once again attributed to the strong presence of Cu on the surface of the catalyst. In addition, both $Cu_{50}Ni_{50}$/SDC and $Cu_{20}Ni_{80}$/SDC

showed good stability within the temperature range used. No CH_4 was observed during any of the experiments.

SDC showed high yields during the experiments and approached equilibrium at high temperatures (<650°C). This is may be caused by the oxygen vacancies present when Samarium is inserted within the Ceria crystal lattice. These oxygen vacancies may actively participate in the reaction, as shown in Chapter 4.

A.3 Conclusion

SDC demonstrated better yields of CO at most temperatures using the three Cu_xNi_{1-x} metals. These trends were previously observed in Chapter 4 with only the equi-massic mixture. Similar observations were found by Ismail [3]. He tested both supports without the presence of a metal catalyst and found good yield of CO at high temperatures. He similarly found the SDC showed higher yields than YSZ.

These increases in CO yield may be caused by the high number of oxygen vacancy sites found using SDC. In contrast to YSZ (0.074 oxygen vacancy per cation), SDC (0.1 oxygen vacancy per cation) has over 1.5 times the stoichiometric oxygen vacancies. Nonetheless, both supports may participate actively in the reaction.

Both supports were also found to be stable at high temperatures when Cu_xNi_{1-x} catalysts of x = 50 and 20 were used. The Cu rich catalysts showed signs of deactivation over time. In addition, there was no CH_4 observed during the experiments. A Cu rich alloy found on the surface of the catalyst may cause the absence of CH_4. A Ni rich alloy combined with the presence of Ni in the Cu rich surface may be the main contributor to the stability of the catalysts observed at the high operating temperatures.

A.4 References

[1] Y. Liu and D. Liu, “Study of bimetallic Cu-Ni/ gamma Al2O3 catalysts for carbon dioxide hydrogenation,” *J. Hydrog. Energy*, vol. 24, pp. 351–354, 1999.

[2] W. Wang, S. Wang, X. Ma, and J. Gong, “Recent advances in catalytic hydrogenation of carbon dioxide.,” *Chem. Soc. Rev.*, vol. 40, no. 7, pp. 3703–27, Jul. 2011.

[3] M. Ismail, “Model Development and Validation of Samaria Doped Ceria (SDC) Based Solid Oxide Fuel Cell Operating with Practical Fuels,” Univiersity of Waterloo, 2013.